NASA TECHNICAL NOTE

NASA TN D-4298

c. 1

NASA TN D-4298

ANALYTICAL AND EXPERIMENTAL STUDY OF DYNAMIC CHARACTERISTICS OF TURBOPUMPS

by H. Ohashi

George C. Marshall Space Flight Center
Huntsville, Ala.

NATIONAL AERONAUTICS AND SPACE ADMINISTRATION • WASHINGTON, D. C. • APRIL 1968

ANALYTICAL AND EXPERIMENTAL STUDY OF DYNAMIC CHARACTERISTICS OF TURBOPUMPS

By H. Ohashi

George C. Marshall Space Flight Center
Huntsville, Ala.

NATIONAL AERONAUTICS AND SPACE ADMINISTRATION

For sale by the Clearinghouse for Federal Scientific and Technical Information
Springfield, Virginia 22151 – CFSTI price $3.00

TABLE OF CONTENTS

LIST OF ILLUSTRATIONS

LIST OF ILLUSTRATIONS (Continued)

LIST OF ILLUSTRATIONS (Continued)

LIST OF ILLUSTRATIONS (Concluded)

LIST OF TABLES

DEFINITION OF SYMBOLS

Symbol	Definition	Units
A	Passage area	m^2
A_n	Fourier coefficient	dimensionless
$C(\omega, \sigma)$	Coupling function	dimensionless
f	Frequency of fluctuation	Hz
g	Constant complex number	m^2/s
G_o	Constant complex number	m^2/s
h	Normalized pressure fluctuation	dimensionless
ℓ	Chord length of airfoil	m
L	Meridional length of turbopump	m
n	Rotational speed of turbopump	rev./s, (rps)
N	Number of airfoils	dimensionless
p	Pressure	N/m^2
Δp	Deviation of pressure from time-mean value	N/m^2
Q	Flow rate through turbopump	m^3/s
ΔQ	Amplitude of flow fluctuation	m^3/s
r	Radius from axis of rotation	m
R	Constant for conformal transformation	m
s	Spacing of airfoils in cascade	m
$S(\omega, \sigma)$	Sinusoidal gust function	dimensionless
u, v	Induced velocity	m/s
u	Moving velocity of rotor cascade	m/s
U_∞	Through-flow velocity parallel to airfoil	m/s
V	Absolute velocity	m/s
w	Unsteady inlet flow in cascade direction	m/s
W	Relative velocity to rotor cascade	m/s
x, y	Coordinate, parallel and perpendicular to airfoil	m
X, Y	Coordinate, axial and cascade direction	m
γ	Distributed circulation	m/s
Γ	Circulation	m^2/s

DEFINITION OF SYMBOLS (Concluded)

Symbol	Definition	Units
θ	Polar angle	radian
λ	Stagger angle of cascade	radian
ν	Angular velocity = $2 \pi f$	radian/s
ρ	Density of working liquid	kg/m^3
σ	Solidity of cascade = ℓ / s	dimensionless
ϕ	Flow coefficient	dimensionless
Φ	Velocity potential	m^2/s
ψ	Pressure rise coefficient	dimensionless
ω	Reduced frequency	dimensionless
Ω	Gravitational potential	m^2/s^2

SUPERSCRIPTS

$\bar{}$	Pertinent to translatory oscillation
$\sim$	Pertinent to sinusoidal gust oscillation

SUBSCRIPTS

0	Time-mean value
1	Upstream of cascade
2	Downstream of cascade
a	Axial component
C	Due to conduit effect
d	At pump delivery port
qs	Quasi-static condition
R	Rotor cascade
s	At pump suction port
S	Stator cascade
R + S	Due to pumping action of rotor and stator
u	Component parallel to cascade direction
W	Pertinent to wake

ANALYTICAL AND EXPERIMENTAL STUDY OF DYNAMIC CHARACTERISTICS OF TURBOPUMPS

SUMMARY

The response of pressure rise of turbopumps to fluctuating flow rate, termed the "dynamic characteristics," was studied analytically and experimentally. Unsteady flow around a two-dimensional, linear cascade of airfoils was solved and the frequency response of the deflection angle of the cascade was calculated for the periodically oscillating inlet condition. Based on the unsteady cascade theory, the dynamic characteristics of turbopumps were analyzed. As a sample of the theoretical application, an exact method for calculating the dynamic characteristics of a single-stage axial flow pump is shown. For the evaluation of an approximate response, a simplified model theory was also developed, which enables the calculation to be made without entering into the details of the pump design.

An experimental investigation was made to determine the dynamic characteristics of a centrifugal pump. The test showed that the analytical calculation was close to the experimental result. The limiting fluctuating frequency under which the dynamic characteristics agree with the quasi-static ones, was determined from the test result. The time constant of the response of pressure rise to a step-like change of flow rate was also derived.

The entire study was made under incompressible and non-cavitating conditions. If the cavitation occurs in a turbopump, the phenomena change drastically from those described in this study.

INTRODUCTION

The pressure rise through a turbopump* varies with the flow rate. The relationship between them is indicated by the characteristics curve of the pump. This characteristics curve is valid only when the pump operates in the steady-state condition, that is, with a constant flow rate. When the flow rate is no longer steady and changes rapidly, the pressure rise cannot respond quickly enough to follow along the steady-state characteristics curve. This results in a considerable change in the actual characteristics curve. The purpose of this study was to determine analytically and experimentally the correlation between the flow rate oscillation and the resulting pressure rise

* Turbopumps include axial flow pumps, mixed flow pumps, centrifugal pumps etc., which are all classified as turbomachinery.

oscillation of turbopumps, termed dynamic characteristics.

Since the unsteady condition is restricted (in this study) to the case in which the flow rate oscillates sinusoidally around its mean value with a constant frequency, the dynamic characteristics are identical to the frequency response of pressure rise to the flow rate. The dynamic characteristics are especially important for analyzing the stability of a system in which the pump is installed. Figure 1 shows a turbopump whose flow rate, Q, oscillates periodically around its mean value, Q_o, because of some outer disturbances. The pressure at the suction port, p_s, and at the delivery port, p_d, fluctuate also according to the fluctuating flow rate, and the pressure rise through the pump, $p_d - p_s$, fluctuates correspondingly. The amplitude and phase correlations between the pressure rise, $p_d - p_s$, and the flow rate, Q, were the essential information pursued in this study. The rotational speed of the pump was assumed to be constant and unaffected by the fluctuating operation.

Many studies (Reference 1 to 3) have been made to predict analytically the steady state characteristics curves of turbopumps. Most of these are derived from the consideration of the flow field around the cascade of airfoils, because the behavior of the cascade is the principal determinant of the characteristics of the turbopump. For the same reason, the behavior of the cascade is the determining factor of the dynamic characteristics of a turbopump. Therefore, an analysis of the flow through a cascade of airfoils under the oscillating inlet flow condition was made as the first step in the theoretical approach and is described in Section I of this paper. Using this basic result, another analysis was performed to determine the dynamic characteristics of turbopumps and is described in Section II. Experimental research was also conducted to determine the dynamic characteristics of a centrifugal pump. The test results and the comparison with the analytical results are described in Section III. Interest in this study is limited to the incompressible, noncavitating case.

ACKNOWLEDGEMENT

This study was conducted in the Applied Mechanical Research Branch, Propulsion and Vehicle Engineering Laboratory of the George C. Marshall Space Flight Center, NASA, as a Postdoctoral Research Associateship Program of the National Academy of Sciences-National Research Council.

The author would like to express his sincere appreciation to the National Academy of Sciences-National Research Council for providing him with this valuable opportunity for the research. The author's appreciation extends also to all who supported this study at the Marshall Space Flight Center, especially to Dr. R. R. Head, Dr. N. E. Welch, Mr. L. B. Marks and Mr. H. M. Hammac for their thoughtful advice and dedicated support.

SECTION I. ANALYSIS OF OSCILLATING FLOW THROUGH A CASCADE

Two-dimensional, incompressible, inviscid, and noncavitating flow around a cascade of airfoils was analytically determined for a periocically oscillating inlet flow. Figure 2(a) illustrates the inlet condition to the cascade. The unsteady inlet flow, V_1, can be considered as a superposition of a steady inlet flow, V_{10}, and an unsteady flow, w(X, Y, t). The unsteady flow, w, can be further divided into two unsteady components, w' and w'', parallel to the direction of cascade and to the direction of zero-lift, respectively.

The unsteady component, w'', causes no change of circulation around the airfoils, and represents an oscillating translation flow that can be simply superimposed on the flow solution. On the other hand, the unsteady component, w', parallel to the cascade direction produces a related unsteady circulation around the airfoils, which is to be determined in this Section. From the previous consideration, the analysis was conducted specifically for the case in which the unsteady component of the inlet flow is parallel to the cascade direction, as illustrated in Figure 2(b), without losing any generality. The unsteady component, w, now parallel to the cascade direction, is generally a function of time and the coordinates.

There are fundamentally two types of unsteady components in the inlet flow. One is the case in which the unsteady component, w, is expressed as $w = \overline{w}\ \mathrm{Exp}\ (i\nu t)$*. In this case, termed "translatory oscillation," w is instantaneously uniform in the region preceding the cascade and oscillates periodically with the frequency $f = \nu/2\pi$. Translatory oscillation is associated with the oscillation of the flow rate, that is, oscillation of axial velocity, V_a. In the other case, w is expressed as $w = \tilde{w}\ \mathrm{Exp}\ (i\nu t - i\nu X/V_a)$*. This oscillation represents a sinusoidal gust propagating downstream with a velocity of V_a. This case is termed "sinusoidal gust oscillation" and occurs as the result of unsteady circulations of airfoils in the preceding cascade.

To avoid excessive mathematical complexity, the unsteady flow was analyzed for cascades of flat plates having a zero stagger angle for two types of inlet unsteadiness. An additional analysis was performed to show that the results obtained for the cascade of zero stagger angle was also applicable, with proper modification, to the cascades of arbitrary stagger angle.

---

* The physical meaning of a complex number is attributed only to the real part.

Flow Around a Cascade of Nonstaggered Flat Plates for Inlet Flows with Translatory Oscillation

Flow Configuration - Flow through the cascade shown in Figure 3 is considered. This cascade consists of flat plates of length, ℓ, arranged with spacing, s, and zero stagger angle. A vertical translatory oscillation, $w = \bar{w}\ \mathrm{Exp}\ (i\nu t)$, is superimposed on the steady through-flow, U_∞, in the direction of the flat plate. The steady inlet flow with a non-zero angle of attack is not considered here, because it can be easily added to the unsteady flow field. Since the flow is assumed to be two-dimensional, incompressible, and inviscid, the unsteady flow field through the cascade can be obtained by simultaneously solving Euler's equations of motion and the equation of continuity under the given inlet and boundary conditions. The potential flow field that satisfies the given inlet and boundary conditions at any instant agrees with the unsteady solution, as far as the velocity field is concerned.

To determine the circulation of each airfoil, the Kutta-Joukowski theorem is assumed for the entire frequency range. The accuracy of this assumption is not clear in the higher frequency range because of the time lag involved in the formation of the boundary layer around the airfoil. The circulation around each airfoil also fluctuates periodically, and this causes shedding of free vortices into the wake system. The wake of each airfoil, therefore, represents a vortex sheet with varying intensity. The flow field induced by this vortex system must be taken into account. To simplify the analysis, wakes are assumed to be straight and parallel to the direction of through-flow, U_∞.

The circulation of each airfoil, $\bar{\Gamma}$, is divided into three parts, $\bar{\Gamma} = \bar{\Gamma}_0 + \Gamma_1 + \Gamma_1'$. The flow with circulation $\bar{\Gamma}_0$ around the airfoil induces a velocity distribution that tends to cancel the given inlet translatory oscillation, $w = \bar{w}\ \mathrm{Exp}\ (i\nu t)$, on the airfoil. This solution represents a quasi-static flow when the effect of the vortex sheets is not taken into account. On the other hand, vortex sheets induce a downwash on each airfoil. The flow with circulation Γ_1 induces a velocity distribution for canceling the non-uniform part of this downwash on the airfoil, while the flow with circulation Γ_1' induces a velocity distribution for canceling the remaining uniform part. These conditions are indicated schematically in Figure 4.

In this analysis, conformal transformation is used to obtain the potential flow solutions.

Conformal Transformation - A cascade consisting of nonstaggered flat plates in the $z = x + iy$ plane (physical plane) is transformed conformally into a circle of unit radius in the $z' = x' + iy'$ plane by using the following mapping function (Reference 4);

$$z = \frac{s}{2\pi}\left(\ln\frac{R + z'}{R - z'} + \ln\frac{z' + 1/R}{z' - 1/R}\right) \qquad (1\text{-}1)$$

where R is a function of the solidity, $\sigma = \ell / s$, of the cascade;

$$\sigma = \frac{\ell}{s} = \frac{2}{\pi} \ln \frac{R + 1}{R - 1} \tag{1-2}$$

As shown in Figure 5, the origin of the z-plane is located at the center of an airfoil, and the x-axis is chosen parallel to the airfoil. Therefore, $z = \pm \ell/2$ describes the trailing and leading edge of the airfoil. These points transform into $z' = \pm 1$ in the z'-plane. Obviously, the flow around the airfoil in the physical plane corresponds to the flow outside or inside of the unit circle in the z'-plane, and $z = \pm \infty$ in the z-plane is transformed into $z' = \pm R$ or $\pm 1/R$ in the z'-plane.

Determination of $\overline{\Gamma}_0$ - The flow field, which has the constant induced flow on the airfoil just opposite to the inlet translatory oscillation, w, can be determined by the proper distribution of vortices in the z'-plane as illustrated in Figure 6. The solution, which includes no circulation around the airfoil, can be obtained in the z'-plane by locating vortices $-\Gamma_\infty = -\,sw$ at $z' = 1/R$ and Γ_∞ at $z' = -1/R$. On the other hand, the solution that produces circulation $\overline{\Gamma}_0$ around each airfoil is obtained in the z'-plane by locating $\overline{\Gamma}_0/2$ at $z' = \pm 1/R$ and $-\overline{\Gamma}_0/2$ at $z' = \pm R$. The assumed Kutta-Joukowski theorem requires that the total velocity induced by these vortices approach zero at the trailing edge ($z' = 1$), and this leads to the result

$$\overline{\Gamma}_0 = \frac{4\,s\,R}{R^2 + 1}\,\overline{w}\,\mathrm{Exp}\,(i\nu t) \tag{1-3}$$

Determination of Γ_1' - The circulation distribution γ_W in the wakes induces a downwash on each airfoil. This circulation distribution (Figure 4) can be regarded as the sum of (1) γ_W on $x = \ell/2$ to ∞ and $-\Gamma_W = -\int_{\ell/2}^{\infty} \gamma_W\,dx$ at $x = +\infty$, and (2) Γ_W at $x = +\infty$. The former distribution (1) induces the non-uniform part of the downwash, and the latter (2) induces the uniform part on the airfoil. The uniform part is calculated from the equation

$$w = \Gamma_W/2s = 1/2s \int_{\ell/2}^{\infty} \gamma_W\,dx$$

and the necessary circulation for canceling this downwash is determined by the same process that leads to equation (1-3);

$$\Gamma_1' = \frac{4\,s\,R}{R^2 + 1}\,w = \frac{2R}{R^2 + 1}\,\Gamma_W \tag{1-4}$$

Determination of Γ_1 - The solution for the non-uniform part of the downwash is described below. To simplify the analysis, the shedded vortices are assumed to be located on the straight lines starting from each trailing edge into the x-direction. First, the effect of the vortices, Γ_W, at x = x is considered. The uniform downwash of these vortices is subtracted by locating counter-vortices, $-\Gamma_W$, at $x = +\infty$ as shown in Figure 7. This flow field can be obtained in the z'-plane by locating Γ_W at z' = x' and 1/R and $-\Gamma_W$ at z' = 1/x' and R, where x' is the mapped location of Γ_W calculated by the mapping function (equation (1-1)).

To realize the Kutta condition at the trailing edge, circulatory flow around the airfoil is added to the above by locating $\Gamma_1/2$ at $z' = \pm 1/R$ and $-\Gamma_1/2$ at $z' = \pm R$, where Γ_1 satisfies the following relation;

$$\Gamma_1 = 2 \frac{R + 1}{R^2 + 1} \frac{R - x'}{x' - 1} \Gamma_W \tag{1-5}$$

For the case of distributed vortices in wakes, Γ_1 can be obtained by integrating equation (1-5) along the wake;

$$\Gamma_1 = 2 \frac{R + 1}{R^2 + 1} \int_{\ell/2}^{\infty} \frac{R - x'}{x' - 1} \gamma_W \, dx \tag{1-6}$$

In the above derivation, the circulation distribution of each vortex sheet is assumed to be identical.

Unsteady Solution for Translatory Oscillation - According to Helmholtz's theorem regarding the persistence of vorticity, the total circulation of the whole system is assumed to be invariably equal to zero (Reference 5 and 6);

$$\overline{\Gamma} + \int_{\ell/2}^{\infty} \gamma_W \, dx = \overline{\Gamma}_0 + \Gamma_1 + \Gamma_1' + \Gamma_W = 0 \tag{1-7}$$

Putting equation (1-6) into equation (1-7), the following relation is obtained;

$$\overline{\Gamma}_0 + \Gamma_1' + \int_{\ell/2}^{\infty} \left(2 \frac{R + 1}{R^2 + 1} \frac{R - x'}{x' - 1} + 1 \right) \gamma_W \, dx = 0 \tag{1-8}$$

Since the inlet unsteady component is periodic with a frequency of $f = \nu/2\pi$, the entire flow field also oscillates with the same frequency, f. It is also assumed that the vortices in the wakes move downstream with the velocity U_∞ in the x-direction. Therefore, the circulation distribution, γ_W, can be expressed in the form

$$\gamma_W = \frac{2\pi}{s} g \, \mathrm{Exp}\left[i\nu\left(t - x/U_\infty\right)\right] \tag{1-9}$$

where g is a constant complex number that describes the amplitude and the phase of the circulation oscillation in the wakes. Introducing the definition

$$\bar{\Gamma}_0 + \Gamma_1' = \bar{G}_0 \, \mathrm{Exp}\,(i\nu t) \tag{1-10}$$

where $\bar{G}_0$ is a constant complex number, the total circulation around the airfoil, $\bar{\Gamma}$, can be written

$$\bar{\Gamma} = \mathrm{Exp}\,(i\nu t)\left[\bar{G}_0 + g\int_{\ell/2}^{\infty} 2\,\frac{R+1}{R^2+1}\,\frac{R-x'}{x'-1}\,\mathrm{Exp}\,(-i\nu\, x/U_\infty)\,d\left(\frac{2\pi x}{s}\right)\right] \tag{1-11}$$

Since the wake vorticity is produced by the change of circulation around the airfoil, the increment of circulation, $(d\bar{\Gamma}/dt)\,dt$, must be equal and opposite to the circulation in the wake between $x = \ell/2$ and $x = \ell/2 + U_\infty\,dt$. Consequently, the relation $d\bar{\Gamma}/dt = -\gamma_W(\ell/2)\,U_\infty$ is obtained; that is,

$$\frac{d\bar{\Gamma}}{dt} = i\nu\,\mathrm{Exp}\,(i\nu t)\left[\bar{G}_0 + g\int_{\ell/2}^{\infty} 2\,\frac{R+1}{R^2+1}\,\frac{R-x'}{x'-1}\,\mathrm{Exp}\,(-i\nu\, x/U_\infty)\,d\left(\frac{2\pi x}{s}\right)\right]$$

$$= -\gamma_W\,(\ell/2)\,U_\infty = -\frac{2\pi}{s}\,g\,\mathrm{Exp}\,(i\nu t)\,\mathrm{Exp}\,(-i\nu\,\ell/2U_\infty)U_\infty$$

The above treatment gives the correlation between $\bar{G}_0$ and g;

$$-\frac{\bar{G}_0}{g} = \left[\int_{\ell/2}^{\infty} 2\,\frac{R+1}{R^2+1}\,\frac{R-x'}{x'-1}\,\mathrm{Exp}\,(-i\nu\, x/U_\infty)\,d\left(\frac{2\pi x}{s}\right)\right] - i\,\frac{2\pi U_\infty}{\nu s}\,\mathrm{Exp}\left(-i\nu\,\frac{\ell}{2U_\infty}\right) \tag{1-12}$$

Using the relations derived from the mapping function (equation (1-1)),

$$\left.\begin{aligned} \frac{R - x'}{x' - 1} &= \frac{R + 1}{2}\left[\sqrt{\frac{\mathrm{Exp}\left(\frac{2\pi x}{s}\right) - \mathrm{Exp}\,(-\pi\sigma)}{\mathrm{Exp}\left(\frac{2\pi x}{s}\right) - \mathrm{Exp}\,(\pi\sigma)}} - 1\right] \\ \frac{(R+1)^2}{R^2 + 1} &= \frac{2}{1 + \mathrm{Exp}\,(-\pi\sigma)} \end{aligned}\right\} \qquad (1\text{-}13)$$

equation (1-12) is written

$$-\frac{\overline{G}_o}{g} = \mathrm{Exp}\,(-i\pi\omega\sigma)\left[\frac{2\,C(\omega,\sigma)}{1 + \mathrm{Exp}\,(-\pi\sigma)} - \frac{i}{\omega}\right] \qquad (1\text{-}14)$$

where

$$\omega = \frac{\nu s}{2\pi U_\infty} = \frac{fs}{U_\infty} : \text{reduced non-dimensional frequency,} \qquad (1\text{-}15)$$

$$C(\omega,\sigma) = \mathrm{Exp}\,(i\pi\omega\sigma)\int_{\ell/2}^{\infty}\left[\sqrt{\frac{\mathrm{Exp}\left(\frac{2\pi x}{s}\right) - \mathrm{Exp}\,(-\pi\sigma)}{\mathrm{Exp}\left(\frac{2\pi x}{s}\right) - \mathrm{Exp}\,(\pi\sigma)}} - 1\right]\mathrm{Exp}\left(-i\nu\frac{x}{U_\infty}\right)d\left(\frac{2\pi x}{s}\right)$$

$$= \int_0^1\left[\sqrt{\frac{1 - t\,\mathrm{Exp}\,(-2\pi\sigma)}{1 - t}} - 1\right]t^{i\omega - 1}\,dt \qquad (1\text{-}16)$$

$$= -\frac{i}{\omega}\left[\sqrt{\pi}\,\frac{\Gamma(1 + i\omega)}{\Gamma(1/2 + i\omega)} - 1\right] + \sqrt{\pi}\,\frac{\Gamma(i\omega)}{\Gamma(1/2 + i\omega)}\left\{F\left[-1/2,\ i\omega,\ 1/2 + i\omega;\ \mathrm{Exp}\,(-2\pi\sigma)\right] - 1\right\}$$

The function, $C(\omega,\sigma)$, represents the coupling effect between the wake and the airfoil and is expressed by using Gamma function, Γ (Reference 7 and 8), and Gauss's hypergeometric function, F (Reference 9), as in equation (1-16). This coupling function is illustrated in Figure 8. In the case in which the solidity of the cascade is comparatively large, say $\sigma \geqq 1.0$, the second term of $C(\omega, \sigma)$ becomes very small and the function can be approximated only by the first term;

$$C(\omega, \infty) = -\frac{i}{\omega}\left[\sqrt{\pi}\,\frac{\Gamma(1 + i\omega)}{\Gamma(1/2 + i\omega)} - 1\right] \qquad (1\text{-}17)$$

where $C(0, \infty) = \ln 4 = 1.386$.

The integrated flow field can be obtained from the above result as follows:

Upstream of Cascade - Since the total vortices included in the airfoils and wakes are invariably equal to zero (equation (1-7)), there is no induced velocity far upstream of the cascade. Hence, the vertical velocity, w_1, far

upstream of the cascade is identical to the given inlet translatory oscillation;

$$w_1 = w = \bar{w}\ \mathrm{Exp}\ (i\nu t) \tag{1-18}$$

Downstream of Cascade - The induced velocity in the y-direction at x = x downstream of the cascade, $v_2(x, y, t)$, is a function of x, y and t. To simplify the analysis, however, this induced velocity is averaged over one spacing, s, thus giving

$$\bar{v}_2(x,t) = 1/s \int_{-s/2}^{s/2} v_2(x, y, t)\, dy \tag{1-19}$$

As shown in Figure 9, an integration path enclosing the airfoil is set up extending from far upstream to x = x downstream. Using the definition of circulation, the following relation is obtained;

$$-s\,\bar{v}_2 = \bar{\Gamma}_0 + \Gamma_1 + \Gamma_1' + \int_{\ell/2}^{x} \gamma_W\, dx$$

$$= \bar{G}_0\ \mathrm{Exp}\ (i\nu t) + \Gamma_1 + \frac{i}{\omega}\, g\ \mathrm{Exp}\ (i\nu t) \left[\mathrm{Exp}\left(-i\nu \frac{x}{U_\infty}\right) - \mathrm{Exp}(-\pi\sigma) \right] \tag{1-20}$$

From equation (1-4) and (1-7) the following equation is obtained;

$$\Gamma_1' = -\frac{2R}{R^2 + 1} (\bar{\Gamma}_0 + \Gamma_1 + \Gamma_1') = -\frac{2R}{(R+1)^2} (\bar{\Gamma}_0 + \Gamma_1) \tag{1-21}$$

leading to

$$\bar{G}_0\ \mathrm{Exp}\ (i\nu t) = \bar{\Gamma}_0 - \frac{2R}{(R+1)^2} (\bar{\Gamma}_0 + \Gamma_1) = \frac{R^2 + 1}{(R+1)^2}\, \bar{\Gamma}_0 - \frac{2R}{(R+1)^2}\, \Gamma_1 \tag{1-22}$$

The first term of the above equation is given in equation (1-3), and the second term can be written as follows;

$$\Gamma_1 = g\ \mathrm{Exp}\ (i\nu t) \int_{\ell/2}^{\infty} 2\, \frac{R+1}{R^2+1}\, \frac{R - x'}{x' - 1}\, \mathrm{Exp}\left(-i\nu \frac{x}{U_\infty}\right) d\left(\frac{2\pi x}{s}\right)$$

$$= \left[\frac{\dfrac{2\,C(\omega,\sigma)}{1 + \mathrm{Exp}\,(-\pi\sigma)}}{\dfrac{2\,C(\omega,\sigma)}{1 + \mathrm{Exp}\,(-\pi\sigma)} - \dfrac{i}{\omega}} \right] \bar{G}_0\ \mathrm{Exp}\ (i\nu t) \tag{1-23}$$

Substituting equations (1-3) and (1-23) into equation (1-22), $\bar{C}_o$ can be determined:

$$\bar{G}_o = s\,[1 - \mathrm{Exp}\,(-\pi\sigma)]\,\frac{1 + i\omega\,\dfrac{2\,C\,(\omega,\sigma)}{1 + \mathrm{Exp}\,(-\pi\sigma)}}{1 + i\omega\,C\,(\omega,\sigma)}\,\bar{w} \tag{1-24}$$

Using the relations obtained in equations (1-14), (1-23) and (1-24), each term of the right hand of equation (1-20) is related to the given inlet translatory oscillation, and thus the induced velocity, $\bar{v}_2$, becomes

$$\bar{v}_2 = -\frac{1 - \mathrm{Exp}\,(-\pi\sigma)}{1 + i\omega\,C\,(\omega,\sigma)}\,\mathrm{Exp}\,[-i\nu(x - \ell/2)/U_\infty]\,\bar{w}\,\mathrm{Exp}\,(i\nu t) \tag{1-25}$$

The vertical velocity downstream of the cascade is calculated by adding the induced flow field to the given inlet translatory oscillation;

$$\begin{aligned} w_2 &= \bar{w}\,\mathrm{Exp}\,(i\nu t) + \bar{v}_2 \\ &= \bar{w}\,\mathrm{Exp}\,(i\nu t)\left\{1 - \frac{1 - \mathrm{Exp}\,(-\pi\sigma)}{1 + i\omega\,C\,(\omega,\sigma)}\,\mathrm{Exp}\,[-i\nu\,(x - \ell/2)/U_\infty]\right\} \end{aligned} \tag{1-26}$$

In the case in which the frequency of the inlet translatory oscillation approaches zero, $\omega\,C(\omega,\sigma)$ also approaches zero, and

$$w_2 = \bar{w}\,\mathrm{Exp}\,(-\pi\sigma) \tag{1-27}$$

This result, of course, agrees with the solution of the steady flow. When the solidity of the cascade is not too small ($\sigma \geqq 1.0$), equation (1-26) can be approximated as follows;

$$w_2 = \bar{w}\,\mathrm{Exp}\,(i\nu t)\left\{1 - \frac{\Gamma(1/2 + i\omega)}{\sqrt{\pi}\;\Gamma(1 + i\omega)}\,\mathrm{Exp}\,[-i\nu\,(x - \ell/2)/U_\infty]\right\} \tag{1-28}$$

This result is only good for the unsteady inlet flow with translatory oscillation.

The solution obtained in the previous derivation represents a potential flow that is irrotational. In this case, the vortices are concentrated on wake lines starting from each trailing edge, and move downstream with velocity U_∞, as shown in Figure 10. When the cascade follows another cascade, the flow downstream of the first cascade becomes the flow upstream of the second. The real outlet flow from a cascade, therefore, imposes a very complicated inlet condition to the following cascade.

To avoid these difficulties, the real outlet flow is replaced by a simplified outlet flow. The simplification is made by redistributing vortices of γ_W dx on wakes (length = dx) uniformly over the region, s by dx, as shown in Figure 10. This simplified flow is no longer irrotational; however, it has a vertical velocity that is independent of ordinate y. The mean vertical induced velocity, $\overline{v}_2$, of equation (1-25) also describes the vertical velocity of the simplified flow, which is nothing but the sinusoidal gust oscillation.

Flow Around a Cascade of Nonstaggered Flat Plates for Inlet Flows with Sinusoidal Gust Oscillation

Flow Configuration - The inlet flow has a vertical sinusoidal gust oscillation, $w = \tilde{w}\ \mathrm{Exp}\ [i\nu(t - x/U_\infty)]$, propagating with the main through-flow U_∞. The unsteady circulation, $\tilde{\Gamma}$, around the airfoil is divided into three parts, $\tilde{\Gamma} = \tilde{\Gamma}_0 + \Gamma_1 + \Gamma_1'$, as shown in Figure 11. The flow with circulation $\tilde{\Gamma}_0$ induces the downwash which cancels the given inlet sinusoidal gust on the airfoil so that the surface of the airfoil becomes a part of the instantaneous stream line. The flow with circulation Γ_1 and Γ_1' cancels the induced flow by vortices in the wakes and, therefore, has the same relations as in the case of the translatory oscillation.

Determination of $\tilde{\Gamma}_0$ - As shown in Figure 12, the flow in the physical plane is conformally transformed into a unit circle in the z'-plane using the mapping function (equation (1-1)). To obtain a sinusoidal downwash opposite to the gust on the airfoil, a more complicated distribution of vortices in the z'-plane is necessary than in the case of a uniform downwash. A circulation distribution, $\gamma(\theta)$, in the form of

$$\gamma(\theta) = \sum_{n=1}^{\infty} A_n \cos n\theta \qquad (1\text{-}29)$$

is located on the unit circle. The Fourier coefficients, $A_1, A_2, \ldots$, will be determined so that the induced velocity on the airfoil is opposite to the given inlet gust. Since the sum of the distributed circulation, $\int_0^{2\pi} \gamma(\theta)\, d\theta$, is equal to zero, the circulation distribution produces no circulatory flow around the airfoil as a whole.

An additional circulation is superimposed on the flow by locating $\tilde{\Gamma}_0/2$ at $z' = \pm\ 1/R$ and $-\tilde{\Gamma}_0/2$ at $z' = \pm\ R$ to satisfy the Kutta-Joukowski theorem at the trailing edge.

The velocity (u', v') induced by the circulation distribution $\gamma(\theta)$ at $z' = 1$ is

$$(u' - iv')_{z'=1} = \frac{i}{2\pi} \sum_{n=1}^{\infty} \int_0^{2\pi} \frac{A_n \cos n\theta}{1 - \mathrm{Exp}\ (i\theta)}\, d\theta$$

Since the integrand becomes infinity at $z' = 1$ ($\theta = 0$), this integration is carried out along the path shown in Figure 13 and gives

$$(u' - iv')_{z'=1} = \lim_{\epsilon \to 0} \left[\underbrace{\frac{i}{2\pi} \sum_{n=1}^{\infty} \int_{\epsilon}^{2\pi-\epsilon} \frac{A_n \cos n\theta}{1 - \mathrm{Exp}(i\theta)} \, d\theta}_{\text{the above} = 0} + \frac{i}{2\pi} \sum_{n=1}^{\infty} A_n \int_{-\epsilon}^{+\epsilon} \frac{d\theta}{1 - \mathrm{Exp}(i\theta)} \right] = i \frac{\sum_{n=1}^{\infty} A_n}{2} \tag{1-30}$$

Hence, the induced velocity at $z' = 1$,

$$u' = 0, \quad v' = -\frac{\sum_{n=1}^{\infty} A_n}{2}$$

must be canceled by the proper circulatory flow, and this necessarily leads to the result

$$\tilde{\Gamma}_0 = -\pi \frac{R^2 - 1}{R^2 + 1} \sum_{n=1}^{\infty} A_n = -\pi \, \mathrm{sech}(\pi\sigma/2) \sum_{n=1}^{\infty} A_n \tag{1-31}$$

The velocity induced by the circulation $\gamma(\theta)$ at an arbitrary point on the unit circle, $z' = \mathrm{Exp}(i\theta_0)$, is written as follows;

$$(u' - iv')_{z'} = \lim_{\epsilon \to 0} \left[\frac{i}{2\pi} \sum_{n=1}^{\infty} \int_{\theta_0+\epsilon}^{\theta_0+2\pi-\epsilon} \frac{A_n \cos n\theta}{\mathrm{Exp}(i\theta_0) - \mathrm{Exp}(i\theta)} \, d\theta + \frac{i}{2\pi} \sum_{n=1}^{\infty} A_n \cos n\theta_0 \int_{\theta_0-\epsilon}^{\theta_0+\epsilon} \frac{d\theta}{\mathrm{Exp}(i\theta_0) - \mathrm{Exp}(i\theta)} \right]$$

$$= \frac{i}{2} \mathrm{Exp}(-i\theta_0) \sum_{n=1}^{\infty} A_n \mathrm{Exp}(-in\theta_0) \tag{1-32}$$

The velocity field (u, v) in the z-plane can be calculated from the velocity in the z'-plane using the relation

$$(u - iv) = (u' - iv') \frac{dz'}{dz} \tag{1-33}$$

where $\frac{dz'}{dz}$ is derived from the mapping function (equation (1-1));

$$\left(\frac{dz'}{dz}\right)_{z'=\mathrm{Exp}\,(i\theta_0)} = \frac{2\pi}{s} \frac{\left[R^2 - \mathrm{Exp}\,(2i\theta_0)\right]\left[\mathrm{Exp}\,(2i\theta_0) - 1/R^2\right]}{2\,(R + 1/R)\left[\mathrm{Exp}\,(2i\theta_0) - 1\right]} \tag{1-34}$$

Substituting equations (1-32) and (1-34) into equation (1-33), the expression is obtained for the induced velocity in the z-plane;

$$u - iv = \frac{2\pi}{s} \frac{(R + 1/R)^2 - 4\cos^2\theta}{8\,(R + 1/R)\sin\theta} \sum_{n=1}^{\infty} A_n\,\mathrm{Exp}\,(-in\theta) \tag{1-35}$$

or

$$v = \frac{2\pi}{s} \frac{(R + 1/R)^2 - 4\cos^2\theta}{8\,(R + 1/R)\sin\theta} \sum_{n=1}^{\infty} A_n \sin n\theta \tag{1-36}$$

at a point on the airfoil corresponding to $z' = \mathrm{Exp}\,(i\theta)$ in the z'-plane. In the previous derivation, all of the Fourier coefficients are confined to real numbers. If not, the horizontal induced velocity, u', at $z' = 1$ can take a certain finite value that cannot be canceled by adding circulatory flow around the airfoil, and the Kutta-Joukowski condition cannot be satisfied.

Next, the complex Fourier coefficients, A_n, are introduced and replace the real coefficients, A_n, in equation (1-36) with the real part of $A_n\,\mathrm{Exp}\,(i\nu t)$;

$$v = \frac{2\pi}{s} \frac{(R + 1/R)^2 - 4\cos^2\theta}{8\,(R + 1/R)\sin\theta} \sum_{n=1}^{\infty} A_n\,\mathrm{Exp}\,(i\nu t)\sin n\theta \tag{1-37}$$

Since the circulatory flow around the airfoil with circulation $\tilde{\Gamma}_0$ induces no vertical velocity component on the airfoil, equation (1-37) describes the total vertical component. To satisfy the boundary conditions on the airfoil, the vertical induced velocity must be equal and opposite to the given inlet gust. Thus,

$$v + w = v + \tilde{w}\,\mathrm{Exp}\,(i\nu t)\,\mathrm{Exp}\,(-i\nu\, x/U_\infty) = 0 \tag{1-38}$$

Substituting equation (1-37) into equation (1-38), the following equation is obtained;

$$\sum_{n=1}^{\infty} A_n \sin n\theta = -\frac{s}{2\pi} \frac{8\,(R + 1/R)\sin\theta}{(R + 1/R)^2 - 4\cos^2\theta}\,\tilde{w}\,\mathrm{Exp}\left(-i\nu\,\frac{x}{U_\infty}\right) \equiv f(\theta) \tag{1-39}$$

Since the above function, $f(\theta)$, is symmetrical about $\theta = \pi$, the function can be expressed only by a sine series. The Fourier coefficients, $A_1, A_2, \ldots,$ are determined by

$$A_n = 1/\pi \int_0^{2\pi} f(\theta) \sin n\theta \, d\theta \tag{1-40}$$

Hence, the sum of the Fourier coefficients is

$$\sum_{n=1}^{\infty} A_n = 1/\pi \sum_{n=1}^{\infty} \int_0^{2\pi} f(\theta) \sin n\theta \, d\theta \tag{1-41}$$

Using integration by parts, the following equation is obtained;

$$\sum_{n=1}^{\infty} A_n = -\, 1/\pi \sum_{n=1}^{\infty} \underbrace{\left| f(\theta) \frac{\cos n\theta}{n} \right|_0^{2\pi}}_{\text{the above} = 0} + 1/\pi \int_0^{2\pi} f'(\theta) \sum_{n=1}^{\infty} \frac{\cos n\theta}{n} \, d\theta$$

The relation,

$$\sum_{n=1}^{\infty} \frac{\cos n\theta}{n} = -\ln (2 \sin \theta/2), \text{ for } 0 < \theta < 2\pi$$

leads further to the following expression;

$$\sum_{n=1}^{\infty} A_n = -\, 1/\pi \int_0^{2\pi} f'(\theta) \ln (2 \sin \theta/2) \, d\theta$$

$$= -\, 1/\pi \underbrace{\left| f(\theta) \ln (2 \sin \theta/2) \right|_0^{2\pi}}_{\text{the above} = 0} + 1/2\pi \int_0^{2\pi} f(\theta) \cot (\theta/2) \, d\theta$$

This integral will be finally conducted in the z-plane after being transformed by the following relations;

$$-\frac{s}{2\pi} \frac{4(R + 1/R) \sin \theta}{(R + 1/R)^2 - 4\cos^2\theta} \, d\theta = dx,$$

$$\cot \theta/2 = \text{Exp } (\pi\sigma/2) \sqrt{\frac{\text{Exp } \left(\frac{2\pi x}{s}\right) - \text{Exp } (-\pi\sigma)}{\text{Exp } (\pi\sigma) - \text{Exp } \left(\frac{2\pi x}{s}\right)}}$$

The result is

$$\sum_{n=1}^{\infty} A_n = -\frac{s}{\pi} \operatorname{Exp}(-\pi\sigma/2)\left[\operatorname{Exp}(\pi\sigma) - \operatorname{Exp}(-\pi\sigma)\right] \operatorname{Exp}(-i\pi\omega\sigma)\, S(\omega,\sigma)\, \tilde{w} \tag{1-42}$$

where

$$S(\omega,\sigma) = \frac{1}{\pi} \frac{\operatorname{Exp}(\pi\sigma)}{\operatorname{Exp}(\pi\sigma) - \operatorname{Exp}(-\pi\sigma)} \operatorname{Exp}(i\pi\omega\sigma)$$

$$\int_{x=-\ell/2}^{\ell/2} \operatorname{Exp}\left(-i\nu \frac{x}{U_\infty}\right) \sqrt{\frac{\operatorname{Exp}\left(\frac{2\pi x}{s}\right) - \operatorname{Exp}(-\pi\sigma)}{\operatorname{Exp}(\pi\sigma) - \operatorname{Exp}\left(\frac{2\pi x}{s}\right)}}\; d\left(\frac{2\pi x}{s}\right)$$

$$= 1/\pi \int_0^1 \sqrt{\frac{t}{1-t}} \left(\frac{1+B}{t+B}\right)^{1+i\omega} dt,$$

$$B = 1/\left[\operatorname{Exp}(2\pi\sigma) - 1\right]$$

The sinusoidal gust function, $S(\omega,\sigma)$, can be calculated by expanding the integrand into a power series of t, and is written as follows;

$$S(\omega,\sigma) = \frac{1}{2} F\left[1/2,\ 1+i\omega,\ 2;\ 1 - \operatorname{Exp}(-2\pi\sigma)\right] \tag{1-43}$$

$$= \frac{\tanh(\pi\omega)}{\sqrt{\pi}\ \omega} \frac{\Gamma(1+i\omega)}{\Gamma(1/2+i\omega)} F\left[1/2,\ 1+i\omega,\ 1/2+i\omega;\ \operatorname{Exp}(-2\pi\sigma)\right]$$

$$- \frac{\operatorname{Exp}(-\pi\sigma)\operatorname{Exp}(2i\pi\omega\sigma)}{\sqrt{\pi}\,(1-2i\omega)} \frac{\Gamma(1/2+i\omega)}{\Gamma(1+i\omega)} F\left[3/2,\ 1-i\omega,\ 3/2-i\omega;\ \operatorname{Exp}(-2\pi\sigma)\right]$$

This function is illustrated in Figure 14. As seen from equation (1-43), $S(\omega,\sigma)$ oscillates slightly with the reduced frequency ω, since it contains a periodic term, $\operatorname{Exp}(2i\pi\omega\sigma)$. When the solidity of the cascade is not too small, this oscillation is not essential. In the case in which the solidity is comparatively large, this function can be approximated by

$$S(\omega,\infty) = \frac{1}{2} F(1/2,\ 1+i\omega,\ 2;\ 1) = \frac{\tanh(\pi\omega)}{\sqrt{\pi}\ \omega} \frac{\Gamma(1+i\omega)}{\Gamma(1/2+i\omega)} \tag{1-44}$$

$$= \text{complex conjugate of } \frac{1}{1 + i\omega\, C(\omega,\infty)}$$

In the limiting case of $\omega = 0$, the function becomes

$$S(0, \sigma) = \frac{1}{1 + \text{Exp}(-\pi\sigma)} \tag{1-45}$$

By substituting the real part of $\sum_{n=1}^{\infty} A_n \text{ Exp } (i\nu t)$ into equation (1-31), the circulation around the airfoil is found to be

$$\tilde{\Gamma}_0 = 2s\,[1 - \text{Exp}(-\pi\sigma)]\,\text{Exp}(-i\pi\omega\sigma)\,S(\omega, \sigma)\,\tilde{w}\,\text{Exp}(i\nu t) \tag{1-46}$$

Unsteady Solution for Sinusoidal Gust Oscillation - As illustrated in Figure 11, the total circulation, $\tilde{\Gamma}$, around the airfoil consists of $\tilde{\Gamma}_0$, Γ_1 and Γ_1'. Since the total circulation of the system remains invariably zero,

$$\tilde{\Gamma}_0 + \int_{\ell/2}^{\infty} \gamma_W \, dx = \tilde{\Gamma}_0 + \Gamma_1 + \Gamma_1' + \Gamma_W = 0$$

An analysis similar to that leading to equation (1-14) yields the expression

$$-\frac{\tilde{G}_o}{g} = \text{Exp}(-i\pi\omega\sigma)\left[\frac{2\,C(\omega, \sigma)}{1 + \text{Exp}(-\pi\sigma)} - \frac{i}{\omega}\right]$$

where

$$\tilde{G}_o \text{ Exp } (i\nu t) = \tilde{\Gamma}_0 + \Gamma_1' ,$$

$$\gamma_W = \frac{2\pi}{s} g \text{ Exp } [i\nu\,(t - x/U_\infty)]$$

The integrated flow field for a given inlet sinusoidal gust oscillation, $w = \tilde{w}\ \text{Exp}(i\nu t)\ \text{Exp}(-i\nu\, x/U_\infty)$, can be obtained as follows:

Upstream of Cascade - Since the total vortices included in the airfoils and wakes are equal to zero, there is no induced velocity at a sufficient distance upstream of the cascade. Therefore, the vertical velocity, w_1, far upstream is equal to the given inlet sinusoidal gust oscillation;

$$w_1 = w = \tilde{w}\ \text{Exp}(i\nu t)\ \text{Exp}(-i\nu\, x/U_\infty) \tag{1-47}$$

Downstream of Cascade - The induced velocity, $\tilde{v}_2$, at x = x downstream of the cascade is determined in a manner similar to the case of translatory oscillation;

$$- s\,\tilde{v}_2 = \tilde{\Gamma}_0 + \Gamma_1 + \Gamma_1' + \int_{\ell/2}^{x} \gamma_W \, dx \tag{1-48}$$

$$= \tilde{G}_o \, \mathrm{Exp}\,(i\nu t) + \Gamma_1 + \frac{i}{\omega} \, g \, \mathrm{Exp}\,(i\nu t) \left[\mathrm{Exp}\,(-i\nu \, x/U_\infty) - \mathrm{Exp}\,(-\pi\sigma) \right]$$

Further,

$$\tilde{G}_o \, \mathrm{Exp}\,(i\nu t) = \frac{R^2 + 1}{(R+1)^2} \, \tilde{\Gamma}_0 - \frac{2R}{(R+1)^2} \, \Gamma_1 \tag{1-49}$$

where

$$\tilde{\Gamma}_0 = 2 \, s \left[1 - \mathrm{Exp}\,(-\pi\sigma) \right] \mathrm{Exp}\,(-i\pi\omega\sigma) \, S\,(\omega, \sigma) \, \tilde{w} \, \mathrm{Exp}\,(i\nu t),$$

$$\Gamma_1 = \left[\frac{\dfrac{2\,C\,(\omega,\sigma)}{1 + \mathrm{Exp}\,(-\pi\sigma)}}{\dfrac{2\,C\,(\omega,\sigma)}{1 + \mathrm{Exp}\,(-\pi\sigma)} - \dfrac{i}{\omega}} \right] \tilde{G}_o \, \mathrm{Exp}\,(i\nu t)$$

From the above,

$$\tilde{G}_o = s \left[1 - \mathrm{Exp}\,(-2\pi\sigma) \right] \mathrm{Exp}\,(-i\pi\omega\sigma) \, S\,(\omega, \sigma) \, \frac{1 + i\omega \dfrac{2\,C\,(\omega,\sigma)}{1 + \mathrm{Exp}\,(-\pi\sigma)}}{1 + i\omega\, C\,(\omega, \sigma)} \, \tilde{w} \tag{1-50}$$

Each term of equation (1-48) can be expressed in terms of the given inlet sinusoidal gust oscillation, and the induced velocity, $\tilde{v}_2$, becomes

$$\tilde{v}_2 = - \left[1 - \mathrm{Exp}\,(-2\pi\sigma) \right] \frac{S(\omega, \sigma)}{1 + i\omega\, C\,(\omega, \sigma)} \, \tilde{w} \, \mathrm{Exp}\,(i\nu t) \, \mathrm{Exp}\,(-i\nu \, x/U_\infty) \tag{1-51}$$

where $\tilde{v}_2$ represents the mean value on one spacing, s. Finally, the vertical velocity downstream of the cascade is

$$w_2 = \tilde{w} \, \mathrm{Exp}\,(i\nu t) \, \mathrm{Exp}\,(-i\nu \, x/U_\infty) + \tilde{v}_2 \tag{1-52}$$

$$= \tilde{w} \, \mathrm{Exp}\,(i\nu t) \, \mathrm{Exp}(-i\nu \, x/U_\infty) \left\{ 1 - \left[1 - \mathrm{Exp}\,(-2\pi\sigma) \right] \frac{S\,(\omega, \sigma)}{1 + i\omega \, C\,(\omega, \sigma)} \right\}$$

For a comparatively large value of solidity ($\sigma \geqq 1.0$), equation (1-52) can be approximated by

$$w_2 = \tilde{w}\ \mathrm{Exp}\ (i\nu t)\ \mathrm{Exp}\ (-i\nu\ x/U_\infty) \left[1 - \frac{\tanh\ (\pi\omega)}{\pi\omega}\right] \tag{1-53}$$

When $\omega = 0$, $\omega C\,(0, \sigma) = 0$ and $S\,(0, \sigma) = [1 + \mathrm{Exp}\ (-\pi\sigma)]^{-1}$, thus $w_2 = \tilde{w}\ \mathrm{Exp}\ (-\pi\sigma)$. This result agrees with the solution for steady flow. The above result gives the unsteady flow solution only for an inlet flow with sinusoidal gust oscillation. If the inlet flow has combined translatory and sinusoidal gust oscillation, the solution can be obtained by superimposing both flow fields.

When the inlet flow oscillates periodically, the lift acting on the airfoil also oscillates periodically. This unsteady lift is calculated for both translatory and sinusoidal gust oscillation, and is given in the Appendix of Reference 10.

Solution for a Cascade with an Arbitrary Stagger Angle

Flow Approximation and its Accuracy - The dynamic property of a cascade having an arbitrary stagger angle are analyzed. Since the exact solution for this case can be expressed only with impractical mathematical complexity, an approximate method is adopted. Flow through a staggered cascade of flat plates, as shown in Figure 15 (a), is considered. The inlet flow is a superposition of through-flow, U_∞, in the direction of the flat plate (x-axis) and a translatory or sinusoidal gust oscillation in the direction of the cascade. First, the flow fields through nonstaggered and staggered cascades having the same solidity are compared (Figure 16). Both inlet flows are assumed to be steady and have the same through-flow, U_∞, and the same w in the cascade direction.

The influence coefficient, κ, of the staggered cascade (Reference 4) is

$$\kappa = \frac{\Gamma\sigma}{\Gamma\sigma = 0} = \frac{4s}{\pi\ell} \frac{R}{R^2 + 1} \frac{\cos\ \theta_T}{\cos\ \lambda} \tag{1-54}$$

where R and θ_T are characteristic numbers included in the mapping function that transforms a staggered cascade into a unit circle in the z'-plane, as illustrated in Figure 15 (b). R and θ_T are determined by solving the following equations simultaneously;

$$\left.\begin{aligned} \sigma = \ell/s = 1/\pi \Bigg(&\cos\ \lambda \ln \frac{R^2 + 2R\cos\ \theta_T + 1}{R^2 - 2R\cos\ \theta_T + 1} \\ &+ 2\sin\ \lambda \tan^{-1} \frac{2R\sin\ \theta_T}{R^2 - 1}\Bigg) \\ \tan\ \theta_T = \frac{R^2 - 1}{R^2 + 1} &\tan\ \lambda \end{aligned}\right\} \tag{1-55}$$

The ratio of the circulation of staggered and nonstaggered cascades is written

$$\frac{\Gamma}{\Gamma_{\lambda=0}} = \frac{\Gamma/\Gamma_{\sigma=0}}{\Gamma_{\lambda=0}/\Gamma_{\lambda,\sigma=0}} \quad \frac{\Gamma_{\sigma=0}}{\Gamma_{\lambda,\sigma=0}} = \frac{\kappa}{\kappa_{\lambda=0}} \frac{\Gamma_{\sigma=0}}{\Gamma_{\lambda,\sigma=0}} \tag{1-56}$$

Since $\Gamma_{\sigma=0}/\Gamma_{\lambda,\sigma=0}$ indicates the circulation ratio of the isolated airfoil, this ratio is proportional to the vertical velocity component in the y-direction, and thus,

$$\frac{\Gamma_{\sigma=0}}{\Gamma_{\lambda,\sigma=0}} = \frac{w \cos\lambda}{w} = \cos\lambda \tag{1-57}$$

From equation (1-54), (1-56) and (1-57),

$$\frac{\Gamma}{\Gamma_{\lambda=0}} = \frac{\frac{R}{R^2+1}\cos\theta_T}{\left(\frac{R}{R^2+1}\right)_{\lambda=0}} = \text{function of } (\sigma, \lambda) \tag{1-58}$$

Figure 17 shows the numerical values of equation (1-58). Note that the circulation ratio remains close to unity if the solidity, σ, does not become too small. From the definition, $\bar{\Gamma}_0/(\bar{\Gamma}_0)_{\lambda=0}$ and $\Gamma_1'/(\Gamma_1')_{\lambda=0}$ are exactly the same as $\Gamma/\Gamma_{\lambda=0}$ of equation (1-58) and are approximately unity. Through a similar comparison it can also be concluded that $\tilde{\Gamma}_0/(\tilde{\Gamma}_0)_{\lambda=0}$ and $\Gamma_1/(\Gamma_1)_{\lambda=0}$ remain close to unity if the solidity, σ, does not become too small. The above comparison shows that the result obtained for a nonstaggered cascade can also be applied to a staggered cascade with reasonable accuracy, provided that the unsteady flow component in the direction of cascade is the same for both cascades.

This approximation is, of course, not sufficiently accurate for determining the steady flow solution. However, since we are mainly interested in the dynamic characteristics of cascades, this approximate method seems to be reasonable.

Results

Translatory Oscillation Case

At a sufficient distance upstream of the cascade;

U_∞ in the x-direction,

$w_1 = \bar{w}\ \mathrm{Exp}\ (i\nu t)$ in the cascade direction.

Downstream of the cascade;

U_∞ in the x-direction,

$$w_2 = \bar{\bar{w}} \text{ Exp } (i\nu t) \left\{1 - \frac{[1 - \text{Exp } (-\pi\sigma)]}{1 + i\omega\, C\,(\omega, \sigma)} \text{ Exp } \left[-i \frac{\nu}{U_\infty} (x - y \tan \lambda - \frac{\ell}{2})\right]\right\} \quad (1\text{-}59)$$

in the cascade direction, where

$$\omega = \frac{\nu s}{2\pi U_\infty} = \frac{\nu s}{2\pi V_a} \cos \lambda$$

Sinusoidal Gust Oscillation Case

At a sufficient distance upstream of the cascade;

U_∞ in the x-direction,

$w_1 = \tilde{\bar{w}} \text{ Exp } (i\nu t) \text{ Exp } \left[-i \frac{\nu}{U_\infty} (x - y \tan \lambda)\right]$ in the cascade direction.

Downstream of the Cascade

U_∞ in the x-direction,

$$w_2 = \tilde{\bar{w}} \text{ Exp } (i\nu t) \text{ Exp } \left[-i \frac{\nu}{U_\infty} (x - y \tan \lambda)\right] \left\{1 - \frac{[1 - \text{Exp } (-2\pi\sigma)]\ S\,(\omega, \sigma)}{1 + i\omega\, C\,(\omega, \sigma)}\right\} \quad (1\text{-}60)$$

in the cascade direction

SECTION II. ANALYTICAL STUDY OF DYNAMIC CHARACTERISTICS OF TURBOPUMPS

Using the results obtained in the previous Section, a theoretical analysis was performed to determine the relationship between pressure rise and flow rate through a turbopump when the flow rate fluctuates periodically around its mean value at a constant frequency and while the rotational speed of the turbopump is constant.

There is a wide variety of principles of turbopump construction ranging from the single-stage axial flow pump to the multi-stage centrifugal pump. Since the working principle of the axial flow pump is based purely on the performance of a linear cascade, the axial flow pump offers the most fundamental case for theoretical application. Therefore, a method for determining the dynamic characteristics of a single-stage axial flow pump is described first. This method serves as an example of the theoretical approach for determining the dynamic characteristics of an arbitrary turbopump. A simple method is also derived for the case when approximate dynamic characteristics are sufficient. This method determines the dynamic characteristics without entering into the details of pump design.

In these analyses, the flow was assumed to be incompressible and inviscid. The effect of eventual cavitation in the pumps is not considered.

Dynamic Characteristics of a Single-Stage Axial Flow Pump

Pressure Difference Due to Oscillating Through-Flow in Conduit - The analysis was conducted on the axial flow pump illustrated in Figure 18. This pump has only one stage consisting of a rotating blade row (rotor) and a following stationary blade row (stator). The rotor is driven by a prime mover at a constant rotational speed, n. The flow rate through the pump, Q, is assumed to fluctuate periodically with a frequency, f, around its mean value, Q_o. Assuming also the sinusoidal fluctuation, the instantaneous flow rate is

$$Q(t) = Q_o + \Delta Q \, \mathrm{Exp}\,(i\nu t), \tag{2-1}$$

$$\nu = 2\pi f$$

where the physical meaning of a complex number is attributed only to its real part.

In the actual pump, the flow pattern around the rotor and stator varies with radius, r. For the calculation of dynamic characteristics, however, a representative radius, r_m, is chosen for the analysis as shown below;

$$r_m = \sqrt{\frac{r_t^2 + r_h^2}{2}} \tag{2-2}$$

where r_t and r_h are outer and inner radii of annular passage. This representative radius has been used often for the analysis of steady-state characteristics and has proved to give good results (Reference 11).

By developing the cylindrical flow surface of radius r_m into a plane, a two-dimensional flow is obtained as shown in Figure 19, where the rotor cascade moves straight in the cascade direction with a constant velocity, $u = 2\pi n r_m$.

Since an incompressible, two-dimensional flow is assumed, the axial velocity, V_a, remains constant upstream and downstream of the rotor and stator.

The flow pattern of an axial flow pump is in most cases the free vortex type, especially when the pump is not provided with inlet guide vanes as illustrated in Figure 18.

The free vortex type flow pattern assures the constant axial velocity over the entire radius, and thus

$$V_a(t) = \frac{Q(t)}{\pi(r_t^2 - r_h^2)} = V_{ao} + \Delta V_a \, \mathrm{Exp}\,(i\nu t) \tag{2-3}$$

where

$$V_{ao} = \frac{Q_o}{\pi(r_t^2 - r_h^2)} \quad , \quad \Delta V_a = \frac{\Delta Q}{\pi(r_t^2 - r_h^2)}$$

The mean velocity triangle at each station is illustrated in Figure 19.

The pressure difference between the delivery and suction ports of the pump, $(p_d - p_s)$, oscillates periodically corresponding to the fluctuating flow rate. As the first step, the pressure difference will be calculated when there are no cascades between suction and delivery ports. This case represents an oscillating flow in a conduit with varying sectional area as shown in Figure 20. If only one-dimensional flow in the conduit is assumed, the velocity in the conduit, V(X, t) is

$$V(X,\ t) = \frac{Q(t)}{A(X)} = \frac{Q_o}{A(X)} + \frac{\Delta Q}{A(X)} \, \mathrm{Exp}\,(i\nu t) \tag{2-4}$$

where A(X) is the sectional area at distance X downstream of the suction reference point.

The pressure gradient, $\partial p/\partial X$, in the conduit can be calculated by substituting equation (2-4) into the equation of motion for a non-viscous, incompressible fluid

$$-\frac{1}{\rho}\frac{\partial p}{\partial X} = \frac{\partial V}{\partial t} + V\frac{\partial V}{\partial X} \tag{2-5}$$

In the usual design practice, the change rate of sectional area, $\partial A(X)/\partial X$, is made as small as possible to reduce fluid losses, and this results in a small change rate of through-flow velocity, $\partial V/\partial X$.

From the above, the first term of equation (2-5) is predominantly larger than the second term, and consequently

$$\frac{\partial p}{\partial X} = - \rho \frac{\partial V}{\partial t} = - \rho i\nu \frac{\Delta Q}{A(X)} \text{Exp}\,(i\nu t)$$

By integrating the above pressure gradient from the suction port to the delivery port,

$$p_d - p_s = - \rho i\nu \text{Exp}\,(i\nu t) \frac{\Delta Q}{A_o} \int_{X=0}^{L} \frac{A_o}{A(X)}\, dX$$

$$= - \rho i\nu \Delta V_a L_{eq} \text{Exp}\,(i\nu t) \qquad (2\text{-}6)$$

where

$A_o = \pi(r_t^2 - r_h^2)$: area of annular passage,

$$L_{eq} = \int_{X=0}^{L} \frac{A_o}{A(X)}\, dX \quad : \text{ equivalent length.}$$

The above pressure difference occurs independently of pumping action and is regarded as an inherent property of the conduit.

The dimensionless pressure difference, h_C, indicating the conduit effect is thus

$$h_C = \frac{(p_d - p_s)_C}{\frac{\rho}{2} u^2} = - 2i\nu \frac{\Delta V_a}{u} \frac{L_{eq}}{u} \text{Exp}\,(i\nu t)$$

$$= - 2i\omega \frac{L_{eq}}{r_m} \frac{\Delta Q}{Q_o} \phi \text{Exp}\,(i\nu t) \qquad (2\text{-}7)$$

where

$\omega = \frac{\nu r_m}{u} = \frac{f}{n}$: reduced frequency of pump,

$\phi = \frac{V_{ao}}{u}$: flow coefficient.

As seen from equation (2-7), h_C always varies with 90° delay to the fluctuation of flow rate throughout the entire frequency range, and the magnitude is proportional to the frequency, f, at a constant fluctuation ratio, $\Delta Q/Q_o$.

Change of Pressure Rise Through Rotor - The rotor cascade consists of arbitrary airfoils arranged with arbitrary spacing and stagger angle as indicated by a broken line in Figure 21. This cascade is then substituted by a cascade of flat plates that have the same chord length as that of the airfoil and are located parallel to the zero-lift inlet direction of the original airfoils in the cascade.

The absolute inlet velocity into the rotor has no component in the cascade direction and has only the axial component $V_a = V_{ao} + \Delta V_a \text{ Exp } (i\nu t)$, which oscillates periodically.

The relative inlet velocity, W, into the rotor is obtained by superimposing axial velocity on the constant peripheral velocity, u, vectorially.

It is now assumed that the flow field corresponding to the mean steady inlet flow, W_{10}, has been solved already by an appropriate method (Reference 12 and 13), and that the mean pressure rise through the rotor has been determined from this flow field. The deviation of pressure rise from its mean value is determined below.

The unsteady axial component, $\Delta V_a \text{ Exp } (i\nu t)$, upstream of rotor is divided into two components, $\Delta V_a \sec \lambda_R \text{ Exp } (i\nu t)$, in the direction parallel to the flat plate, and $\bar{w}_1 = -\Delta V_a \tan \lambda_R \text{ Exp } (i\nu t)$, in the cascade direction where λ_R is the stagger angle of the simplified rotor cascade.

The component, $\Delta V_a \sec \lambda_R \text{ Exp } (i\nu t)$, which is parallel to the zero-lift direction of the original cascade, induces no circulation around airfoils and thus passes through without causing any change of flow field. On the other hand, $\bar{w}_1$ in the cascade direction represents a translatory oscillation of inlet flow and induces a fluctuating circulation around the airfoils.

The solution for this case is already obtained in Section I as follows: For upstream of rotor,

$$\bar{w}_1 = \bar{w} \text{ Exp } (i\nu t)$$

where

$$\bar{w} = -\Delta V_a \tan \lambda_R \tag{2-8}$$

For downstream of rotor,

$$\bar{w}_2 = \bar{w}_1 + \bar{v}_2 \tag{2-9}$$

where

$$\bar{v}_2 = \Delta V_a \tan \lambda_R \frac{1 - \mathrm{Exp}(-\pi\sigma_R)}{1 + i\omega_R\, C(\omega_R, \sigma_R)} \mathrm{Exp}(i\nu t)\, \mathrm{Exp}\left[-i\nu(X - \frac{\ell_R}{2}\cos\lambda_R)/V_{ao}\right],$$

$$\omega_R = \frac{\nu s_R}{2\pi U_\infty} = \frac{\cos\lambda_R}{N_R\,\phi}\,\omega$$

In the above relation, s_R is the spacing of the rotor cascade and N_R is the number of rotor blades. The coordinate systems, (x, y) and (X, Y), are illustrated in Figure 21.

The flow field downstream of the rotor cascade is obtained by superimposing $\Delta V_a \sec \lambda_R \mathrm{Exp}(i\nu t)$ in the x-direction and $\bar{w}_2$ of equation (2-9) in the Y-direction. The superposition of $\Delta V_a \sec \lambda_R \mathrm{Exp}(i\nu t)$ and the first term of equation (2-9) produces a simple oscillating flow, $\Delta V_a \mathrm{Exp}(i\nu t)$, in the axial direction that is equal to the given inlet unsteady condition. The disturbance induced by the rotor cascade exists only in the second term of equation (2-9). The flow field downstream of the rotor is, therefore, the superposition of the mean flow, W_{20} (steady); axial oscillation, $\Delta V_a \mathrm{Exp}(i\nu t)$; and the induced disturbance, $\bar{v}_2$, in the cascade direction as illustrated in Figure 21. The associated pressure change is calculated from this flow field.

The basic equation for determining the pressure of incompressible, potential flow is

$$\frac{p}{\rho} + \frac{\partial\Phi}{\partial t} + \Omega + \frac{1}{2}V^2 = F(t) \qquad (2\text{-}10)$$

where

- Φ velocity potential
- Ω potential due to gravity
- V resultant velocity of fluid
- F arbitrary function to fit initial condition

The gravitational potential, Ω, produces merely the hydrostatic pressure field. Therefore, the potential, Ω, is omitted hereafter by considering the difference of real pressure and hydrostatic pressure.

To calculate the pressure by equation (2-10), it is necessary to determine the so-called "impulsive pressure, $\rho(\partial\Phi/\partial t)$." Since the velocity potential of the mean steady flow is also steady with respect to time and does not contribute to impulsive pressure, only the velocity potential of unsteady flow is significant.

The unsteady velocity potential is divided into three parts; Φ_1 is due to through flow, Φ_2 is due to vertical translatory flow, and Φ_3 is due to induced flow as shown in Figure 22 (a), (b) and (c).

The superimposition of through-flow and vertical translatory flow gives the oscillating flow in the axial direction. Using the X, Y coordinate system shown in Figure 21,

$u = \Delta V_a \text{ Exp } (i\nu t)$ in X-direction

$v = 0$ in Y-direction

and thus,

$$\Phi_1 + \Phi_2 = \Delta V_a \text{ X Exp } (i\nu t)$$

Differentiating the velocity potential as to time, the impulsive pressure is

$$\rho \frac{\partial(\Phi_1 + \Phi_2)}{\partial t} = \rho i\nu \, \Delta V_a \text{ X Exp } (i\nu t)$$

This impulsive pressure results in the same pressure difference given by equation (2-6), and was already taken into account as a part of h_C in equation (2-7). Therefore, the contribution of Φ_1 and Φ_2 to the impulsive pressure need not be considered again.

The flow corresponding to Φ_3 is induced by vortices in the airfoils as well as in the wakes and has the velocity and pressure distribution that are a function of X, Y, and t downstream of the cascade. However, as far as this real downstream flow is approximated by the simplified flow as shown in Figure 22 (d), it is obvious from the equation of motion that the pressure, p_2, is instantaneously constant anywhere downstream of the cascade. Thus, the pressure downstream of the cascade is equal to the mean pressure at the exit line of the cascade at any instant.

The detailed analysis on the effect of Φ_3 on the pressure at the exit line of the cascade (Reference 14) leads to the conclusion that the impulsive pressure, $\rho(\partial\Phi_3/\partial t)$, produces a local pressure gradient between two adjacent blades, but its mean value over one spacing becomes zero. Since only the mean pressure over a spacing is of interest, the contribution of Φ_3 to the downstream pressure, p_2, can be omitted from consideration.

It has become obvious that the impulsive pressure term, as well as the gravitational potential term, can be dropped from equation (2-10).

The pressure is finally calculated by

$$\frac{p}{\rho} + \frac{1}{2} V^2 = F(t) \qquad (2\text{-}11)$$

From the velocity triangle in Figure 21, the instantaneous velocity head upstream of the rotor is

$$1/2 \{[V_{ao} + \Delta V_a \text{ Exp } (i\nu t)]^2 + W_{u_{10}}{}^2\}$$

where the subscript u denotes the component in the cascade direction.

On the other hand, the velocity head at the exit of the cascade is from equation (2-9)

$$1/2 \left\{ \left[V_{ao} + \Delta V_a \text{ Exp } (i\nu t) \right]^2 + \left[W_{u_{20}} + \Delta V_a \tan \lambda_R \frac{1 - \text{Exp } (-\pi\sigma_R)}{1 + i\omega_R \, C(\omega_R, \sigma_R)} \text{ Exp } (i\nu t) \right]^2 \right\}$$

From equation (2-11), the deviation of pressure rise from its time-mean value, Δp_R, is

$$\frac{\Delta p_R}{\rho} = 1/2 \left(W_{u_{10}}{}^2 - \left\{ W_{u_{20}} + \Delta V_a \tan \lambda_R \frac{[1 - \text{Exp } (-\pi\sigma_R)]}{1 + i\omega_R \, C(\omega_R, \sigma_R)} \text{ Exp } (i\nu t) \right\}^2 \right)$$

$$- 1/2 \left(W_{u_{10}}{}^2 - W_{u_{20}}{}^2 \right)$$

$$\cong - W_{u_{20}} \cdot \Delta V_a \frac{\tan \lambda_R [1 - \text{Exp } (-\pi\sigma_R)]}{1 + i\omega_R \, C(\omega_R, \sigma_R)} \text{ Exp } (i\nu t) \qquad (2\text{-}12)$$

In the above, ΔV_a is assumed to be small and the term of $\Delta V_a{}^2$ is neglected. The dimensionless pressure change is then

$$h_R = \frac{\Delta p_R}{\frac{\rho}{2} u^2} = - 2 \tan \lambda_R \frac{1 - \text{Exp } (-\pi\sigma_R)}{1 + i\omega_R \, C(\omega_R, \sigma_R)} \frac{W_{u_{20}}}{u} \frac{\Delta Q}{Q_o} \phi \text{ Exp } (i\nu t) \qquad (2\text{-}13)$$

Change of Pressure Rise Through Stator - The inlet flow to the stator contains two kinds of inlet unsteadiness. The oscillating axial component, ΔV_a Exp $(i\nu t)$, produces a translatory inlet oscillation, $\bar{w}_1 = - \Delta V_a \tan \lambda_S$ Exp $(i\nu t)$, to the stator similar to the case of the rotor. Besides this, the disturbance velocity induced by the rotor generates a simulated sinusoidal gust oscillation upstream of the stator and makes the flow through the stator more complicated than the flow through the rotor.

The flow downstream of the stator includes two kinds of distrubance, one resulting from translatory inlet oscillation, and the other from sinusoidal gust oscillation.

The flow caused by the oscillation of axial flow is solved in exactly the same way as in the case of the rotor. The flow downstream of the stator is

represented by

$\Delta V_a \text{ Exp } (i\nu t)$ in the X-direction,

$$\bar{v}_2 = \Delta V_a \tan \lambda_S \frac{1 - \text{Exp } (-\pi\sigma_S)}{1 + i\omega_S C(\omega_S, \sigma_S)} \text{Exp } (i\nu t) \text{Exp } \left[-i\nu(X - \frac{\ell_S}{2} \cos \lambda_S)/V_{ao}\right]$$

in the Y-direction

where coordinate (X, Y) is illustrated in Figure 23.

On the other hand, the flow upstream of the stator contains a sinusoidal gust expressed generally as

$$\tilde{w}_1 = \tilde{w} \text{ Exp } (i\nu t) \text{ Exp } (-i\nu X/V_{ao})$$

where $\tilde{w}$ must be specifically so determined that the disturbance induced by the rotor can be properly transmitted into the coordinate system of the stator. From the condition that the above equation at $X = -[d + \ell_S/2(\cos \lambda_S)]$ coincides with equation (2-9) at $X = \ell_R/2(\cos \lambda_R)$, the inlet sinusoidal gust to the stator has the form

$$\tilde{w}_1 = -\Delta V_a \tan \lambda_R \frac{1 - \text{Exp } (-\pi\sigma_R)}{1 + i\omega_R C(\omega_R, \sigma_R)} \text{Exp}\left[-i\nu(d + \frac{\ell_S}{2} \cos \lambda_S)/V_{ao}\right] \quad (2\text{-}14)$$

$$\text{Exp } (i\nu t) \text{ Exp } (-i\nu X/V_{ao})$$

The solution for a given inlet sinusoidal gust is solved in the previous Section in which the flow, $\tilde{w}_2$, downstream of the cascade is known

$$\tilde{w}_2 = \tilde{w}_1 + \tilde{v}_2 = \tilde{w}_1 \left\{1 - [1 - \text{Exp } (-2\pi\sigma_S)] \frac{S(\omega_S, \sigma_S)}{1 + i\omega_S C(\omega_S, \sigma_S)}\right\} \quad (2\text{-}15)$$

where

$$\omega_S = \frac{\nu s_S}{2\pi U_\infty} = \frac{\cos \lambda_S}{N_S \phi} \omega$$

and

s_S is the spacing of the stator cascade,
N_S is the number of the stator blades.

The first term of equation (2-15) is a sinusoidal gust oscillation, which merely passes through without any change, while the second term indicates the induced disturbance because of the inlet gust flow. The entire flow field is obtained by superimposing the steady mean flow, the translatory oscillation flow, and the sinusoidal gust oscillation flow as illustrated in Figure 23.

For the calculation of pressure, it is necessary to consider the effect of impulsive pressure, $\rho(\partial\Phi/\partial t)$. So far as the translatory oscillating inlet flow into the stator is concerned, the effect of impulsive pressure is restricted to the generation of pressure gradients within a spacing as in the case of the rotor, and thus can be omitted from the consideration.

Besides the translatory oscillation, the flow around the stator is accompanied by the sinusoidal gust oscillation, which is no longer irrotational flow and for which the velocity potential does not exist. This circumstance makes the determination of pressure very difficult, since the fundamental relation for pressure, equation (2-10), does not hold for rotational flow. To avoid this difficulty, the real sinusoidal gust inlet flow is replaced by the modified flow field as illustrated in Figure 24 (a).

In the modified flow, the inlet flow has no gust oscillation and is consequently irrotational. Instead of this steady inlet flow, the airfoil itself oscillates with the velocity $-\tilde{w}_1$ in the cascade direction, so that the airfoil encounters the same relative velocity to the fluid. Even through this exchange of inlet and boundary conditions, the same circulation distribution will be obtained in the airfoil and in the wake as that of the original flow, provided $|\tilde{w}_1| \ll V_{a0}$. This replacement, however, has an essential advantage because there exists a velocity potential. Therefore, the effect of impulsive pressure will be calculated from the modified flow field.

The unsteady velocity potential of modified flow is divided into two parts, Φ_4 and Φ_5. The potential Φ_4 is generated by the unsteady vortices in the airfoil and wake that are conditioned by the oscillating motion of the airfoil.

An analysis similar to that leading to the result $\rho(\partial\Phi_3/\partial t)$ has no effect on an average pressure of rotor cascade, gives the conclusion that the impulsive pressure, $\rho(\partial\Phi_4/\partial t)$, generates merely a pressure gradient between two adjacent blades, and has no effect on the average pressure over one spacing. Since we are not interested in the local pressure but rather in the average pressure, the effect of impulsive pressure, $\rho(\partial\Phi_4/\partial t)$, can be dropped from equation (2-10).

Besides the unsteady circulation, each airfoil has a steady, distributed circulation, $\gamma_0(X)$, over its airfoil. The total steady circulation Γ_0 of the airfoil is the sum of distributed circulation, and thus,

$$\Gamma_0 = \int_{X=-\frac{\ell}{2}\cos\lambda}^{\frac{\ell}{2}\cos\lambda} \gamma_0(X)\, dX = (V_{u_{20}} - V_{u_{30}})s$$

In the case when the airfoil does not move, this steady circulation causes no change of velocity potential as to time and produces no impulsive pressure.

In the modified flow, however, the airfoil is in an oscillating motion, and this causes an associated time-dependent velocity potential field, Φ_5.

Now the velocity potential can be calculated of a strip of cascade with width dX, which is moving with velocity $-\tilde{w}_1$ in the cascade direction, cf. Figure 24 (b). The time-differential of the velocity potential at point 1 sufficiently upstream of the strip is

$$\left(\frac{\partial \Phi_5}{\partial t}\right)_1 = \left(\frac{\partial \Phi_5}{\partial Y}\right)_1 \left(\frac{\partial Y}{\partial t}\right)_1 = \frac{\gamma_o \, dX}{2s} \tilde{w}_1$$

Since only the relative motion between point 1 and the strip is essential, the point 1 is supposed to move with velocity $\partial Y/\partial t = \tilde{w}_1$ in the above derivation, instead of considering the strip as moving with $-\tilde{w}_1$.

From the same analysis, the time-differential of the velocity potential at point 2 sufficiently downstream of the strip is

$$\left(\frac{\partial \Phi_5}{\partial t}\right)_2 = - \frac{\gamma_o \, dX}{2s} \tilde{w}_1$$

From the above, the difference of time-differential across the cascade becomes

$$\left(\frac{\partial \Phi_5}{\partial t}\right)_1 - \left(\frac{\partial \Phi_5}{\partial t}\right)_2 = \frac{\gamma_o \tilde{w}_1}{s} dX \qquad (2\text{-}16)$$

The integration of equation (2-16) over the airfoil gives the total difference of time-differential due to total circulation on the airfoil; thus,

$$\left(\frac{\partial \Phi_5}{\partial t}\right)_1 - \left(\frac{\partial \Phi_5}{\partial t}\right)_2 = \frac{1}{s} \int_{X = -\frac{\ell}{2} \cos \lambda}^{\frac{\ell}{2} \cos \lambda} \gamma_o (X) \, \tilde{w}_1 (X, t) \, dX$$

$$= \frac{\tilde{w}}{s} \operatorname{Exp} (i\nu t) \int_{-\frac{\ell}{2} \cos \lambda}^{\frac{\ell}{2} \cos \lambda} \gamma_o (X) \operatorname{Exp} (-i\nu X / V_{ao}) \, dX \qquad (2\text{-}17)$$

To carry on the above integration, the distribution of $\gamma_o (X)$ must be given, which is different in each case according to the geometrical shape of the airfoil.

It is assumed here, however, that the circulation distribution changes linearly from its maximum at the leading edge to zero at the trailing edge. Thus,

$$\gamma_o(X) = \frac{\Gamma_o}{\ell \cos \lambda}\left(1 - \frac{2X}{\ell \cos \lambda}\right) \tag{2-18}$$

Substituting equation (2-18) into equation (2-17) and integrating over the airfoil, we obtain

$$\left(\frac{\partial \Phi_5}{\partial t}\right)_1 - \left(\frac{\partial \Phi_5}{\partial t}\right)_2 = \frac{i\Gamma_o \tilde{w}}{\pi \omega \ell} \operatorname{Exp}(i\nu t)\left[\frac{\sin \pi\omega\sigma}{\pi\omega\sigma} - \operatorname{Exp}(i\pi\omega\sigma)\right] \tag{2-19}$$

where

$$\omega = \frac{\nu s}{2\pi U_\infty} = \frac{\nu s \cos \lambda}{2\pi V_{ao}}$$

This result should be considered for the calculation of pressure around the stator.

The pressure downstream of the exit edge of the stator is considered to be constant for the same reason as for the rotor, and the pressure difference upstream of the stator and at the exit edge of the stator is calculated by equation (2-10).

The deviation of pressure rise Δp_S, through the stator from its time-mean value is thus,

$$\frac{\Delta p_S}{\rho} = \frac{1}{2}\left[V_{u_{20}}{}^2 - (V_{u_{30}} + \bar{v}_2 + \tilde{v}_2)^2\right] + \left[\left(\frac{\partial \Phi_5}{\partial t}\right)_1 - \left(\frac{\partial \Phi_5}{\partial t}\right)_2\right] - \frac{1}{2}\left(V_{u_{20}}{}^2 - V_{u_{30}}{}^2\right)$$

Substituting equations (2-14), (2-15) and (2-19) into the above and neglecting the term of $\Delta V_a{}^2$ gives

(2-20)

$$\frac{\Delta p_S}{\rho} \cong -V_{u_{30}}\Delta V_a\left\{\tan\lambda_R \frac{1 - \operatorname{Exp}(-\pi\sigma_R)}{1 + i\omega_R\, C(\omega_R, \sigma_R)} \frac{1 - \operatorname{Exp}(-2\pi\sigma_S)}{1 + i\omega_S\, C(\omega_S, \sigma_S)} S(\omega_S, \sigma_S) \operatorname{Exp}\left[-i\nu(d + \ell_S \cos\lambda_S)/V_{ao}\right]\right.$$

$$\left. + \tan\lambda_S \frac{1 - \operatorname{Exp}(-\pi\sigma_S)}{1 + i\omega_S\, C(\omega_S, \sigma_S)}\right\} \operatorname{Exp}(i\nu t) - i(V_{u_{20}} - V_{u_{30}})\Delta V_a \tan\lambda_R \frac{1 - \operatorname{Exp}(-\pi\sigma_R)}{1 + i\omega_R\, C(\omega_R, \sigma_R)} \frac{\left[\frac{\sin \pi\omega_S\sigma_S}{\pi\omega_S\sigma_S} - \operatorname{Exp}(i\pi\omega_S\sigma_S)\right]}{\pi\omega_S\sigma_S} \operatorname{Exp}\left[-i\nu(d + \frac{\ell_S}{2}\cos\lambda_S)/V_{ao}\right] \operatorname{Exp}(i\nu t)$$

The dimensionless pressure change is then

(2-21)

$$h_S = \frac{\Delta p_S}{\frac{\rho}{2} u^2} = -2\Bigg(\Big\{\tan\lambda_R \frac{1 - \mathrm{Exp}(-\pi\sigma_R)}{1 + i\omega_R\, C(\omega_R, \sigma_R)} \frac{1 - \mathrm{Exp}(-2\pi\sigma_S)}{1 + i\omega_S\, C(\omega_S, \sigma_S)} S(\omega_S, \sigma_S)\, \mathrm{Exp}\Big[-i\nu(d + \ell_S \cos\lambda_S)/V_{ao}\Big] + \tan\lambda_S \frac{1 - \mathrm{Exp}(-\pi\sigma_S)}{1 + i\omega_S\, C(\omega_S, \sigma_S)}\Big\} \frac{V_{u_{30}}}{u}$$

$$+ \tan\lambda_R \frac{1 - \mathrm{Exp}(-\pi\sigma_R)}{1 + i\omega_R\, C(\omega_R, \sigma_R)} \frac{i\Big[\frac{\sin\pi\omega_S\,\sigma_S}{\pi\,\omega_S\,\sigma_S} - \mathrm{Exp}(i\pi\omega_S\,\sigma_S)\Big]}{\pi\,\omega_S\,\sigma_S} \frac{(V_{u_{20}} - V_{u_{30}})}{u}\, \mathrm{Exp}\Big[-i\nu(d + \frac{\ell_S}{2}\cos\lambda_S)/V_{ao}\Big]\Bigg)\frac{\Delta Q}{Q_o}\,\phi\,\mathrm{Exp}(i\nu t)$$

The total unsteady pressure difference between the delivery and the suction ports of the pump is obtained by summing up h_C, h_R, and h_S:

$$h = \frac{P_d - P_s}{\frac{\rho}{2} u^2} - \left(\frac{P_d - P_s}{\frac{\rho}{2} u^2}\right)_0 = h_C + h_R + h_S \qquad (2\text{-}22)$$

In the case of f = 0, the above becomes

$$h_{qs} = -2\Big\{\tan\lambda_R[1 - \mathrm{Exp}(-\pi\sigma_R)]\,[1 - \mathrm{Exp}(-\pi\sigma_S)\frac{V_{u_{30}}}{u}]$$

$$+ \tan\lambda_S\,[1 - \mathrm{Exp}(-\pi\sigma_S)]\frac{V_{u_{30}}}{u}\Big\}\,\frac{\Delta V_a}{u}$$

and agrees, of course, with the pressure change when the axial velocity increases steadily by ΔV_a, assuming the flow through a cascade of flat plates without losses.

Using the result obtained, a sample calculation is carried on for a typical single-stage axial flow pump. The basis of the calculation and the result are both illustrated in Figure 25. As seen from this result, h_S has a phase delay that increases nearly proportional to the reduced frequency. The reason for this delay is that a part of this pressure fluctuation is caused by the sinusoidal gust oscillation produced by the rotor, and the gust requires time to reach the stator where the disturbance velocity is converted into pressure.

It is also worth mentioning that the pressure change due to conduit effect, h_C, increases proportional to the frequency, f, and thus becomes predominantly larger than the pressure change through the rotor and stator, $h_R + h_S$, in the higher frequency range. When the frequency exceeds a certain limit, the compressibility effect of the working liquid and the piping system becomes apparent and the above analysis can no longer be applied.

Simplified Dynamic Characteristics of Turbopumps

Although there are a wide variety of principles of turbopump construction, it is fundamentally possible to calculate the dynamic characteristics of individual turbopumps by applying the method developed in the previous paragraph. However, the more complicated the pump, the more difficult, and perhaps even impractical, is the analytical calculation. In this paragraph, a more simple and practical calculation of the dynamic characteristics will be developed for the case when approximate dynamic characteristics are sufficient.

In Figure 26, the shape of turbopumps is different in each case. In all cases, however, all of the energy input to the working liquid is produced in the rotor. A part of this input is converted into pressure in the rotor, and the rest is converted into pressure in the following stator or diffusor.

For the calculation of simplified dynamic characteristics, the following assumptions are made;

1. The angular momentum of inlet flow into the rotor is steady.

2. The increase of velocity head at the outlet edge of the rotor is converted into pressure rise in the following stator or diffusor without any time delay. In other words, the stator or diffusor is very narrow and follows very close to the outlet of the rotor.

Under the above assumptions, the change of pressure rise through the rotor, Δp_R, is given by equation (2-12)

$$\frac{\Delta p_R}{\rho} = - W_{u_{20}} \Delta V_a \frac{\tan \lambda_R \left[1 - \mathrm{Exp}\left(-\pi \sigma_R\right)\right]}{1 + i\omega_R \, C(\omega_R, \sigma_R)} \mathrm{Exp}\,(i\nu t)$$

where λ_R, σ_R, ω_R are the stagger angle, solidity, and reduced frequency of the rotor cascade, respectively. In the case of the radial and the mixed flow impeller, the cascade on the representative stream surface is no longer a pure linear cascade, as it is in the case of the axial flow pump. Therefore, the result obtained for the axial flow stage does not hold for pumps of other types in the exact meaning.

It is, however, quite reasonable to replace this non-linear cascade through an equivalent linear cascade. For example, an equivalent linear cascade of a circular cascade (radial flow impeller) can be obtained by transforming the circular cascade conformally into a linear cascade using a proper mapping function. For radial and mixed flow pumps, therefore, the cascade parameters, λ_R, σ_R, and ω_R, are taken not from the original cascade but from the equivalent linear cascade. In the same way, axial velocity V_a, means meridian velocity in this case.

From the previous assumption, the change of pressure rise through the stator is equal to the increase of dynamic pressure at the exit of the rotor; thus,

$$\frac{\Delta p_S}{\rho} = 1/2 \left[(V_{u_{20}} - \bar{v}_2)^2 - V_{u_{20}}{}^2 \right]$$

$$\cong - V_{u_{20}} \Delta V_a \frac{\tan \lambda_R \left[1 - \mathrm{Exp}\ (-\pi\sigma_R) \right]}{1 + i\omega_R\ C(\omega_R,\ \sigma_R)} \mathrm{Exp}\ (i\nu t)$$

The total change of pressure becomes

$$\frac{\Delta p_R + \Delta p_S}{\rho} = - u \cdot \Delta V_a \frac{\tan \lambda_R \left[1 - \mathrm{Exp}\ (-\pi\sigma_R) \right]}{1 + i\omega_R\ C(\omega_R,\ \sigma_R)} \mathrm{Exp}\ (i\nu t)$$

or by making it dimensionless,

$$h_{R+S} = \frac{\Delta p_R + \Delta p_S}{\frac{\rho}{2} u^2} = - 2 \frac{\tan \lambda_R \left[1 - \mathrm{Exp}\ (-\pi\sigma_R) \right]}{1 + i\omega_R\ C(\omega_R,\ \sigma_R)} \frac{\Delta Q}{Q_o} \phi\ \mathrm{Exp}\ (i\nu t) \quad (2\text{-}23)$$

where

$$\omega_R = \frac{\nu s_R}{2\pi U_\infty} = \frac{\cos \lambda_R}{N_R \phi} \omega = \frac{\cos \lambda_R}{N_R \phi} \frac{f}{n}$$

In the case where the solidity of the rotor cascade, σ_R, is comparatively large, namely about $\sigma_R \geqq 1.0$, the above can be simplified further

$$h_{R+S} = - 2 \tan \lambda_R \frac{\Gamma(1/2 + i\omega_R)}{\sqrt{\pi}\ \Gamma(1 + i\omega_R)} \frac{\Delta Q}{Q_o} \phi\ \mathrm{Exp}\ (i\nu t) \quad (2\text{-}24)$$

The numerical value of $\dfrac{\Gamma(1/2 + i\omega)}{\sqrt{\pi}\ \Gamma(1 + i\omega)}$ is listed in Table I.

In Figure 27, $h_{R+S}/2 \tan \lambda_R \dfrac{\Delta Q}{Q_o} \phi$ is illustrated in the form of a polar diagram. In the case of $f = \omega_R = 0$, equation (2-24) becomes

$$(h_{R+S})_{qs} = - 2 \tan \lambda_R \frac{\Delta Q}{Q_o} \phi\ \mathrm{Exp}\ (i\nu t)$$

and agrees with the result when the flow rate changes quasi-statically. The ratio, $h_{R+S}/(h_{R+S})_{qs} = \Gamma(1/2 + i\omega_R)/\sqrt{\pi}\ \Gamma(1 + i\omega_R)$, is also plotted in Figure 28

as the Bode diagram, which shows the frequency response by using gain (db) and phase shift. From this diagram two limiting reduced frequencies, $(\omega_R)_L = 0.3$ and $(\omega_R)_H = 30$, are introduced. At a reduced frequency lower than $(\omega_R)_L$, the characteristics of a turbopump agree practically with that of steady-state operation; that is, the relation between flow rate and pressure rise can be expressed by the usual steady-state characteristics curve. On the other hand, at a reduced frequency higher than $(\omega_R)_H$, the fluctuation of pressure rise becomes almost negligible even though the flow rate fluctuates periodically. At such a high frequency, the pressure difference due to the oscillating flow in a conduit, h_C, becomes extremely large.

Since $\omega_R = \frac{\cos \lambda_R}{N_R \phi} \frac{f}{n}$, the corresponding absolute limiting frequencies, f_L and f_H, become

$$\left.\begin{aligned} f_L &= 0.3 \frac{N_R \phi}{\cos \lambda_R} n \\ f_H &= 30 \frac{N_R \phi}{\cos \lambda_R} n = 100 f_L \end{aligned}\right\} \qquad (2\text{-}25)$$

In the previous analysis, the dynamic characteristics of turbopumps are described in the form of frequency responses. It is fundamentally possible to calculate the response of pressure rise for an arbitrary change of flow rate based on the frequency response.

The time constant of turbopumps can be calculated roughly by approximating the response of Figure 28 to that of the first order lag element (transfer function is $K/(Ts + 1)$) and by assuming $(\omega_R)_L = 0.3$ represents the break point. The result is,

$$\text{Time constant, } T = \frac{1}{0.3} \frac{\cos \lambda_R}{2\pi N_R \phi n} \qquad (2\text{-}26)$$

The above shows only the pressure change through a single-stage turbopump. In the case of a multi-stage turbopump, the overall dynamic characteristics are calculated by summing up the characteristics of each stage.

$$(h_{R+S})_{\text{overall}} = \sum_{\text{stage}} h_{R+S}$$

SECTION III. EXPERIMENTAL STUDY OF DYNAMIC CHARACTERISTICS OF A CENTRIFUGAL PUMP

The dynamic characteristics of turbopumps were studied experimentally in this Section. The experiment was conducted specifically using a centrifugal pump that was available from the commercial market for common industrial use. The fluctuating flow was generated mechanically by a reciprocating piston attached to the delivery pipe line of the pump.

The instantaneous flow rate and pressures were measured and recorded on oscillograph and magnetic tape, which enabled both visual and computer evaluation to be made of the measurements. The test result was compared with the theoretical prediction that was calculated based on the analysis of the previous Section.

This study was limited to the incompressible case. The experiment was, therefore, carried for the frequency range in which the compressibility effect is negligible or of secondary importance. Since the occurence of cavitation seriously deteriorates the assumption of incompressibility, cavitation in the test pump was suppressed as far as possible.

Experimental Arrangement

Test Equipment - The test equipment consisted of three main systems; a pumping system, a pulsating system, and a measurement/control system. Figure 29 shows the three-dimensional arrangement of the main hardware.

Pumping system - A centrifugal pump for common industrial use was selected for the test pump because of its simple, robust construction and popular use. Table II describes the details of the test pump.

The pump was driven by a 30 HP induction motor through a continuous speed change gear. The moment of inertia of this driving system was so large that the fluctuation of input torque to the pump during unsteady operation caused no detectable change of rotational speed, so long as the frequency of fluctuation exceeded 1 Hz.

The working liquid (city water) was fed to the pump from a head tank, which was located 10 m (33 ft) above the pump level, contained 26 m^3 (7,000 gallons) of water, and supplied 11 N/cm^2 (16 psi) boost pressure to the pump inlet. This boost pressure corresponded to Net Positive Suction Head of 21 N/cm^2 (30 psi) and allowed the pump to operate cavitation-free even under the severe test condition of large pressure fluctuation.

Suction and delivery accumulators were attached to the suction and delivery pipe line, respectively. The cushioning action of their air reservoirs served to absorb the flow fluctuation in the pipe line. Therefore, the flow fluctuation generated by the pulsating system could be restricted between the two accumulators, avoiding undesirable pressure surge in the long suction and delivery pipe lines.

The flow rate was regulated by adjusting a control valve. In the case of fluctuating flow rate, only the mean flow rate, Q_o, could be controlled by this valve. The distance between the pump and the control valve was designed to be as short as practically possible in order to obtain highest possible resonance frequency. This resonance frequency determined the upper limit of test frequency range from which any reasonable incompressible result can be reduced. Figure 30 illustrates the detail of test arrangement around the pump.

Pulsating system - Fluctuating flow through the pump was generated by a 3 1/4-inch diameter reciprocating piston attached to the delivery pipe between pump outlet and control valve, as shown in Figure 30.

The instantaneous flow rate, Q, increases as the piston pulls out, while Q decreases as the piston pushes in. The fluctuation of flow rate, $Q - Q_o$, is fundamentally proportional to the piston velocity. The piston was connected to a hydraulic actuator, whose motion was electronically controlled to trace an exact sine wave with desired amplitude and frequency. Therefore, the fluctuating flow, $Q - Q_o$, is also sinusoidal unless some other deteriorating effects, such as compressibility, lack of hydraulic power etc., distort the wave form. A 20 hp hydraulic pump was used for feeding the actuator with 1,700 N/cm^2 (2,500 psi) constant pressure hydraulic oil.

Measurement and control system - Figure 31 illustrates schematically the main measurement and control system. Suction pressure, p_s, delivery pressure, p_d, and differential pressure, $p_d - p_s$, are measured by variable-reluctance type pressure pickups. The deflection diaphram of these pickups is interchangeable, so that a diaphram of proper rating is built in for each test pressure range. The natural frequency of these pickups ranges between 15 and 25 kHz, according to their diaphram thickness, and is obviously far above the frequency range which is of main interest in this study.

Flow rate is measured simutaneously by two different kinds of flowmeters, a turbine flowmeter and a magnetohydrodynamic (MHD) flowmeter. A 2-inch diameter turbine flowmeter was in installed on the delivery line between the pulsator and the control valve, and aimed to meter accurate flow rate under steady-state operation. It could not, however, respond quickly enough to indicate the instantaneous flow rate under unsteady operation because of its relatively slow Digital to Analog converter, which indicated rather the mean flow rate, Q_o, in a higher frequency range, $f > 50$ Hz.

A homemade MHD flowmeter was installed on the delivery line between pump outlet and pulsator. This flowmeter consists of an acrylic pipe, a magnet of DC exitation and two gold-plated electrodes. The output potential from the electrodes was directly proportional to the instantaneous flow rate, Q, provided that the flux density across the pipe remains constant. The main advantage of this flowmeter was its very quick response, which was of special importance in this study. One problem associated with this method was the drift of output potential due to the asymmetry of the electro-chemical potential around both electrodes. This drift made it difficult to measure the flow rate continuously over a long time span with sufficient accuracy. In this experiment, however, the MHD flowmeter was operated continuously for about 20 seconds

with practically negligible drift. The rate of flow fluctuation, $\Delta Q/Q_o = (Q_{max} - Q_{min})/2Q_o$, was estimated directly by observing the output of MHD flowmeter displayed on the screen of the syncroscope standing by the test pump.

To check the magnitude of the mechanical vibration of the piping system, a small piezoelectric accelerometer was cemented on the surface of the delivery pipe between the pulsator and the control valve. This measurement was used to detect the mechanical resonance of the piping system as well as to detect the hyraulic resonance of liquid contained in the piping system.

The displacement of the actuator plunger was also measured by using a potentiometer that was built in the actuator. This measurement checked the actual motion of the pulsator piston which was supposed to be sinusoidal.

Seven electrical signals, each representing one of the above measurements, were fed to the main amplifier unit, and were recorded both on an oscillograph and a magnetic tape; the former for the conventional visual observation, the latter for evaluation and processing by digital computer. Necessary calibration was conducted to determine the overall conversion factor of each measurement.

The rotational speed of the test pump was set to a desired value by adjusting the gear ratio of Varidrive transmission. The rotational speed itself is measured by a digital counter that counts directly the number of revolutions per second. This counter also determines the exact flow rate by counting the pulse signals from the turbine flowmeter.

A DC power source with automatic current control supplied a constant current of 20 A to the magnet of the MHD flowmeter.

The control system of the actuator consisted of a servomatic analyzer and a servo amplifier. The servomatic analyzer generated a sine wave signal of the desired intensity and frequency, while the servo amplifier intensified this signal and fed the control current to the regulator valve of the actuator. The feedback control minimizes any deviation of the actuator motion from the predetermined one. The attenuation of the initial signal generated by the servomatic analyzer was adjusted so that the rate of flow fluctuation, $\Delta Q/Q_o$, was a desired value.

Test Program - An experiment was conducted in accordance with the test program described in Table III. Series 1 and 2 include preliminary tests that were intended to determine the nature and magnitude of the pressure fluctuation inherent to this test arrangement without applying a forced fluctuation with the pulsator.

The main test was performed at three different rotational speeds of the test pump, n = 60, 30 and 15 rps (series 3 through 14). At each rotational speed, four series of tests were conducted. First, a steady-state characteristics curve was determined by varying the flow rate Q from zero to maximum without applying any forced fluctuation. (The dynamic characteristics can be discussed only in connection with the steady-state characteristics.)

Pulsating tests were performed at two different mean flow rates, Q_o, corresponding to the design flow rate (maximum efficiency point) and to half of the design flow rate, respectively. The rate of flow fluctuation, $\Delta Q/Q_o$, was adjusted to 0.1 so long as the pulsating system could realize this condition. Otherwise, the fluctuation rate was maintained at the maximum available value. In most cases, the maximum fluctuation rate decreased rapidly when the fluctuation frequency exceeded 30 Hz. The maximum frequency available from this pulsating system was slightly over 100 Hz, but only with a very small fluctuation rate.

A linearity test was added to determine the effect of the fluctuation rate, $\Delta Q/Q_o$, on the whole phenomena, varying the fluctuation rate from 0.02 to the maximum available value at relatively low frequencies, 3 and 10 Hz. As the last test, series 15 determined the pressure difference between the pump suction and the delivery due to the oscillating flow generated by the pulsator without running the test pump. This pressure difference, Δp_C, was essentially indifferent to the pumping action itself and merely resulted from the conduit effect of the pump casing. This test provided information that was necessary to divide the change of pressure difference between the pump delivery and the suction, $\Delta p = (p_d - p_s) - (p_d - p_s)_0$, into two essentially different groups, that is, into the pressure difference due to the conduit effect of the pump, Δp_C, and the change of pressure rise through the pump, Δp_{R+S}.

An oscillograph recording was made for all test series, but a tape recording was made only for the test series that required computer processing.

Test Results

Steady-State Characteristics - From the test series 3, 7 and 11, steady-state characteristics of the test pump at n = 60, 30 and 15 rps were obtained. The pressure rise through pump, $p_d - p_s$, and the flow rate, Q, were made nondimensional using the following relations;

$$\left.\begin{aligned} &\text{pressure rise coefficient,} \quad \psi = (p_d - p_s) / \frac{1}{2} \rho u_2^2 \\ &\text{flow coefficient,} \quad \phi = Q/\pi\, d_2\, b_2\, u_2 \end{aligned}\right\} \qquad (3\text{-}1)$$

where d_2, b_2, u_2 are outer diameter, exit width, peripheral velocity of pump impeller, respectively.

Figure 32 shows the nondimensional steady-state characteristics of the test pump. The design point of this pump was located at $\phi = 0.1137$ $(=\phi_D)$ where the efficiency of the pump reached its maximum value. As previously mentioned, pulsating tests were performed both at $\phi = \phi_D$ and $\phi = 1/2\ \phi_D$.

The slope of the characteristics curve is read from Figure 32 as;

$$\frac{d\psi}{d\phi} = -5.94 \quad \text{at } \phi = \phi_D,$$

$$= -3.44 \quad \text{at } \phi = \frac{1}{2}\phi_D.$$

The change of pressure rise, Δp_{R+S}, corresponding to a change of flow rate, $Q - Q_o$, can be determined from the above slope when the flow fluctuation is quasi-static.

Pulsating Test

Data and Their Reduction - Pulsating tests were conducted in test series 4, 5, 6 at n = 60 rps, in series 8, 9, 10 at n = 30 rps, and in series 12, 13, 14 at n = 15 rps.

Figure 33 shows a typical oscillograph recording as a sample that illustrates the amplitude-time histories of seven measurements, from bottom to top, suction pressure, p_s, delivery pressure, p_d, differential pressure, $p_d - p_s$, flow rate Q by MHD flowmeter, displacement of the actuator plunger, acceleration of the delivery pipe, and flow rate Q by turbine flowmeter. This test was a part of series 4 and was conducted under the condition n = 60 rps, Q_o = 200 gpm ($\phi = \phi_D$), f = 10 Hz, $\Delta Q/Q_o \approx 0.1$.

The time passes from right to left on the oscillograph record and each abscissa represents a particular time, which can be interpreted from the time mark recorded at the topmost edge. This time mark is also simultaneously recorded on the magnetic tape to synchronize both recordings.

Despite the effort to obtain a flow fluctuation as perfectly sinusoidal as possible, the one indicated by MHD flowmeter showed in some cases an appreciable deviation from the initial intention. This deviation resulted partly from the compressibility of the water column, and partly from the nonharmonic motion of the pulsator piston, which had a tendency to be quicker during pull-out motion than during push-in motion, especially in a higher frequency range. The pressure fluctuation was also not a simple harmonic but contained many higher harmonics that represented either multiple harmonics of basic pressure fluctuation or standing vibrations of the water column enclosed in the piping system. The latter could not be eliminated even with the perfect excitation of fluctuating flow.

Because of the presence of these harmonics, it became practically impossible to evaluate the correct amplitude and phase correlation between flow rate and pressure rise through the visual observation of oscillograph records. Nevertheless, oscillograph recording is the best means for visualization and understanding of the whole pheonomena involved.

Test results were recorded also on the multi-channel magnetic tape for computer processing. For each test condition, the slice time of recorded tape was determined through the visual observation of corresponding oscillograph records, so that each slice could contain representative measurements for

4 seconds, excluding any measurement under transient or irregular circumstances. First, each slice of the tape was fed to an Analog-to-Digital converter, in which the input data on the tape were digitized at the sample rate of 500 per second to furnish the digital input data for the computer. An IBM 7094 computor was used for the processing, operating with the Random Vibration Analysis Program (RAVAN, Reference 15). The program was developed by the Computation Laboratory of George C. Marshall Space Flight Center, NASA, to perform various statistical analyses of random processes normally associated with flight and captive tests and is capable of computing various statistical functions, such as auto-correlation functions, power spectral density distribution functions, root-mean-square (rms) amplitude distribution functions, probability density distribution function of single input functions; cross-correlation functions for positive and negative lag time, cross power spectral density distribution functions, cross phase correlation functions, and coherence distribution function of two independent input functions (Reference 16). These computed functions are available in the form of graphs prepared by a Stromberg-Carlson 4020 automatic plotter.

Figure 34-1 through 34-18 show a part of the plotter outputs for the test condition that is equal to that of Figure 33. Flow rate Q by MHD flowmeter, change of pressure difference, Δp, suction pressure, p_s, and delivery pressure, p_d, were analyzed as a single input function, and the result is shown in Figure 34-1, -2, -3, -4, -8, -9, -12, -13, -14 and -18. On the other hand, cross correlation analyses were conducted for two couples of input functions, (Δp and Q) and (p_s and p_d), as shown in Figure 34-5, -6, -7, -10, -11, -15, -16, and -17.

From these results the amplitude and phase correlation of flow and pressure fluctuation can be determined far more exactly than can be done by the visual observation of oscillograph recordings. Besides the accuracy, the computed coherence allows the estimation of the reliability of that accuracy.

Linearity Test - Figure 35 describes the amplitude and the phase correlation of flow and pressure fluctuation. The flow fluctuation, $Q - Q_o$, is expressed by the real part of a rotating vector, $\Delta Q \text{ Exp } (i\nu t)$, and the phase of pressure fluctuation is correlated to that of flow fluctuation. The change of pressure difference in the quasi-static operation condition, Δp_{qs}, can be determined from the slope of the steady-state characteristics curve and has 180° phase delay to that of flow fluctuation. The fluctuating pressures, Δp, Δp_{qs}, Δp_{R+S} etc., were made nondimensional by dividing through the corresponding dynamic pressure, $\rho u_2^2/2$, thus giving h, h_{qs}, h_{R+S} etc.

Linearity tests conducted in series 6, 10 and 14 were to determine the effect of the magnitude of flow fluctuation, $\Delta Q/Q_o$, on the response of pressure difference. The result shown in Figure 36-1 (n = 60 rps), 36-2 (n = 30 rps) and 36-3 (n = 15 rps) indicates that the nondimensional change of pressure difference, h, has the amplitude proportional to the rate of flow fluctuation, $\Delta Q/Q_o$, and the constant phase shift over the tested range of $\Delta Q/Q_o$. Since the h_{qs} is also proportional to $\Delta Q/Q_o$, the above result means that the amplitude and phase correlation between h and h_{qs} remains constant, indifferent to the magnitude of flow fluctuation.

These linearity tests were conducted at relatively low frequencies, at f = 3 and 10 Hz. At the higher frequency range where the compressibility of the water column becomes significant, good linear relationship cannot be expected as in the incompressible case.

Dynamic Characteristics Test - Figures 37 through 42 show the amplitude ratio and phase shift of h/h_{qs} as the function of fluctuation frequency, f, at six different test conditions. Because the pressure difference due to conduit effect, Δp_C, increases proportional to the frequency, the amplitude of h/h_{qs} increases also with the increase of frequency. The phase shift varies from zero at f = 0 to around 90° at the frequencies where the Δp_C becomes predominantly larger than Δp_{R+S}.

The effect of compressibility becomes appreciable when the frequency exceeds 30 Hz. The intensity of pressure fluctuation increases rapidly as the frequency becomes close to the resonance frequency of the pumping system, around 120 Hz. Figure 43 illustrates the change of pressure difference, Δp, corresponding to the flow fluctuation of ΔQ = 10 gpm using a polar diagram. The pressure difference due to conduit effect, Δp_C, was determined from the pulsating test of series 15 as follows;

amplitude of Δp_C (psi) = 0.0277 ΔQ(gpm) f(Hz),

phase shift of Δp_C = 96° delay to flow fluctuation.

The conduit effect of the pump casing is equivalent to that of a 38.4-inch long pipe with a 2-inch inner diameter.

Subtracting Δp_C from Δp vectorially, the change of pressure rise through the pump, Δp_{R+S}, can be determined. Then, the amplitude and phase correlation between h_{R+S} and h_{qs} can be established.

The amplitude and phase correlation of h_{R+S}/h_{qs} are plotted in Figures 44-1 and 44-2 against the reduced frequency of the rotor cascade,

$$\omega_R = \frac{\cos \lambda_R}{N_R \phi} \frac{f}{n}$$

where λ_R = 55° and N_R = 6.

The data shown in these figures were confined to those that seemed to have no compressibility effect. The test results were relatively scattered in spite of very careful reduction of data by computer. This was mainly because Δp_{R+S} cannot be determined directly but indirectly by subtracting Δp_C from Δp vectorially. Especially in higher frequency range, Δp_{R+S} must be determined as the difference of two vectors, Δp and Δp_C, that are predominantly larger than Δp_{R+S} itself, and the accuracy of obtained Δp_{R+S} inevitably deteriorates.

To compare the test result with the theory, a theoretical curve was drawn which was calculated from equation (2-24) of Section II assuming a simplified

model of turbopumps. The test results showed the tendency for the amplitude ratio of h_{R+S}/h_{qs} to decrease with the increase of the reduced frequency at a slightly faster rate than the simplified model theory predicted. Regarding the phase shift of h_{R+S}/h_{qs}, the experimental shift was definitely larger than that of the simplified model theory. This suggests that the conversion of kinetic energy at the exit of the impeller into the pressure rise in the following volute chamber requires a certain time delay that is neglected in the simplified model theory.

It is, of course, possible to calculate the frequency response of the test pump more accurately by considering the mechanism of pressure recovery in the volute chamber, thus reducing the discrepancy between theory and experiment. Nevertheless, the simplicity and the generality of the simplified model theory seems to be worth even more than its reduced accuracy.

The reduced frequency, $(\omega_R)_L$, at which the dynamic characteristics begin to separate from the quasi-static ones, is read from the test results as

$$(\omega_R)_L = 0.1$$

comparing with $(\omega_R)_L = 0.3$ obtained from the theory.

The time constant of the response of pressure rise to a step-like change of flow rate was calculated by approximating the obtained frequency response to that of a first order lag element and by assuming $(\omega_R)_L = 0.1$ represents the break point. The result is

$$\text{Time constant, } T = \frac{1}{0.1} \frac{\cos \lambda_R}{2\pi N_R \phi n} \qquad (3\text{-}2)$$

Regarding the relation between mean flow rate, Q_o, and corresponding mean pressure rise, $(p_d - p_s)_o$, during the fluctuating operation, it is found that the relation is practically identical to that of the steady-state characteristics curve as far as the rate of flow fluctuation, $\Delta Q/Q_o$, does not exceed the test range.

Fluctuation of Suction and Delivery Pressure - According to the force flow fluctuation, suction pressure, p_s, and delivery pressure, p_d, fluctuate with the same frequency. The amplitude ratio of p_d and p_s is plotted against frequency in Figure 45. In the lower frequency range, the amplitude of p_d is much larger than the amplitude of p_s, because the pressure fluctuation at the suction port is suppressed by the presence of the suction accumulator. At higher frequencies, however, both amplitudes become more or less equivalent.

The phase correlation of p_d and p_s is shown in Figure 46. Since the whole test frequency range is under the resonance frequency, both pressure fluctuations have comparatively less phase difference.

In this study cavitation in the test pump was prevented by supplying a large boost pressure at the suction. In the case in which the boost pressure is not large enough, the fluctuating suction pressure often causes periodic cavitation which introduces strong nonlinearity to the system. Under the cavitating condition, it was observed that the frequency of the predominant pressure fluctuation was not the frequency of forced fluctuation but of subharmonics, f/2, f/3, f/4 etc.

CONCLUSIONS

The response of pressure rise of turbopumps to periodically fluctuating discharge, termed dynamic characteristics, was studied analytically and experimentally.

In Section I, the theoretical basis for the calculation of dynamic characteristics was developed. The incompressible, inviscid flow solution around a cascade of nonstaggered flat plates for a periodically fluctuating inlet flow was determined. Solutions were obtained for two kinds of inlet unsteadiness, namely for translatory oscillation and for sinusoidal gust oscillation.

The possibility of applying the results of the nonstaggered cascade to the cascade of arbitrary stagger angle was sought. This analysis proved that the obtained solution was applicable also to arbitrary cascade with sufficient accuracy.

In Section II, the analytical method for calculating the dynamic characteristics of turbopumps was developed, applying the results obtained in Section I. A single-stage axial flow pump was chosen as the sample case and its exact dynamic characteristics were determined based on the specific data of the rotor and stator cascade.

For the case when even approximate dynamic characteristics are sufficient, a simple method was also derived that enables the calculation to be made without entering into the details of the pump design.

In Section III, the dynamic characteristics of a centrifugal pump were determined experimentally. Pressure at suction and delivery, flow rate, etc. were measured and the correlation between pressure and flow fluctuation was analyzed.

The dynamic characteristics obtained from the experiment were close to those predicted by the simplified model theory of Section II. The limiting

frequency under which the dynamic characteristics closely agreed with the quasi-static ones, was determined experimentally as

$$f = 0.1 \frac{N_R \phi}{\cos \lambda_R} n$$

In the entire study, interest was confined to the incompressible, non-cavitating case. When cavitation occurs in a turbopump, the phenomena change drastically from those described in this work.

REFERENCES

1. Pfleiderer, C.: Die Kreiselpumpen. Springer-Verlag, Berlin, 1961.
2. Kovats, A.: Calculation of Radial-Flow-Impeller Performance Curves by the Modified Airfoil Theory. ASME, No. 58-A-86, 1958.
3. Serovy, G. K., and Lysen, J. C.: Prediction of Axial Flow Turbomachine Performance by Blade-Element Method. Transaction of ASME, Vol. 85, Series A, No. 1, pp. 1 - 8, January 1963.
4. Weinig, F.: Die Strömung und die Schaufeln von Turbomaschinen. Johann Ambrosius Barth, Leipzig, 1935.
5. Von Karman, Th., and Sears, W. R.: Airfoil Theory for Non-Uniform Motion. Journal of the Aeronautical Sciences, Vol. 5, No. 10, pp. 379-390, August 1938.
6. Sears, W. R.: Some Aspects of Non-Stationary Airfoil Theory and its Practical Application. Journal of the Aeronautical Sciences, Vol. 8, No. 3, pp. 104 - 108, January 1941.
7. Nielsen, N.: Die Gammafunktion. Cheslea Pub. Co., New York, 1965.
8. National Bureau of Standards, U. S. Department of Commerce: Table of the Gamma Function for Complex Arguments NBS Applied Mathematics Series, Vol, 34, U. S. Department of Commerce, Washington, D. C., 1954.
9. Bateman, H.: Higher Transcendental Functions. Vol. 1, McGraw-Hill Book Co., New York, 1953.
10. Ohashi, H.: Analysis of Oscillating Flow Through Cascades. Internal Note of George. C. Marshall Space Flight Center, NASA, IN-P&VE-P-66-19, Huntsville, Alabama, 1966.
11. Member of the Staff of Lewis Research Center, NASA: Aerodynamic Design of Axial Flow Compressor. NASA SP-36, Chapter X, Prediction of Off-Design Performance of Multistage Compressors, 1965.
12. Traupel, W.: Die Berechnung der Potentialstömung durch Schaufelgitter. Schweizer Archiv für Angewandte Wissenschaft und Technik, Bd. 10, Heft 12, 1944.

13. Schlichting, H.: Berechnung der reibungslosen inkompressiblen Strömung für vorgegebenes ebenes Schaufelgitter. VDI Forschungsheft, 447, 1955.

14. Ohashi, H.: Analytical Study of Dynamic Characteristics of Turbopumps. Internal Note of George C. Marshall Space Flight Center, NASA, IN-P&VE-P-66-20, Huntsville, Alabama, 1966.

15. Newberry, M. H.: Random Vibration Analysis Program (RAVAN). NASA, Technical Memorandum, TM X-53359, 1965.

16. Vibration Committee of Marshall Space Flight Center, NASA: Vibration Manual. George C. Marshall Space Flight Center, NASA, Huntsville, Alabama, 1966.

BIBLIOGRAPHY

Schultz-Grunow, F.: Pulsierender Durchfluss durch Rohre. Forschung, Bd. 11, Heft 4, pp. 170 - 187, Juli/August 1940.

Thurston, G. B.: Periodic Fluid Flow Through Circular Tubes. Journal of the Acoustic Society of America, Vol. 24, No. 6, pp. 653 - 656, November 1952.

Oppenheim, A. K., and Chilton, E. G.: Pulsating-Flow Measurement, A Literature Survey. Transaction of ASME, Vol. 77, pp. 231-248, February 1955.

Uchida, S.: The Pulsating Viscous Flow Superposed on the Steady Laminar Motion of Incompressible Fluid. ZAMP, Bd. 7, Heft 5, pp. 403-422, July 1956.

Jones, W. P.: Research on Unsteady Flow. Journal of the Aerospace Sciences, Vol. 29, No. 3, pp. 249 - 263, March 1962.

Brown, F. T., and Nelson, S. E.: Step Responses of Liquid Lines with Frequency-Dependent Effects of Visocity. Transaction of ASME, Journal of Basic Engineering, Vol. 87, No. 2, pp. 504-510, June 1965.

Benson, R. S., and Whitfield, A.: An Experimental Investigation of the Non-Steady Flow Characteristics of a Centrifugal Compressor. PIME, Vol. 180, Part 1, 1965-66.

TABLE I. VALUE OF $\Gamma\ (1/2 + i\omega)/\sqrt{\pi}\ \Gamma\ (1 + i\omega)$

$$\frac{\Gamma(\frac{1}{2} + i\omega)}{\sqrt{\pi}\,\Gamma(1 + i\omega)} = R + iI = \rho e^{i\theta}$$

ω	R	I	ρ	$\theta°$
0	1	0	1	0
0.01	1.000	-0.014	1.000	- 0.79
0.03	0.998	-0.041	0.999	- 2.38
0.1	0.975	-0.134	0.984	- 7.81
0.2	0.910	-0.242	0.941	-14.89
0.3	0.826	-0.314	0.884	-20.80
0.5	0.669	-0.372	0.764	-29.04
0.7	0.554	-0.371	0.666	-33.75
1.0	0.447	-0.342	0.563	-37.44
1.5	0.352	-0.297	0.461	-40.12
2	0.299	-0.264	0.402	-41.38
3	0.240	-0.221	0.326	-42.60
5	0.183	-0.174	0.252	-43.57
10	0.127	-0.124	0.178	-44.28
30	0.074	-0.073	0.103	-44.77
100	0.042	-0.042	0.056	-45.00
∞	0	0	0	(-45)

TABLE II. SPECIFICATION OF TEST PUMP

Model / Manufacturer	$1\frac{1}{2}$ CCL / Buffalo Pumps, N.Y.
Suction / Discharge Diameter	2 inch / $1\frac{1}{2}$ inch
Impeller Type	Radial Impeller with Backward Vanes
Outer Diameter	6.632 inch
Exit Width	0.260 inch
Number of Vanes	6
Exit Angle of Vanes	35^{o}
Material	Bronze
Diffusor Type	Vaneless Volute Chamber
Casing Material	Cast Iron
Normal Operating Condition	
Rotational Speed	3,500 rpm (58.33 rps)
Flow Rate	120 gpm
Head Rise	150 ft
Power Required	10 HP

TABLE III. TEST PROGRAM

Series NO.	description of test	test pump n (rps)	test pump Q_o (gpm)	test pump $\Delta Q/Q_o$	actuating system hyd. pump	actuating system f (Hz)	valve settings	measurement main items	record on o-gram	record on tape
1	preliminary test to check pressure fluctuation caused by hyd. pump	0 (stop)	0	0	run (2500 psi)	0	AV: open & closed CV: varied	p_s, p_d, p_d-p_s, Q_{MHD} & $Q_{turb.}$	X	
2	preliminary test to check pressure fluctuation at min. disturbance	0	0 to max.	0	stop	0	DS: closed DV: open CV: varied	ditto	X	
3	steady-state characteristics	60	0 to max.	0	stop	0	regular	ditto	X	
4	pulsating test at $\phi = \phi_D$	60	200	0.1 or less	run	1 to 100	regular	ditto	X	X
5	pulsating test at $\phi = \frac{1}{2}\phi_D$	60	100	0.1 or less	run	1 to 100	regular	ditto	X	X
6	linearity test	60	200	0.02 to max.	run	3 & 10	regular	ditto	X	X
7	steady-state characteristics	30	0 to max.	0	stop	0	regular	ditto	X	
8	pulsating test at $\phi = \phi_D$	30	100	0.1 or less	run	1 to 100	regular	ditto	X	X
9	pulsating test at $\phi = \frac{1}{2}\phi_D$	30	50	0.1 or less	run	1 to 100	regular	ditto	X	X
10	linearity test	30	100	0.02 to max.	run	3 & 10	regular	ditto	X	X
11	steady-state characteristics	15	0 to max.	0	stop	0	regular	ditto	X	
12	pulsating test at $\phi = \phi_D$	15	50	0.1 or less	run	1 to 100	regular	ditto	X	X
13	pulsating test at $\phi = \frac{1}{2}\phi_D$	15	25	0.1 or less	run	1 to 100	regular	ditto	X	X
14	linearity test	15	50	0.02 to max.	run	3 & 10	regular	ditto	X	X
15	pressure fluctuation caused by actuator motion only	0	0	∞	run	1 to 40	regualr	ditto	X	X

Regular valve settings; suction stop v., delivery stop v. (DS), accumulator v. (AV).....open, drain v (DV).....closed, control v. (CV).....adjusted.

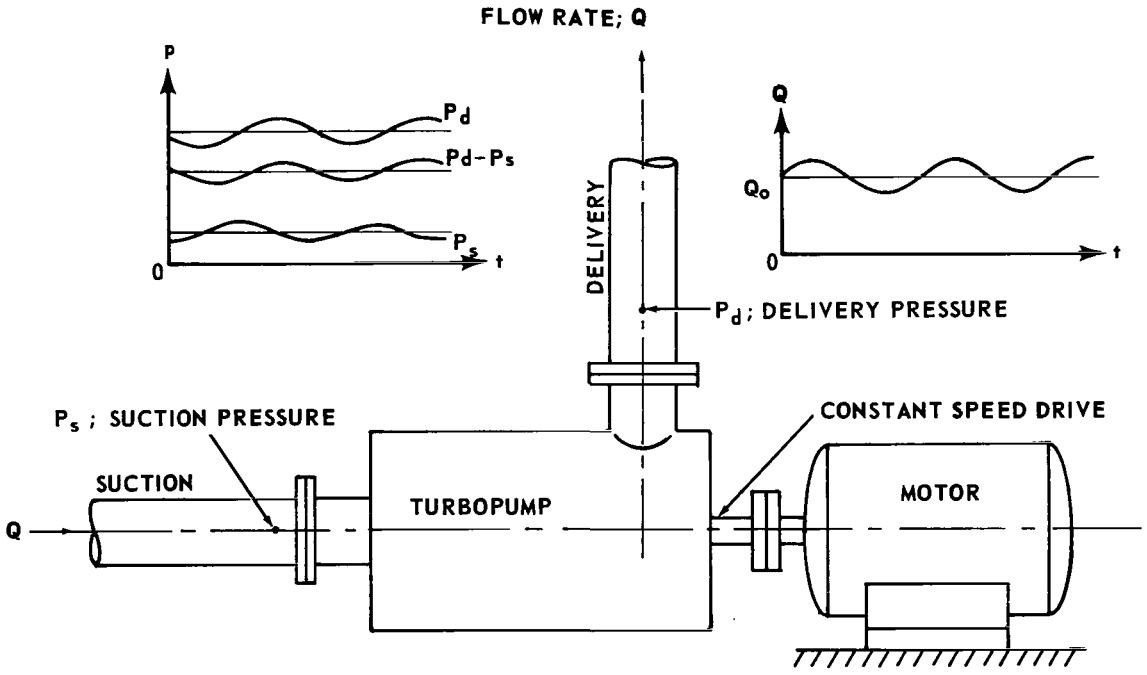

FIGURE 1. UNSTEADY OPERATION OF A TURBOPUMP; FLOW RATE AND PRESSURE FLUCTUATE PERIODICALLY

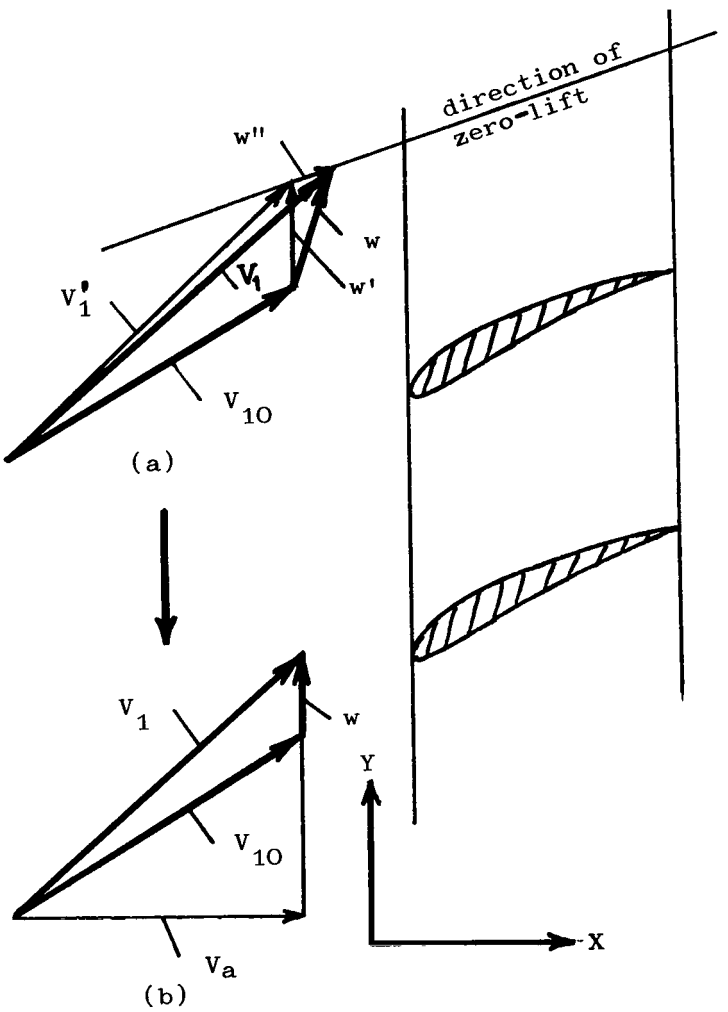

FIGURE 2. UNSTEADY FLOW THROUGH A CASCADE

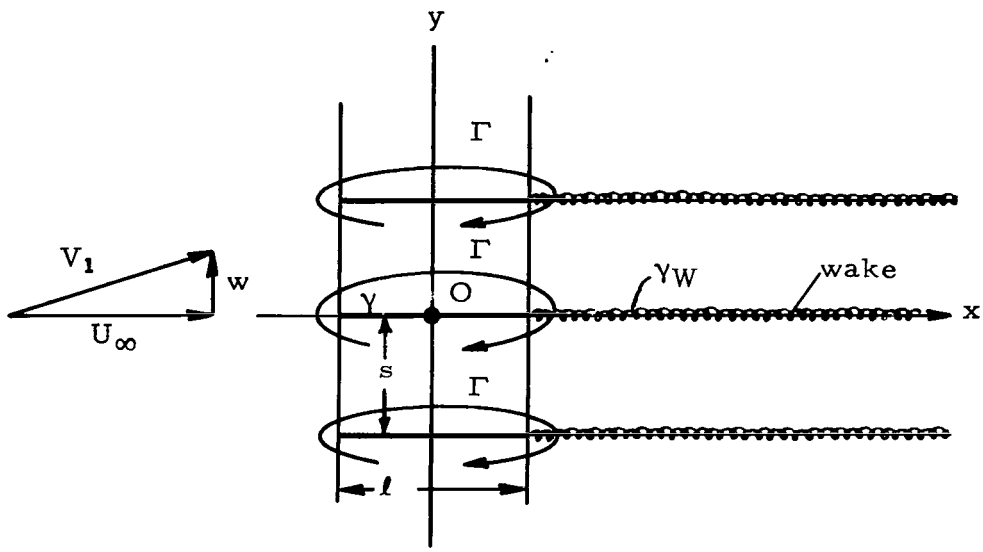

FIGURE 3. FLOW CONFIGURATION AROUND A CASCADE OF NONSTAGGERED FLAT PLATES

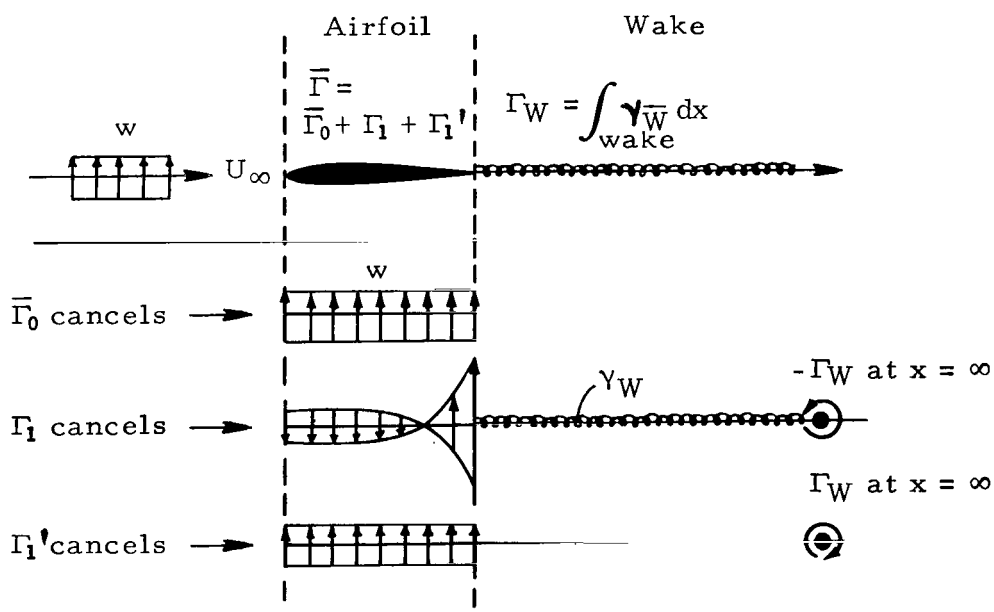

FIGURE 4. THREE KINDS OF CIRCULATION FOR TRANSLATORY OSCILLATION

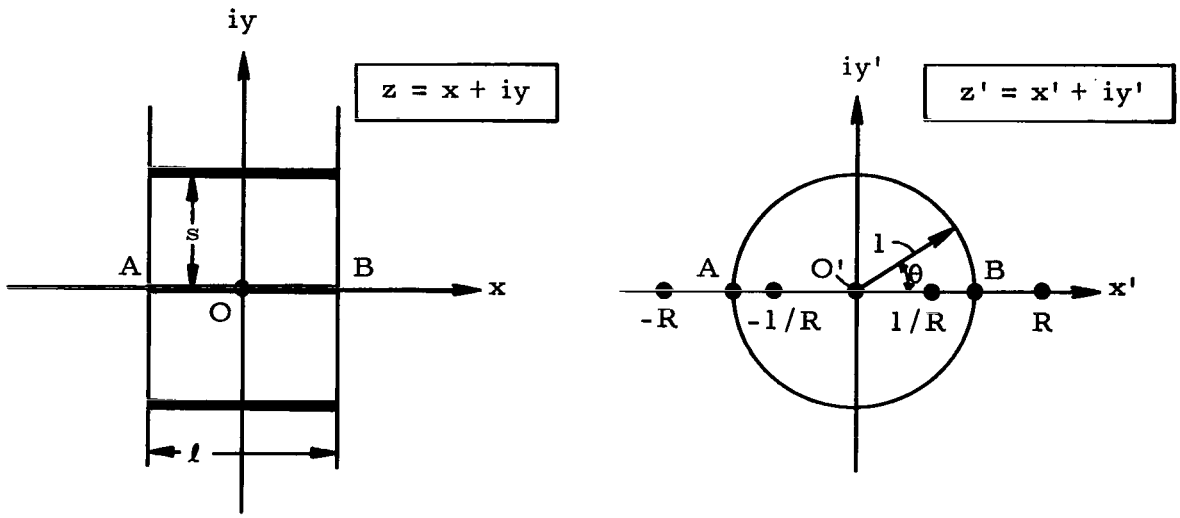

FIGURE 5. CONFORMAL TRANSFORMATION INTO UNIT CIRCLE

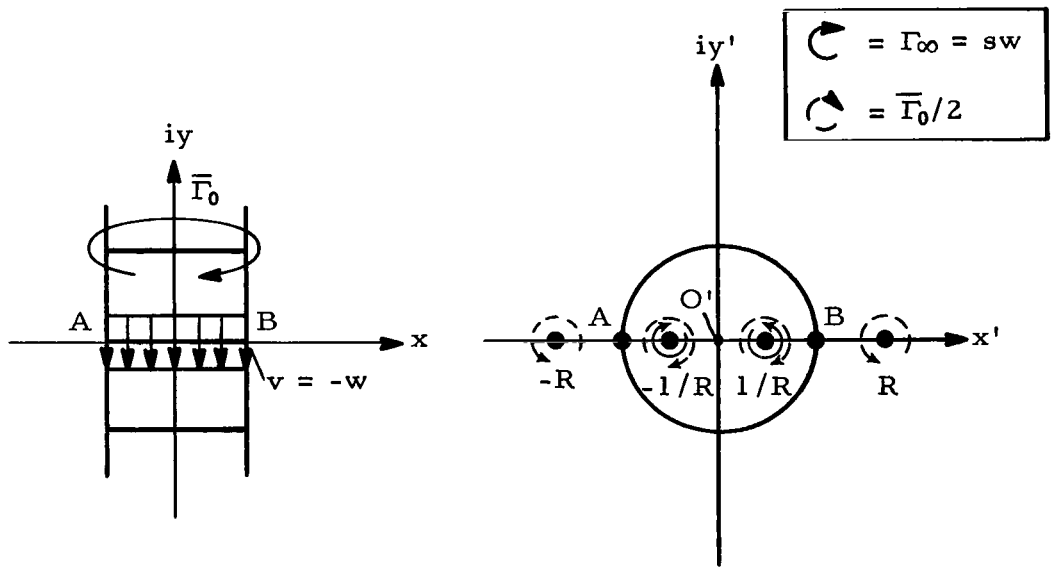

FIGURE 6. DETERMINATION OF $\bar{\Gamma}_0$

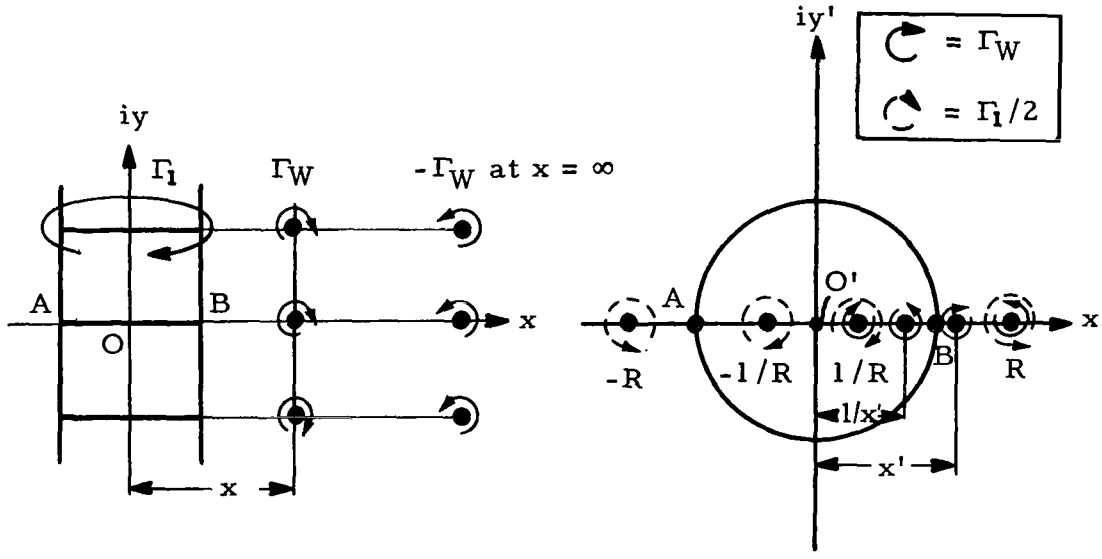

FIGURE 7. DETERMINATION OF Γ_1

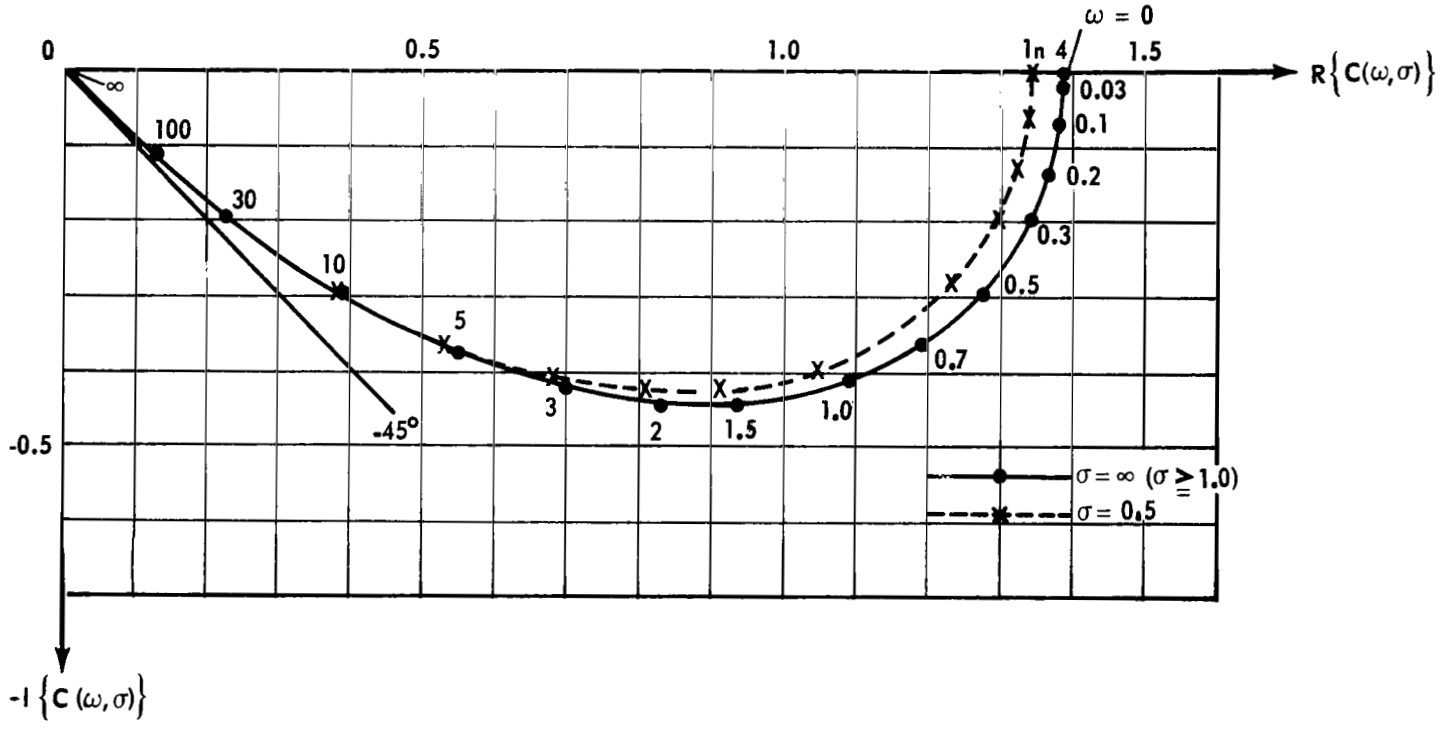

FIGURE 8. COUPLING FUNCTION, $C(\omega, \sigma)$

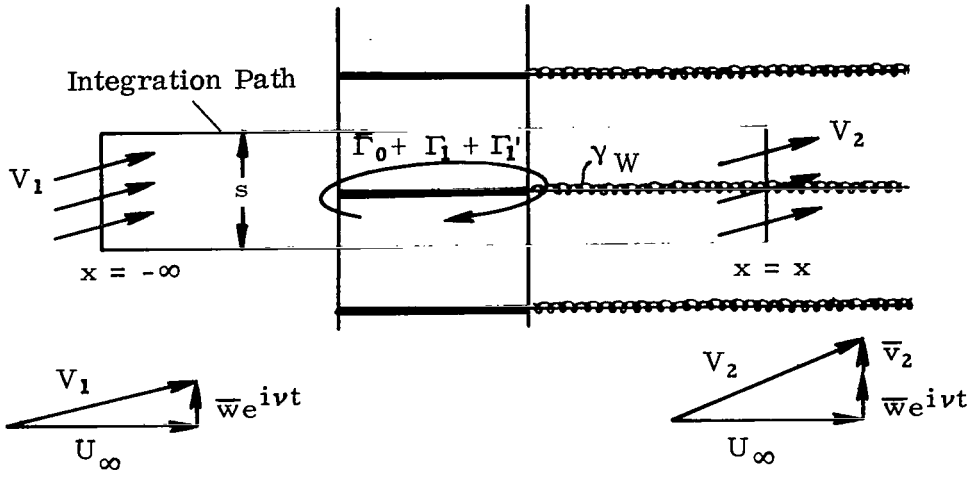

FIGURE 9. CIRCULATION ENCLOSED IN INTEGRATION PATH

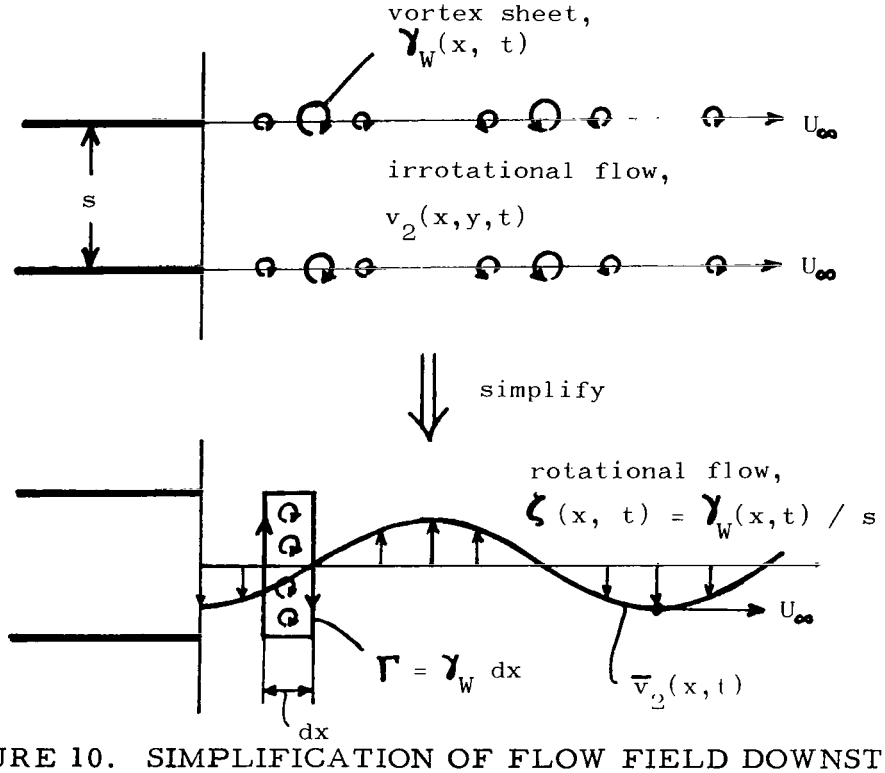

FIGURE 10. SIMPLIFICATION OF FLOW FIELD DOWNSTREAM OF THE CASCADE

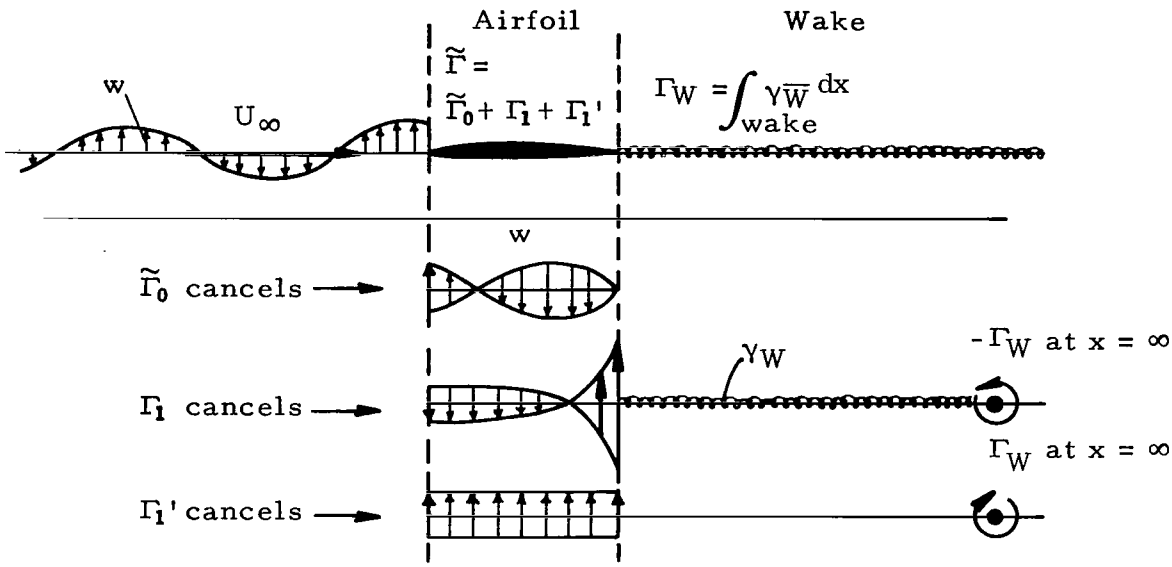

FIGURE 11. THREE KINDS OF CIRCULATION FOR SINUSOIDAL GUST OSCILLATION

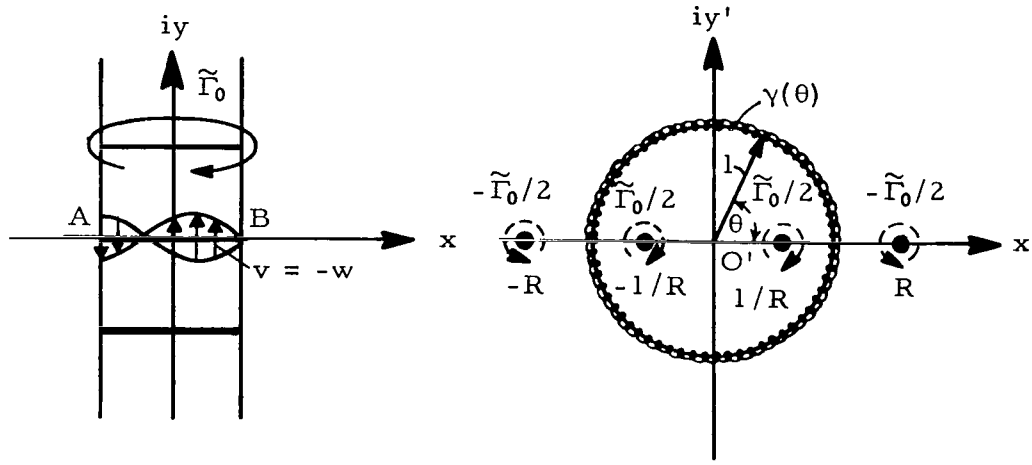

FIGURE 12. DETERMINATION OF $\tilde{\Gamma}_0$

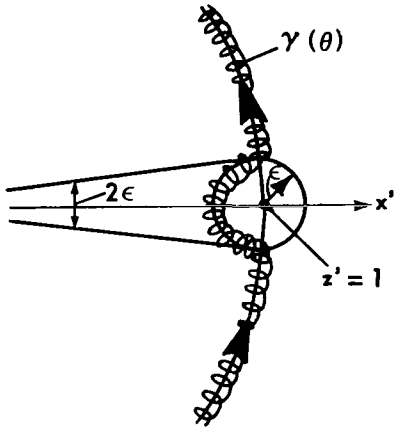

FIGURE 13. INTEGRATION PATH FOR CALCULATION OF INDUCED VELOCITY

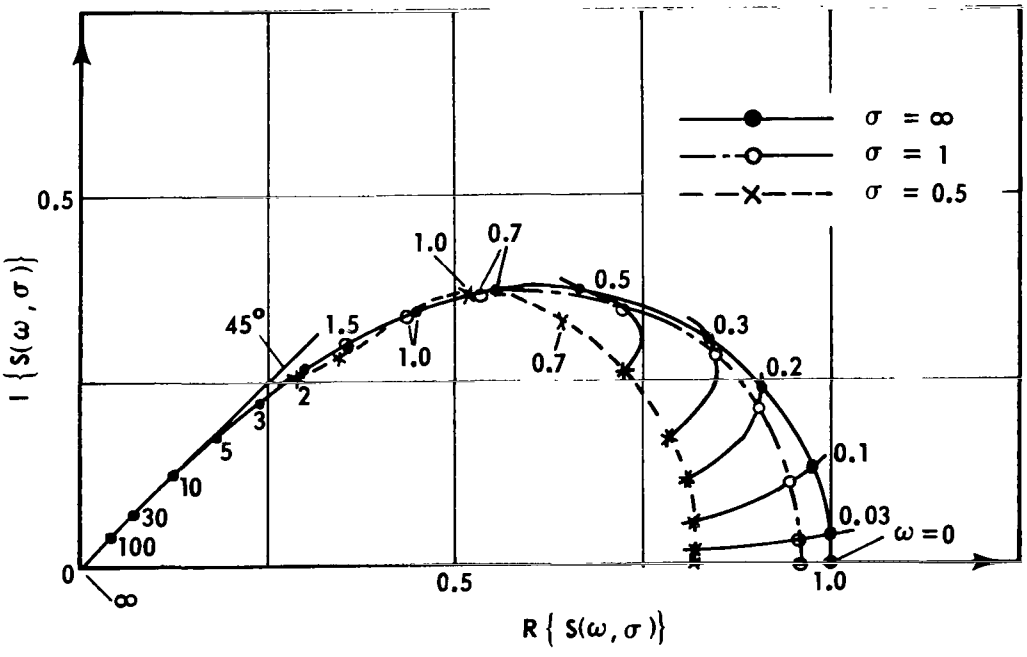

FIGURE 14. SINUSOIDAL GUST FUNCTION, S(ω, σ)

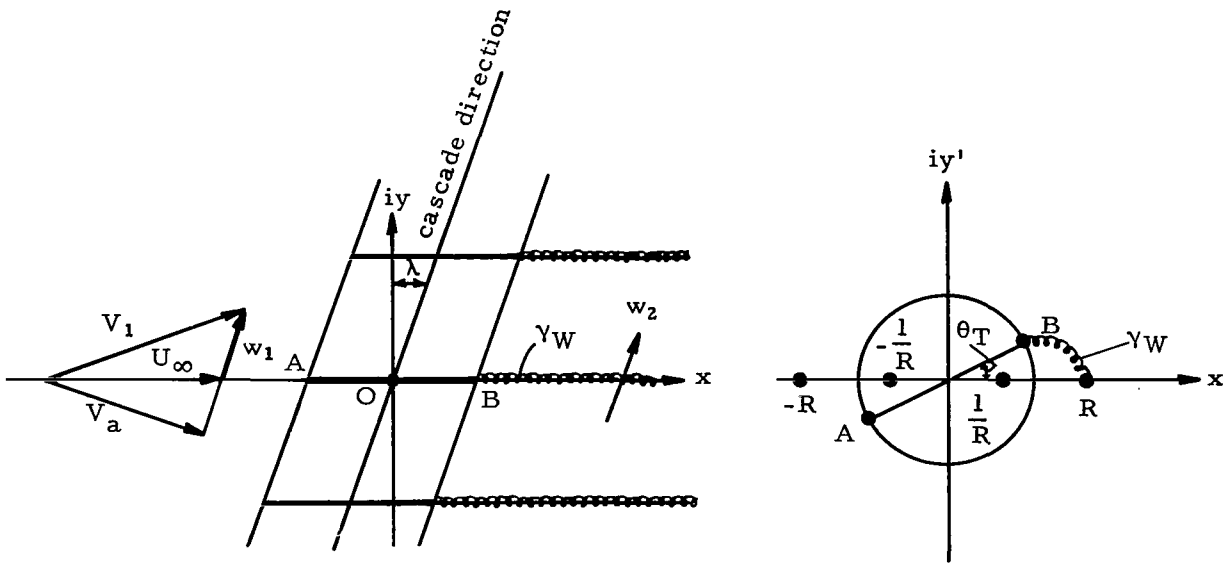

(a) z-plane (b) z'-plane

FIGURE 15. UNSTEADY FLOW THROUGH A STAGGERED CASCADE

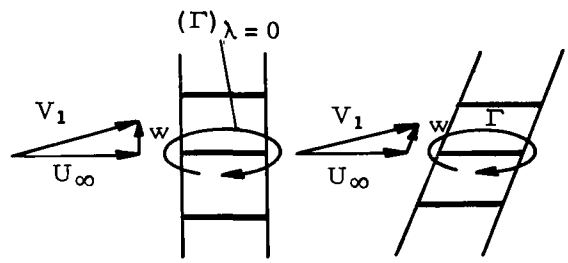

FIGURE 16. COMPARISON OF CIRCULATION FOR STAGGERED AND NONSTAGGERED CASCADES

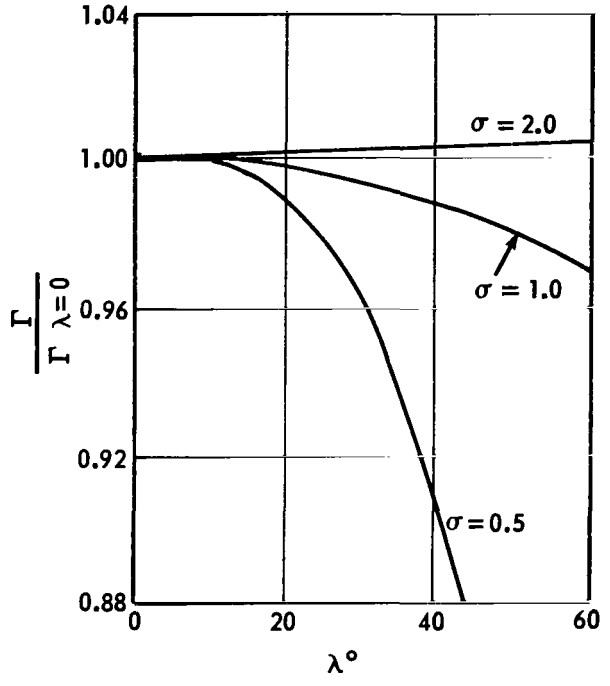

FIGURE 17. EFFECT OF STAGGER ANGLE ON THE CIRCULATION OF AN AIRFOIL IN A CASCADE

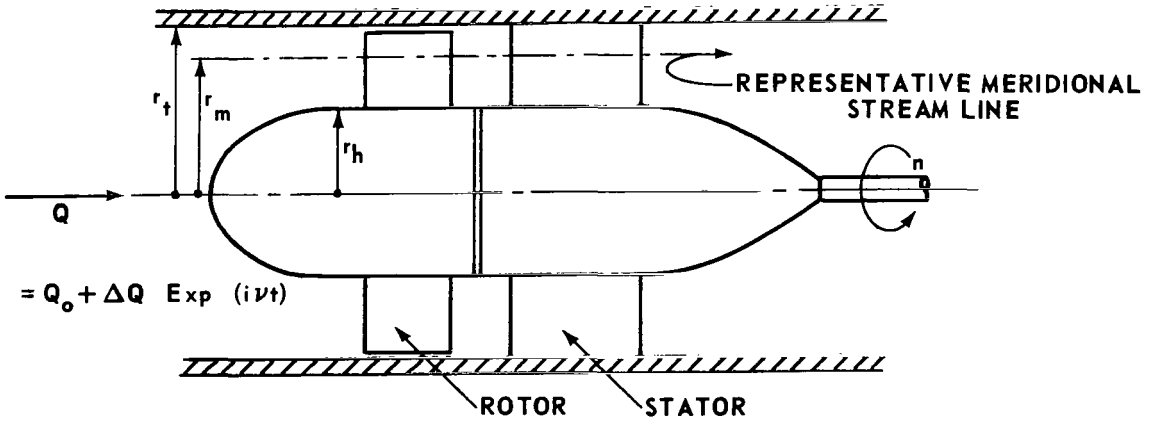

FIGURE 18. SINGLE-STAGE AXIAL FLOW PUMP FOR ANALYSIS

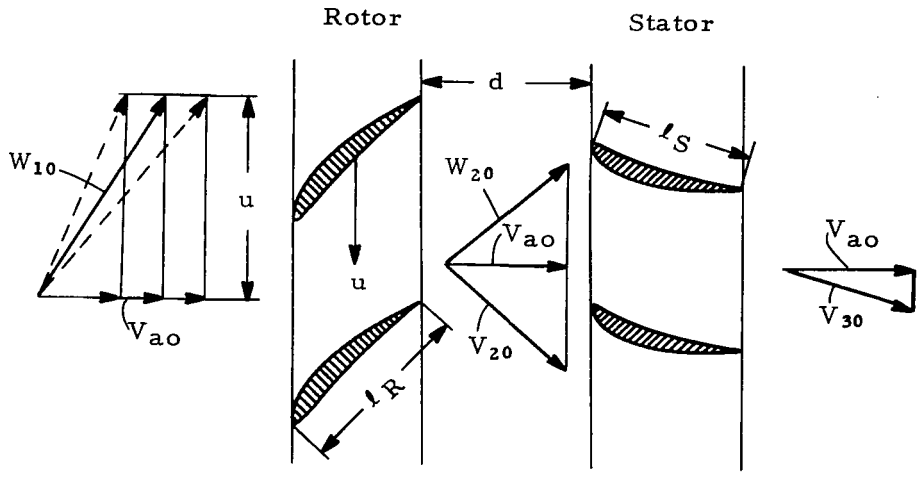

FIGURE 19. MEAN VELOCITY TRIANGLES OF A STAGE

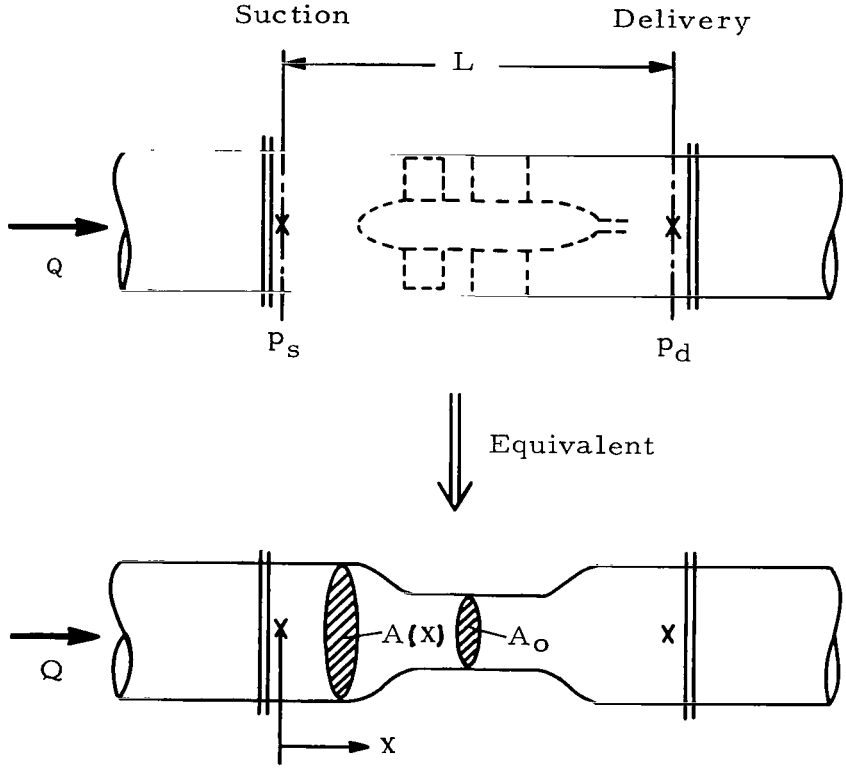

FIGURE 20. PRESSURE FLUCTUATION AS A CONDUIT

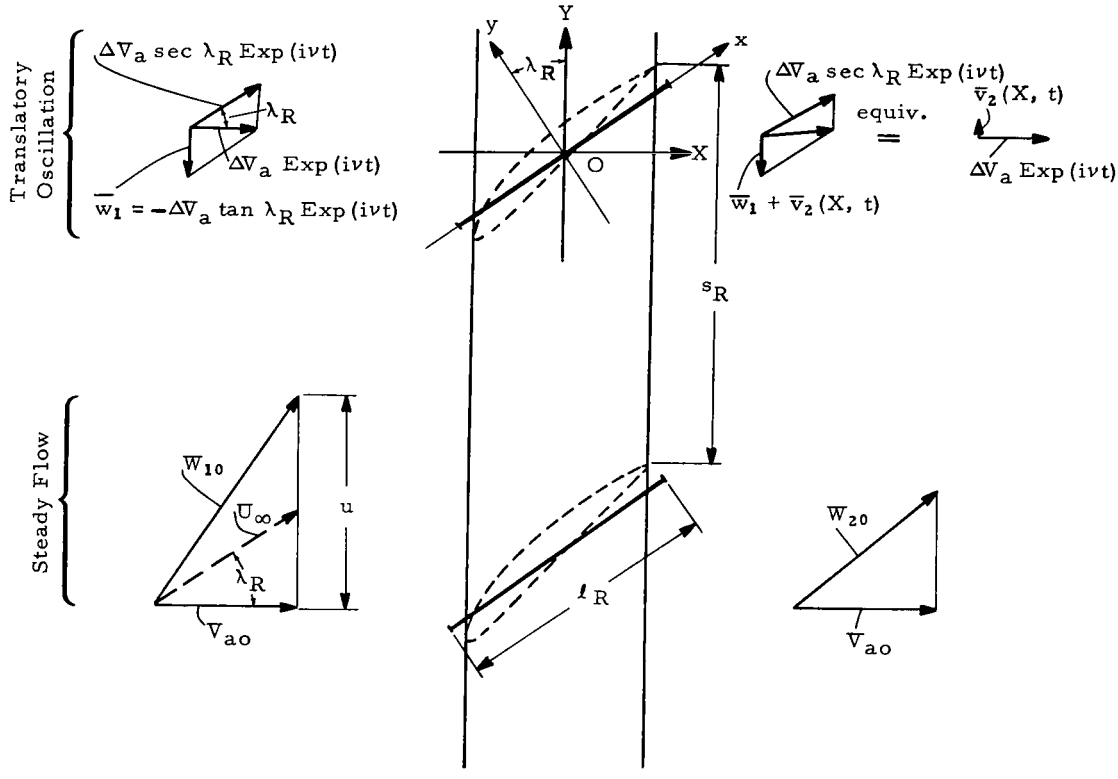

FIGURE 21. STEADY AND UNSTEADY FLOW FIELD AROUND A ROTOR

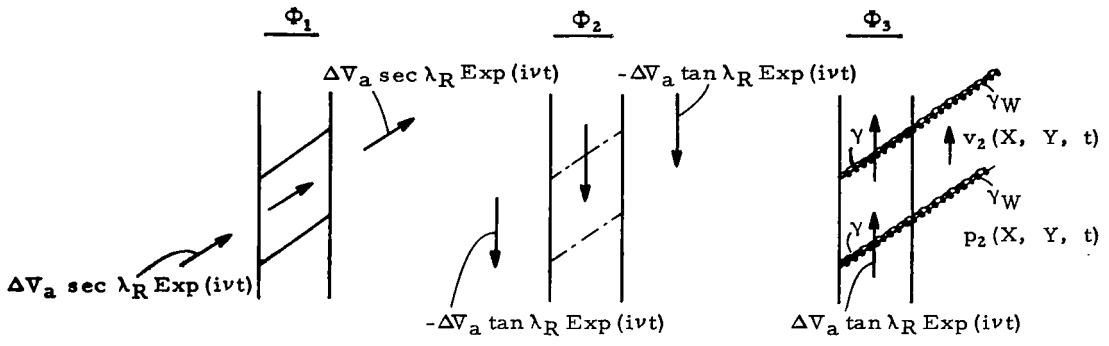

(a) Through-Flow (b) Vertical Flow (c) Induced Flow

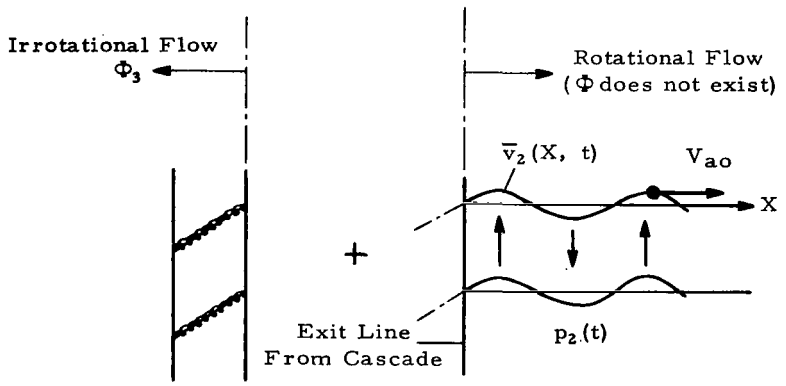

(d) Simplified Induced Flow

FIGURE 22. VELOCITY POTENTIAL CORRESPONDING TO EACH UNSTEADY FLOW ELEMENT

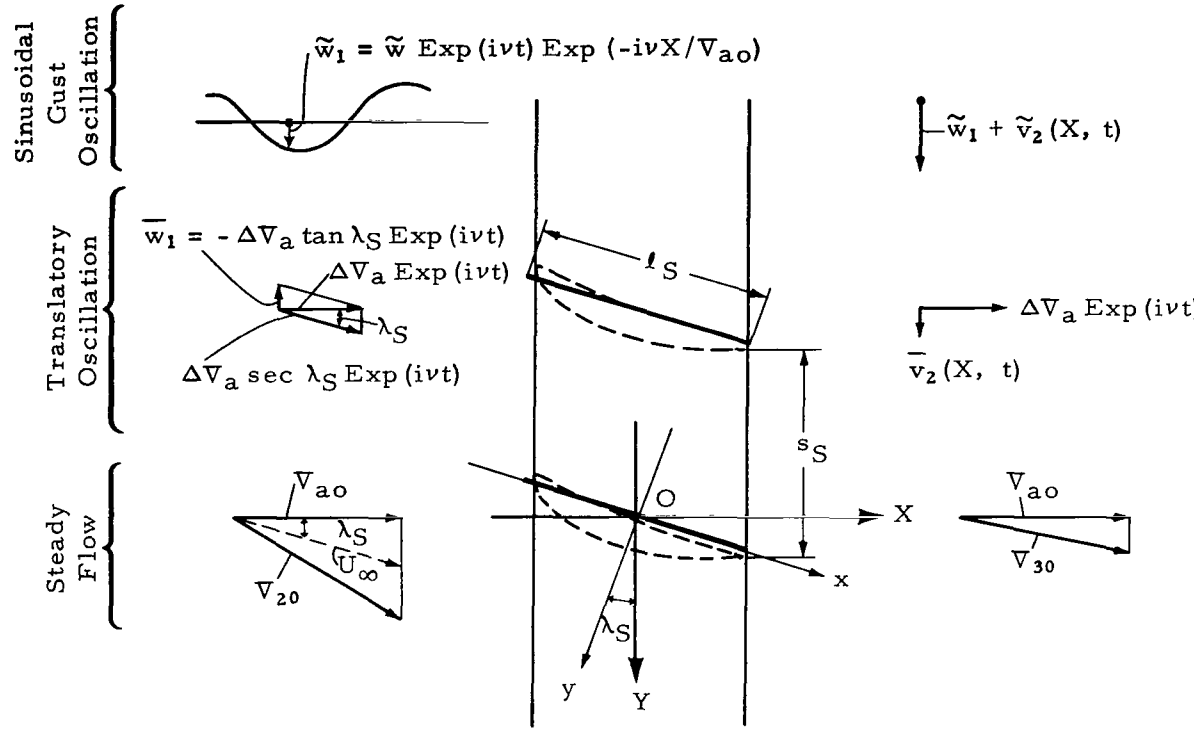

FIGURE 23. STEADY AND UNSTEADY FLOW FIELD AROUND A STATOR

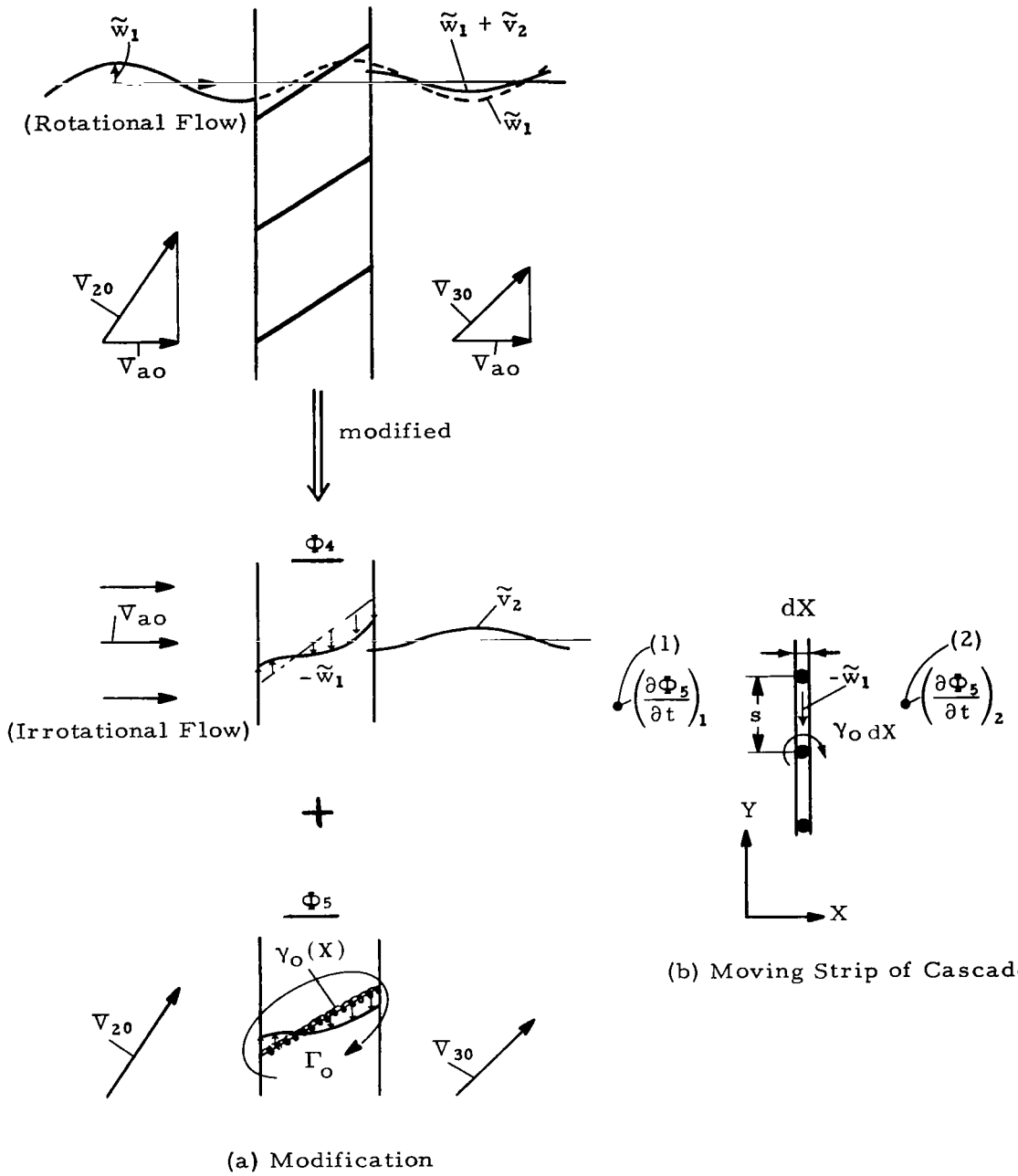

(a) Modification

(b) Moving Strip of Cascade

FIGURE 24. VELOCITY POTENTIAL CAUSED BY SINUSOIDAL GUST OSCILLATION

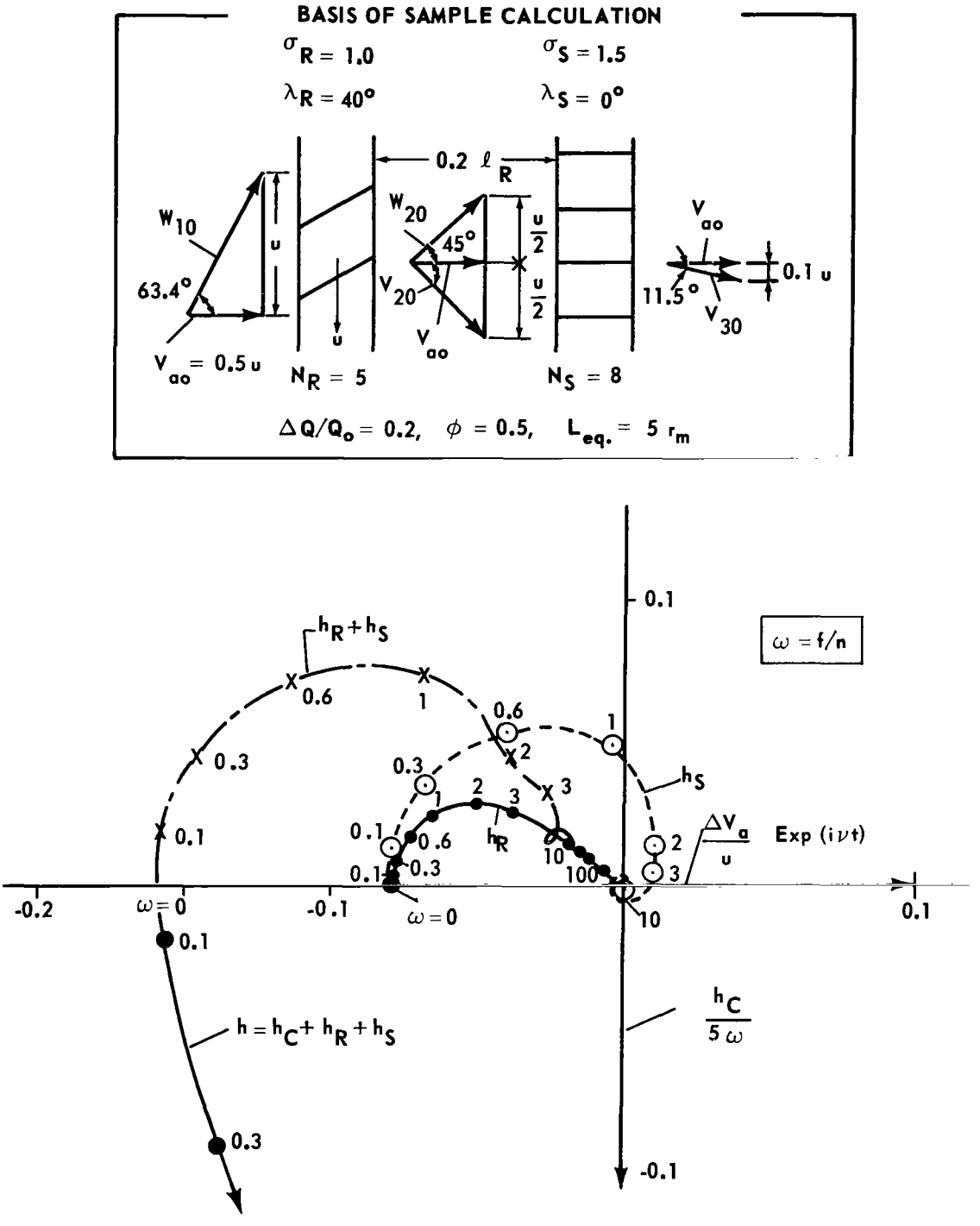

FIGURE 25. DYNAMIC CHARACTERISTICS OF A SINGLE-STAGE AXIAL FLOW PUMP

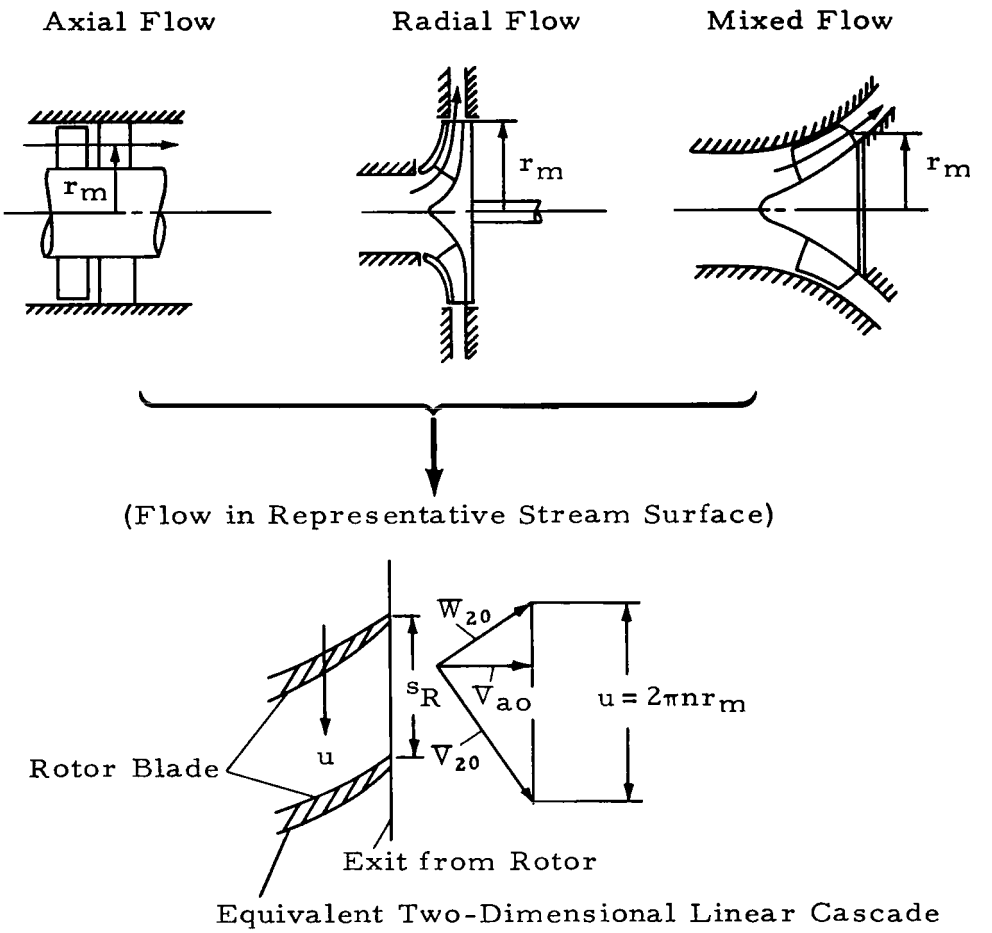

FIGURE 26. CALCULATION OF SIMPLIFIED DYNAMIC CHARACTERISTICS

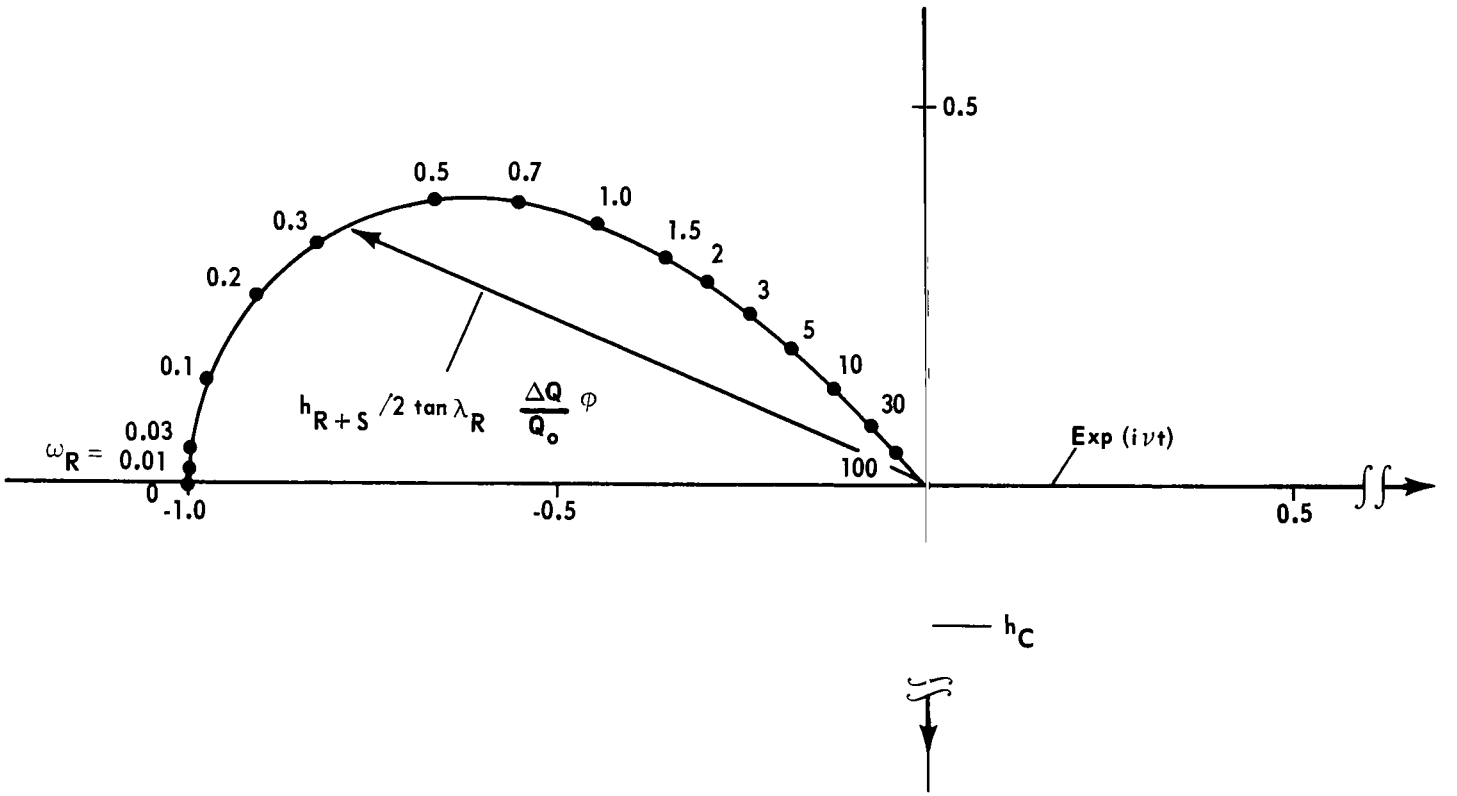

FIGURE 27. SIMPLIFIED DYNAMIC CHARACTERISTICS OF A TURBOPUMP

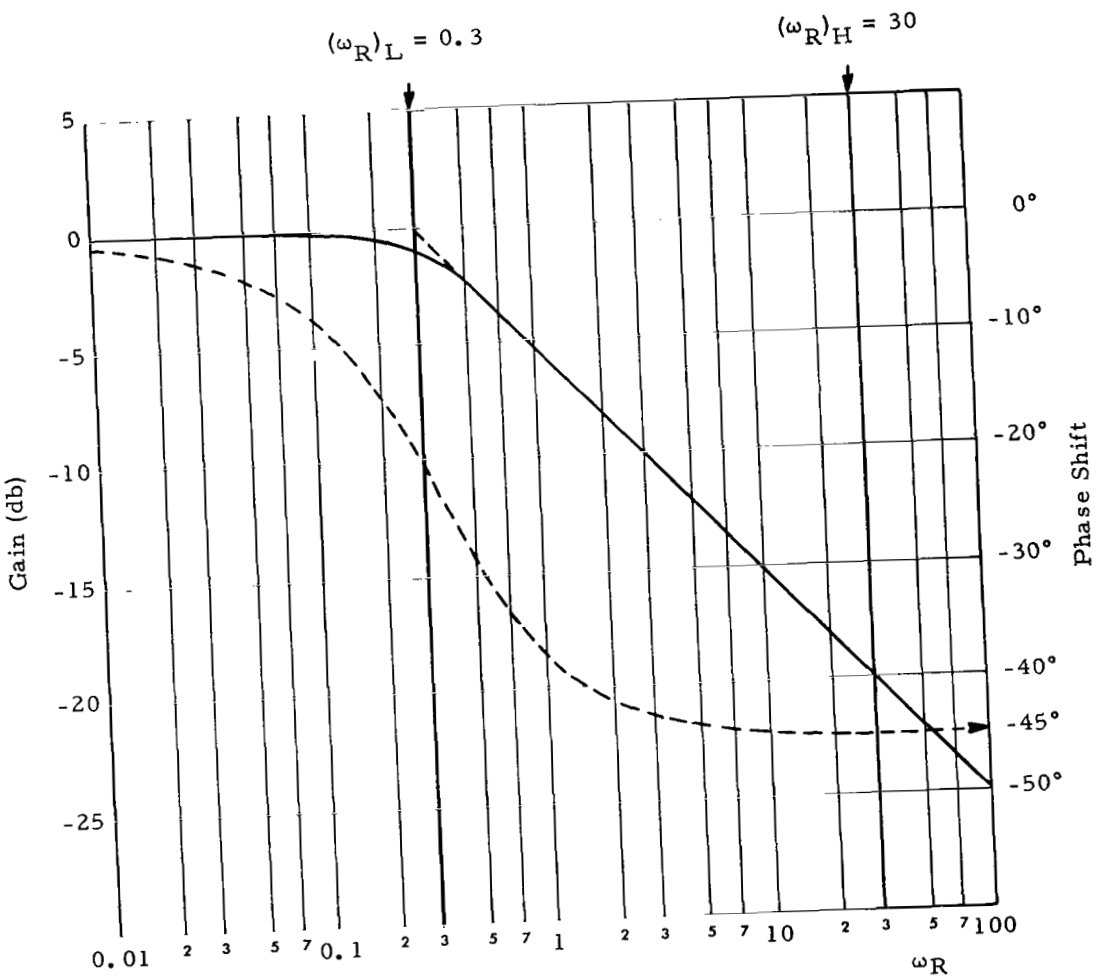

FIGURE 28. BODE DIAGRAM OF $h_R + S/(h_R + S)_{qs}$

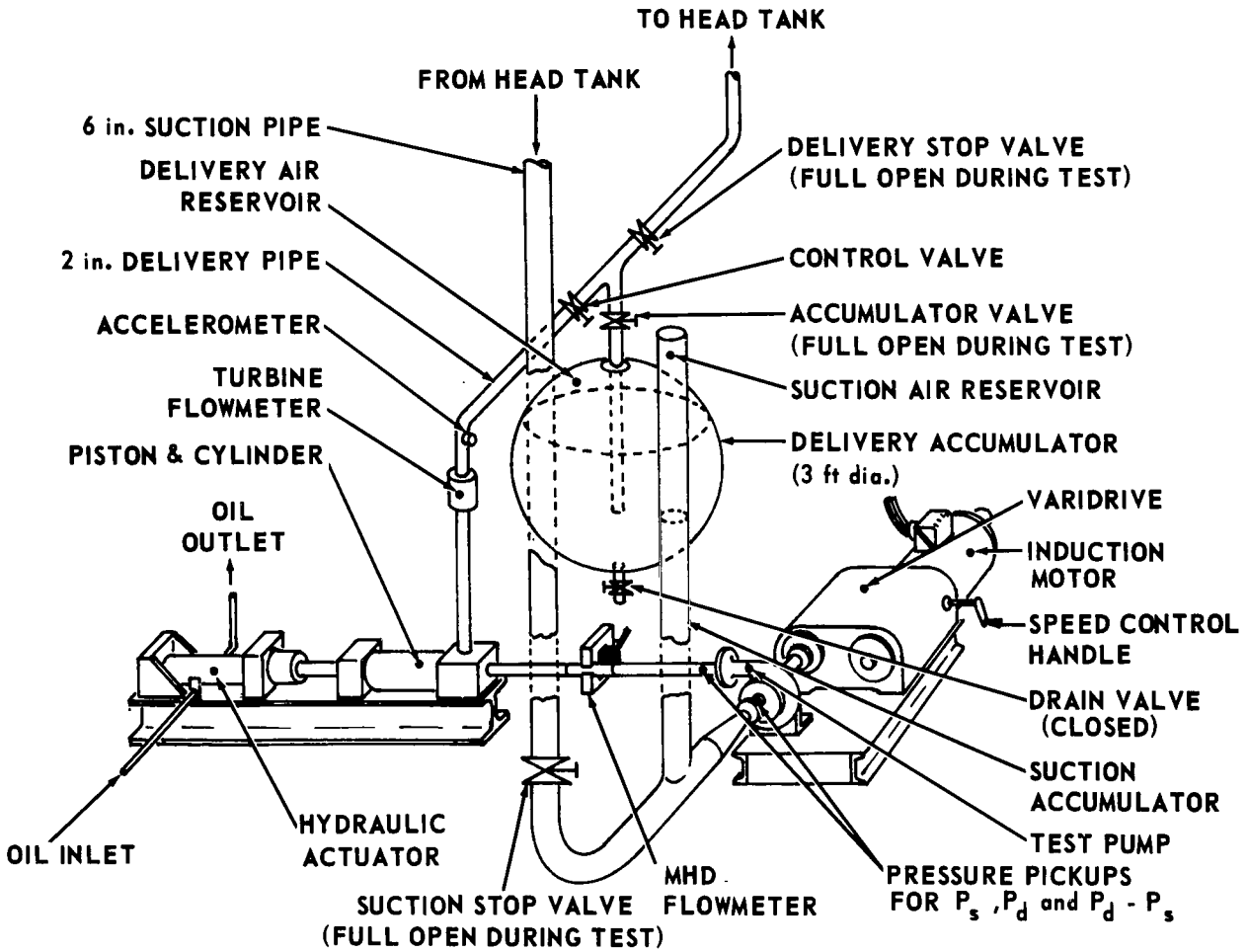

FIGURE 29. SCHEMATIC VIEW OF THE EXPERIMENTAL ARRANGEMENT

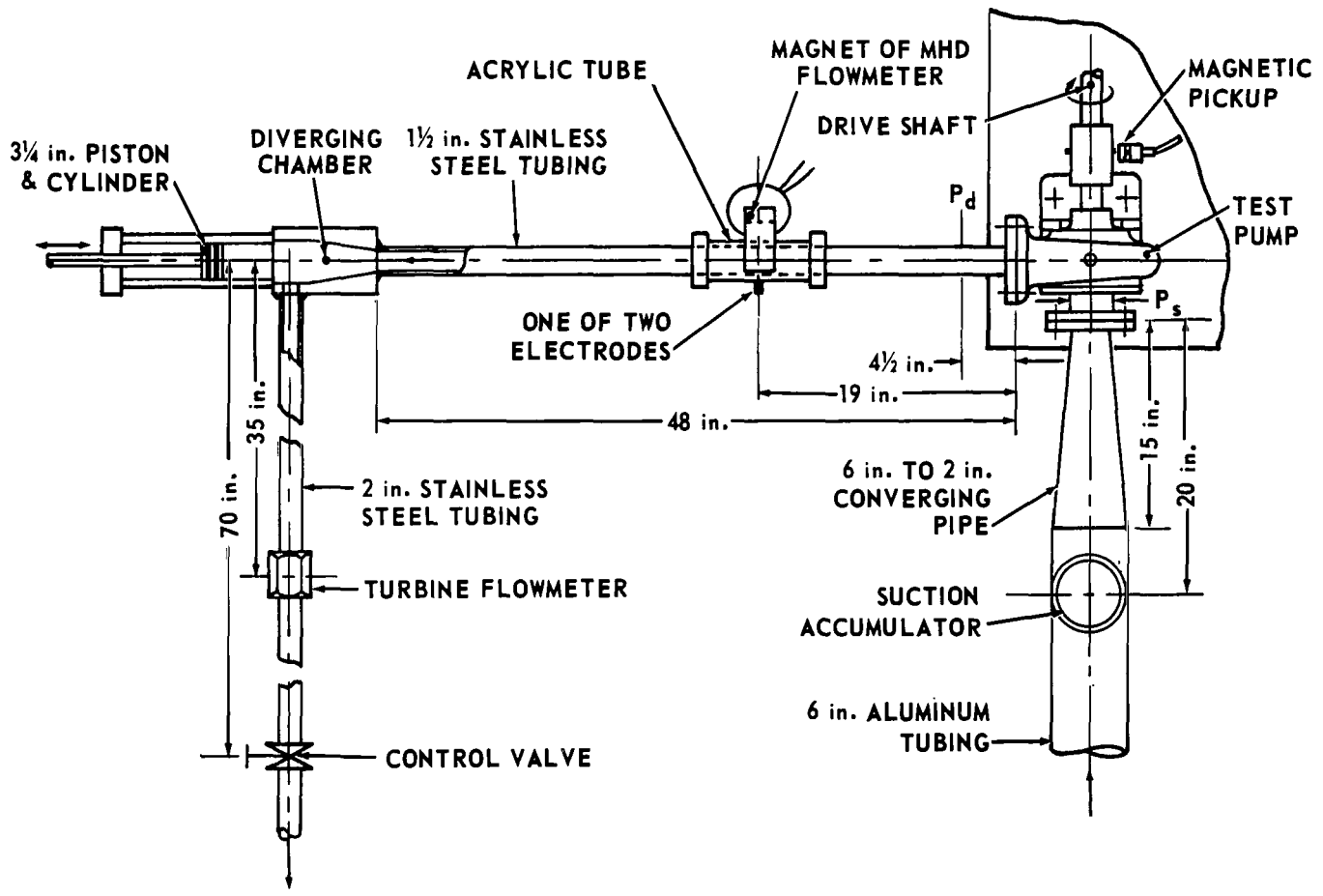

FIGURE 30. DETAILS OF THE PUMPING AND PULSATING SYSTEM

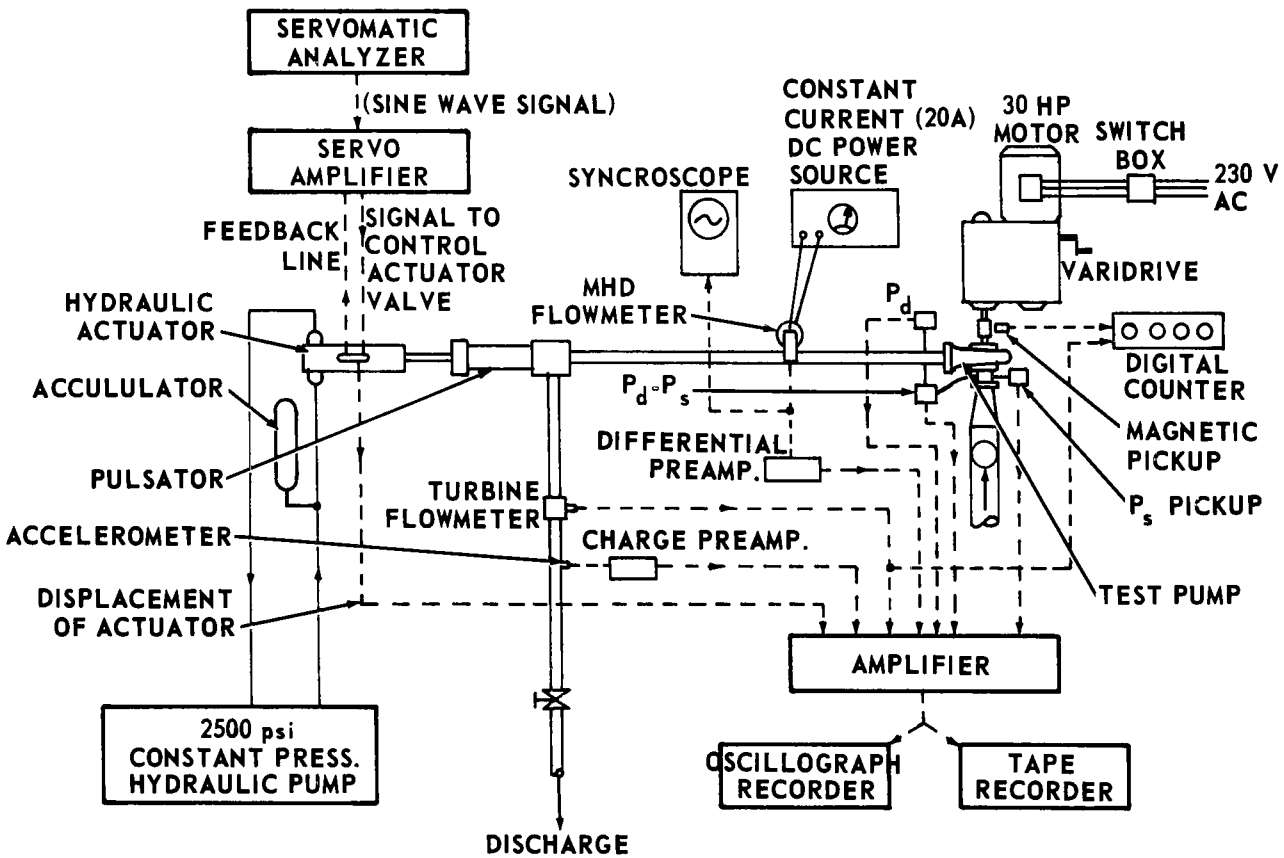

FIGURE 31. SCHEMATIC DIAGRAM OF THE MEASUREMENT AND CONTROL SYSTEM

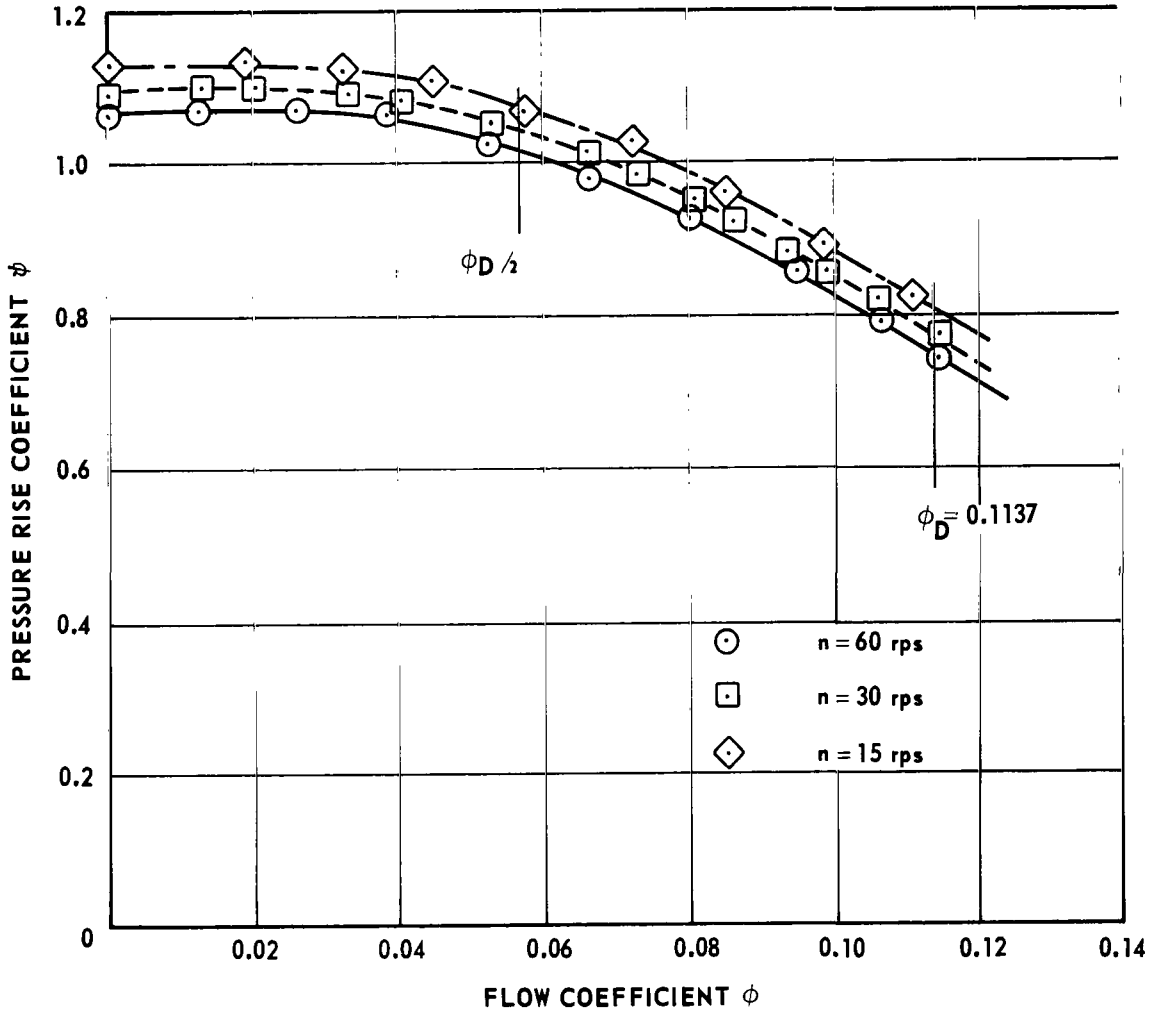

FIGURE 30. NONDIMENSIONAL STEADY - STATE CHARACTERISTICS OF THE TEST PUMP

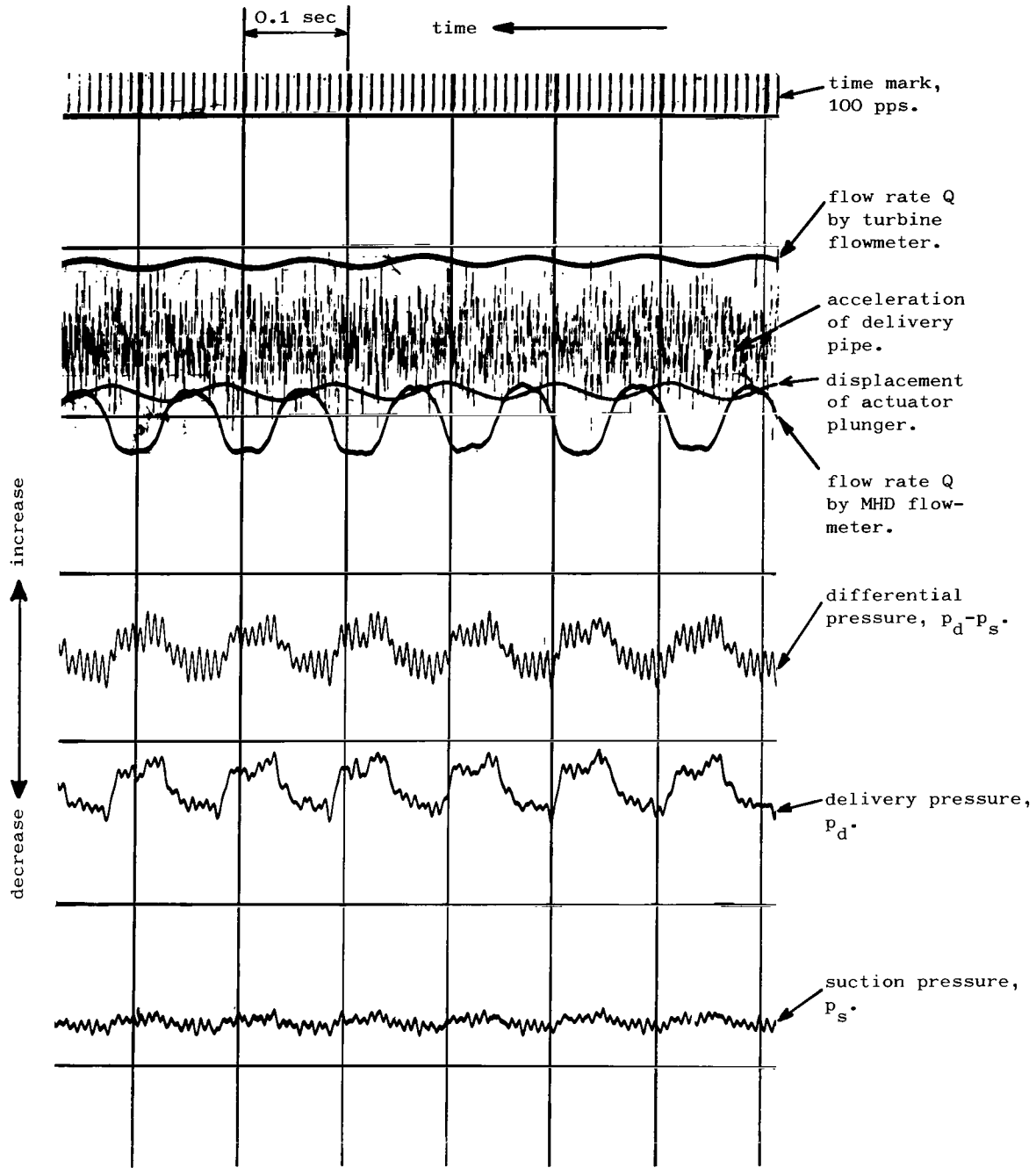

($p_d - p_s$, p_d and p_s were recorded through 100 Hz low-pass filter.)

FIGURE 33. TYPICAL OSCILLOGRAPH RECORDING OF UNSTEADY-STATE OPERATION: n = 60 rps, Q_o = 200 gpm, f = 10 Hz, $\Delta Q/Q_o \approx 0.1$ (SERIES 4)

FIGURE 34-1 TO 34-18 TYPICAL SC 4020 PLOTTER OUTPUTS PROCESSED BY THE RANDOM VIBRATION ANALYSIS PROGRAM (RAVAN): n = 60 rps, Q_o = gpm, f = 10 Hz, $\Delta Q/Q_o \approx 0.1$ (SERIES 4)

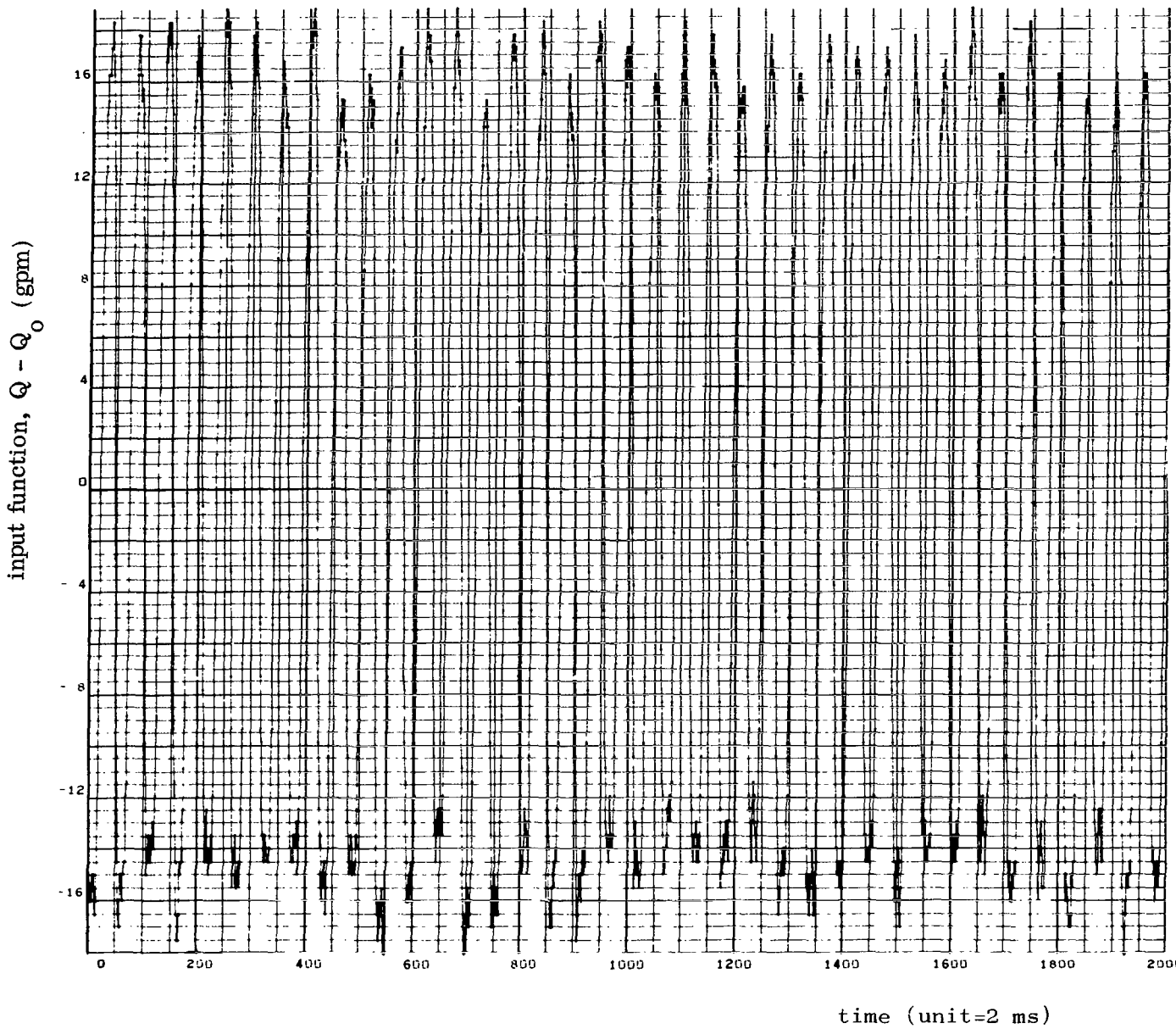

FIGURE 34-1. PLOT OF Q - Q_o INPUT FUNCTION VERSUS TIME

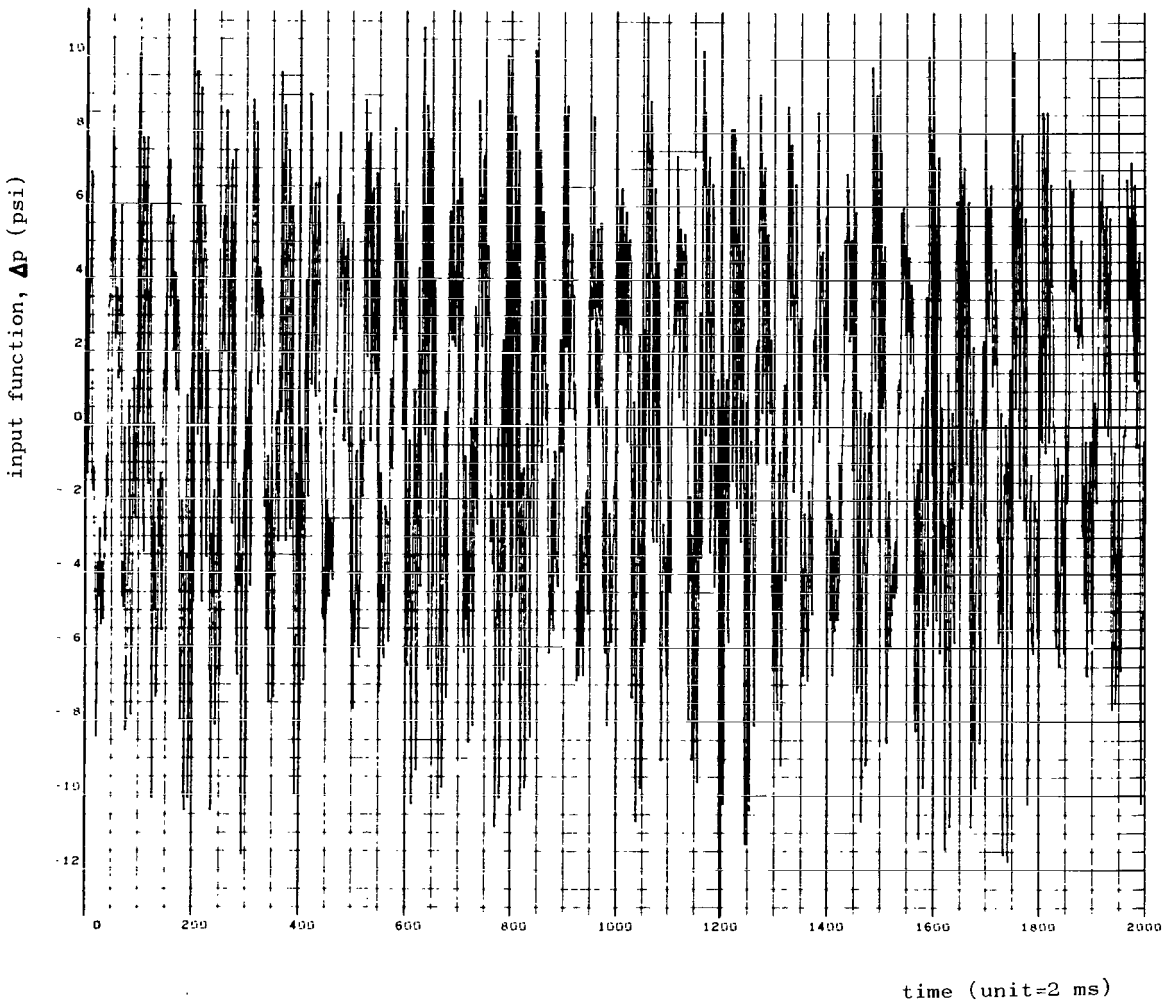

FIGURE 34-2. PLOT OF $\Delta p = (p_d - p_s) - (p_d - p_s)_o$ INPUT FUNCTION VERSUS TIME

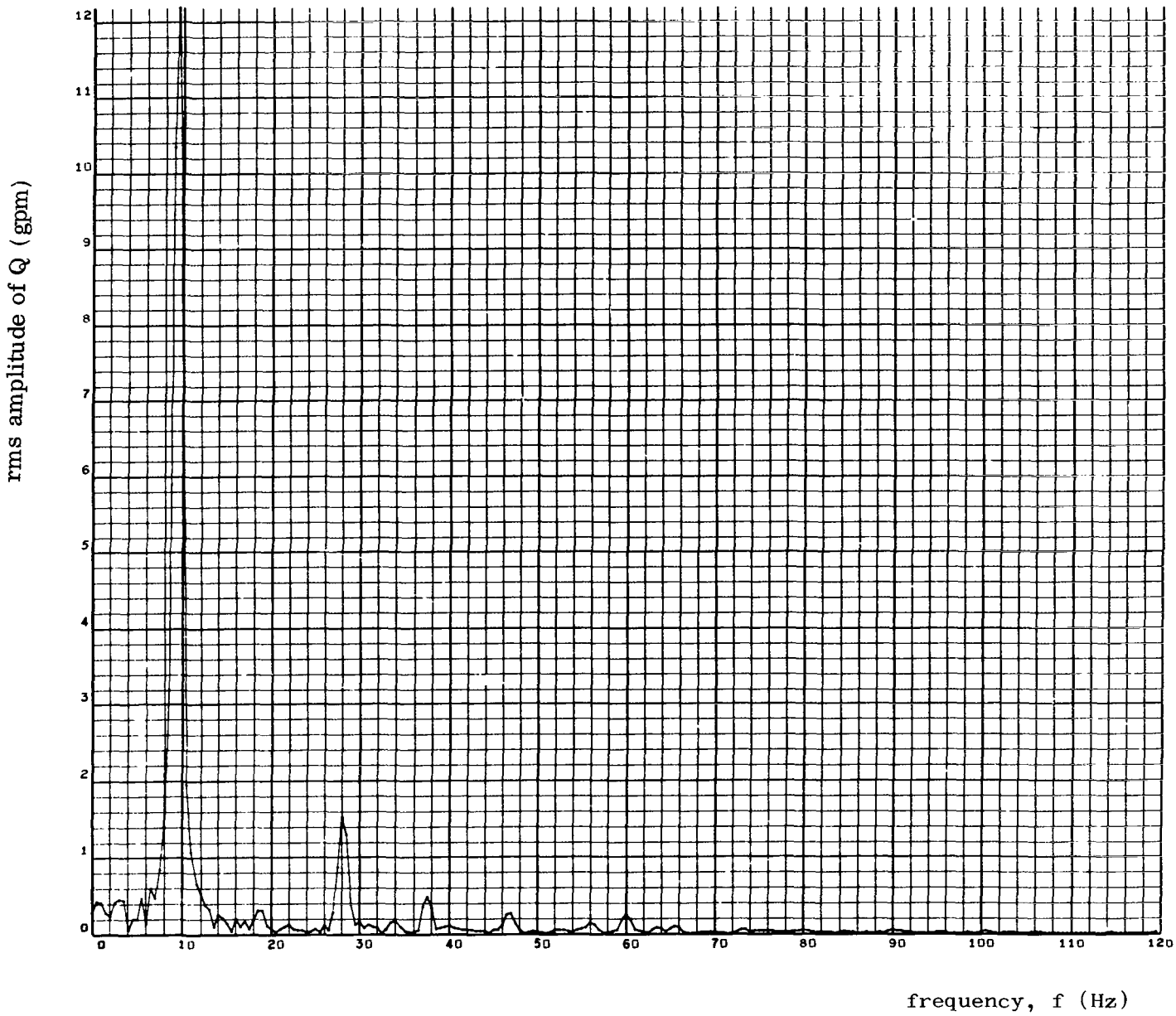

FIGURE 34-3. rms AMPLITUDE DISTRIBUTION OF Q VERSUS FREQUENCY

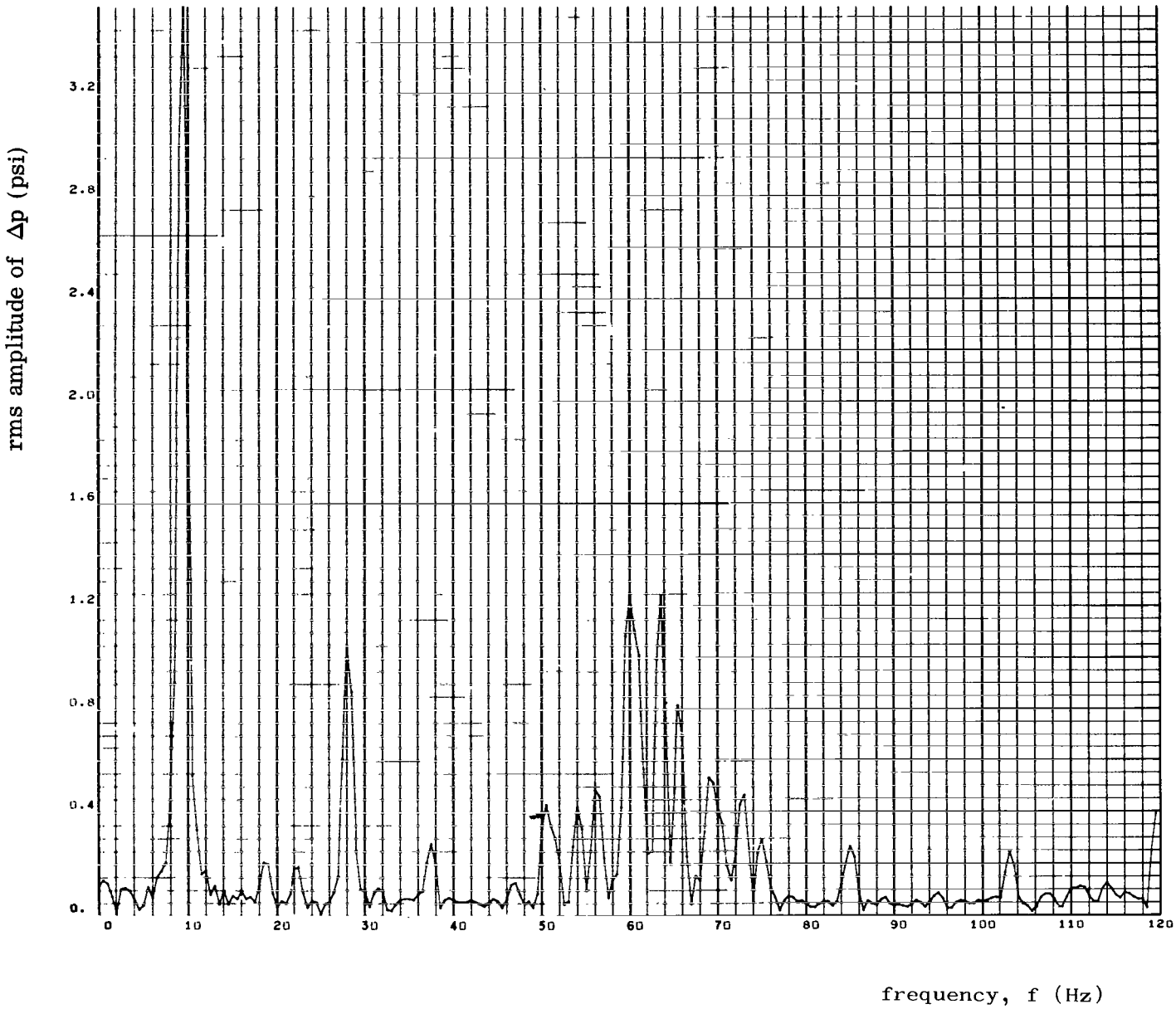

FIGURE 34-4. rms AMPLITUDE DISTRIBUTION OF PRESSURE RISE, Δp, VERSUS FREQUENCY

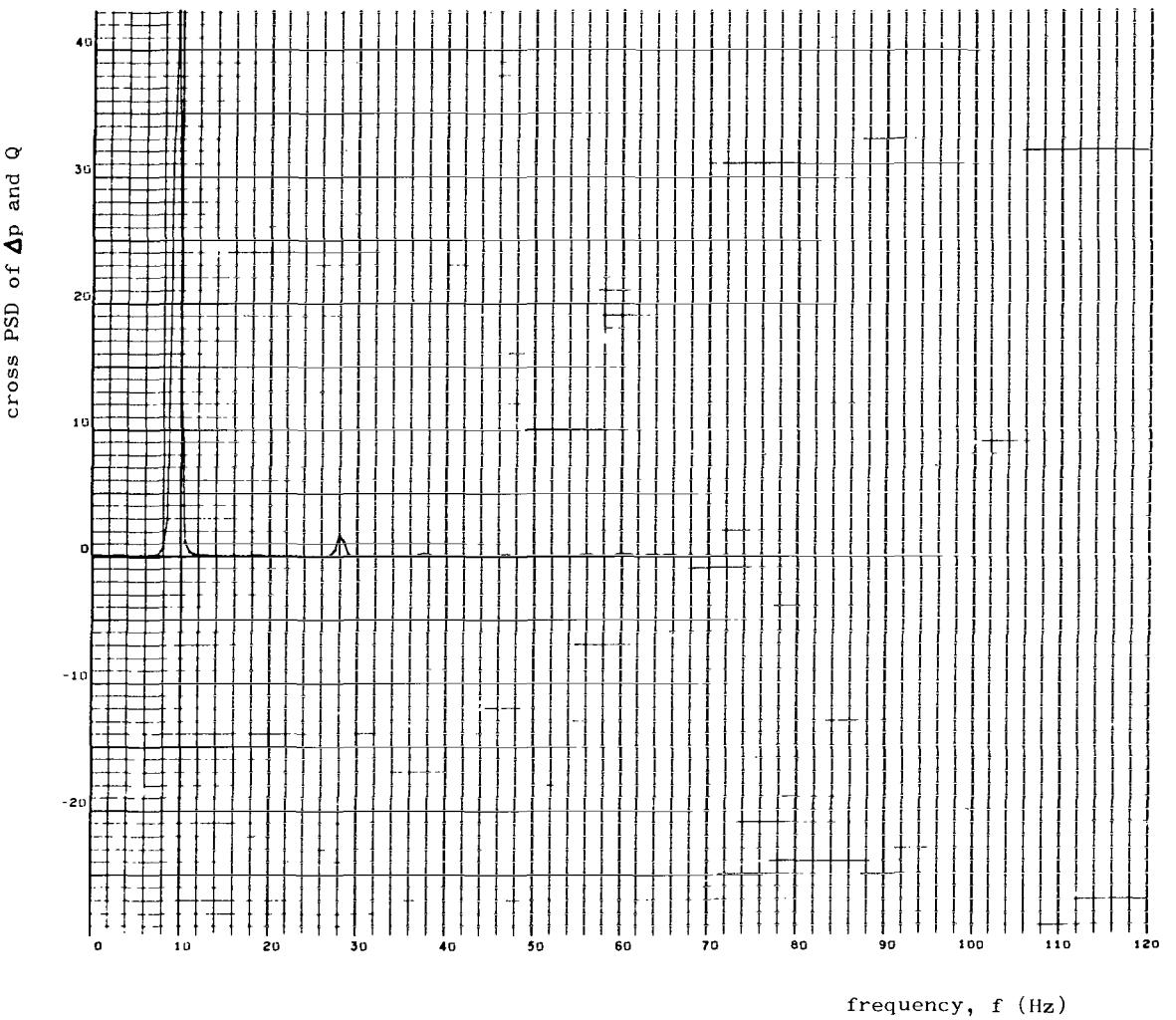

FIGURE 34-5. CROSS POWER SPECTRAL DENSITY OF Δp AND Q VERSUS FREQUENCY

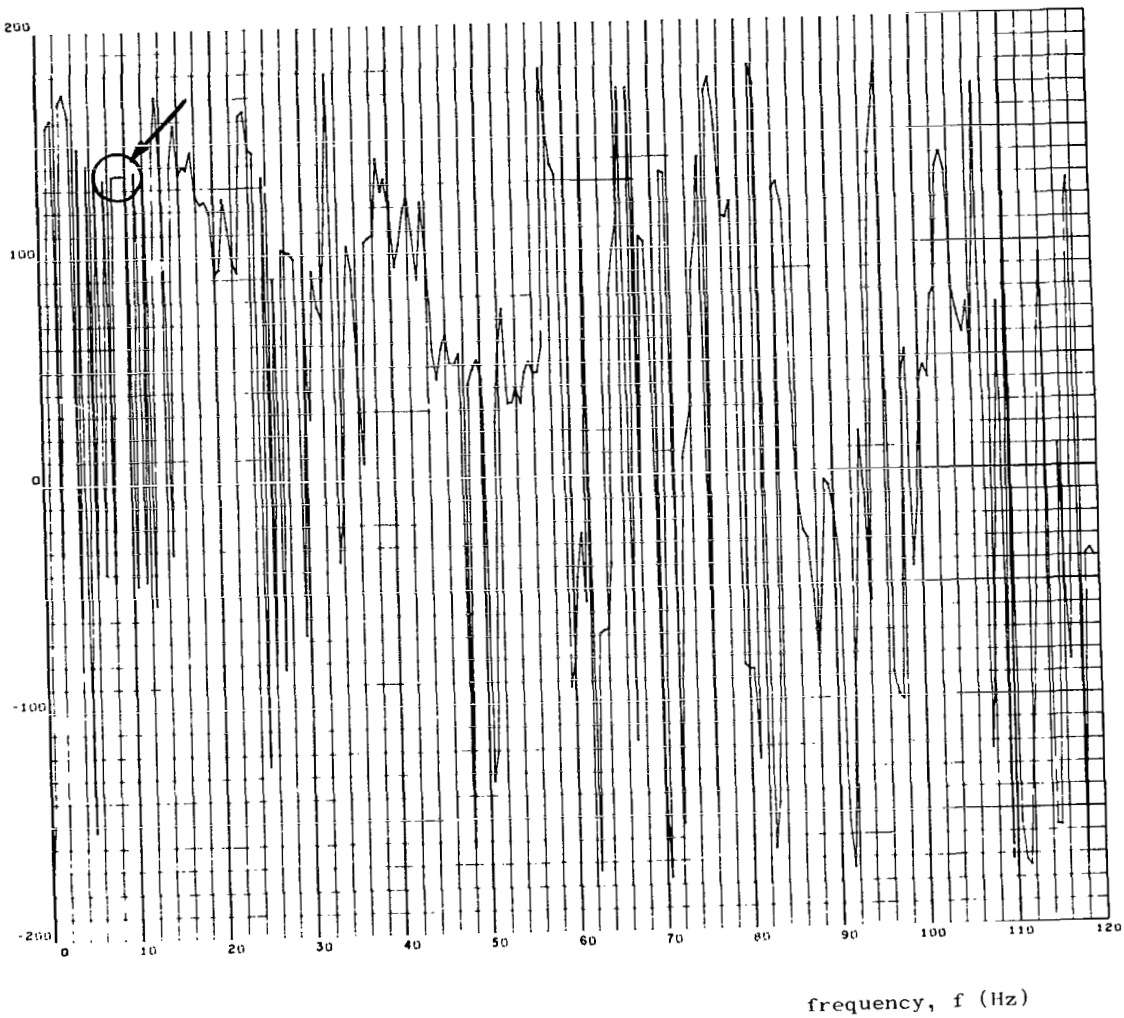

FIGURE 34-6. CROSS PHASE CORRELATION OF Δp AND Q VERSUS FREQUENCY

FIGURE 34-7. COHERENCE OF Δp AND Q VERSUS FREQUENCY

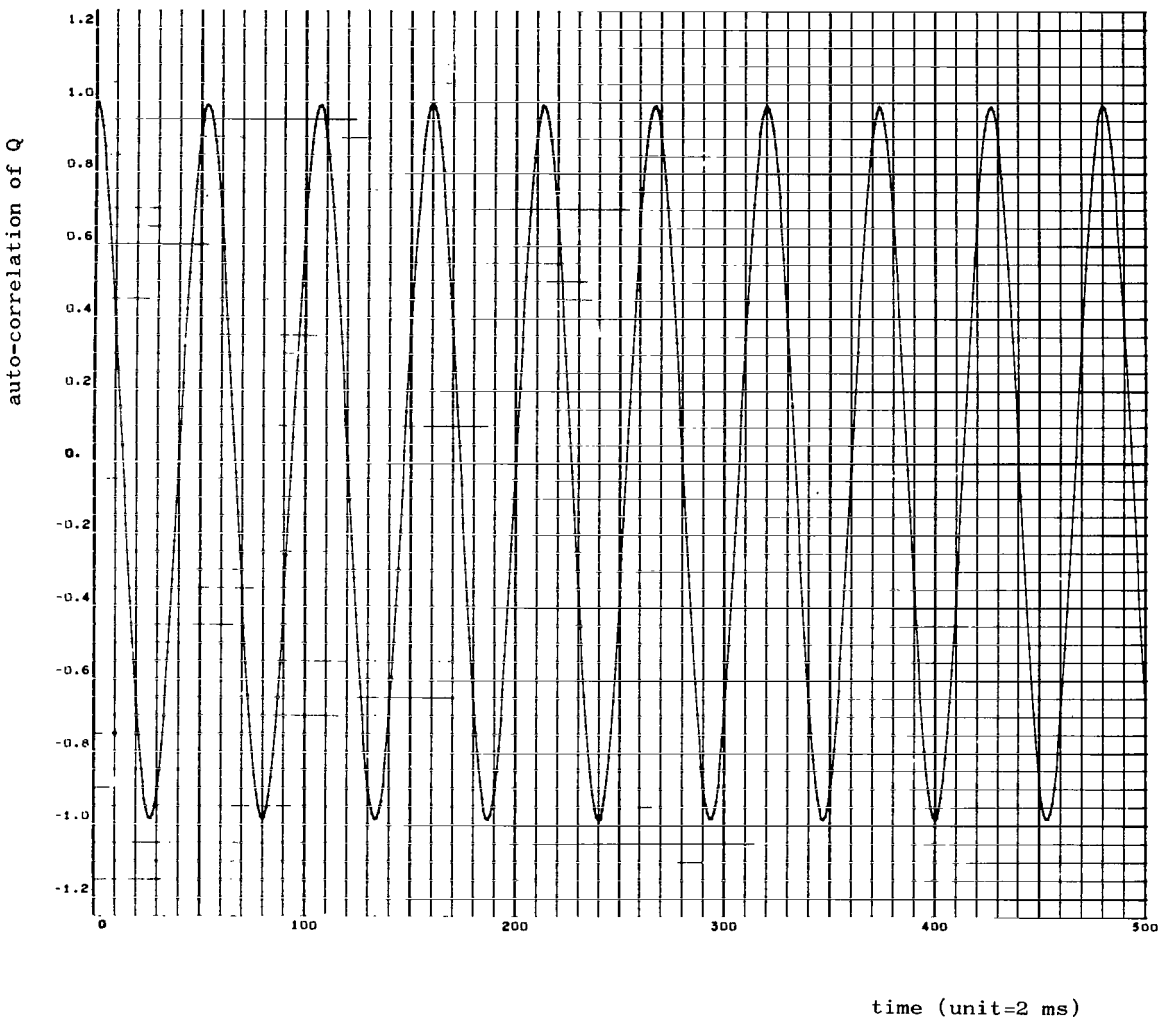

FIGURE 34-8. AUTO-CORRELATION OF Q VERSUS LAG TIME

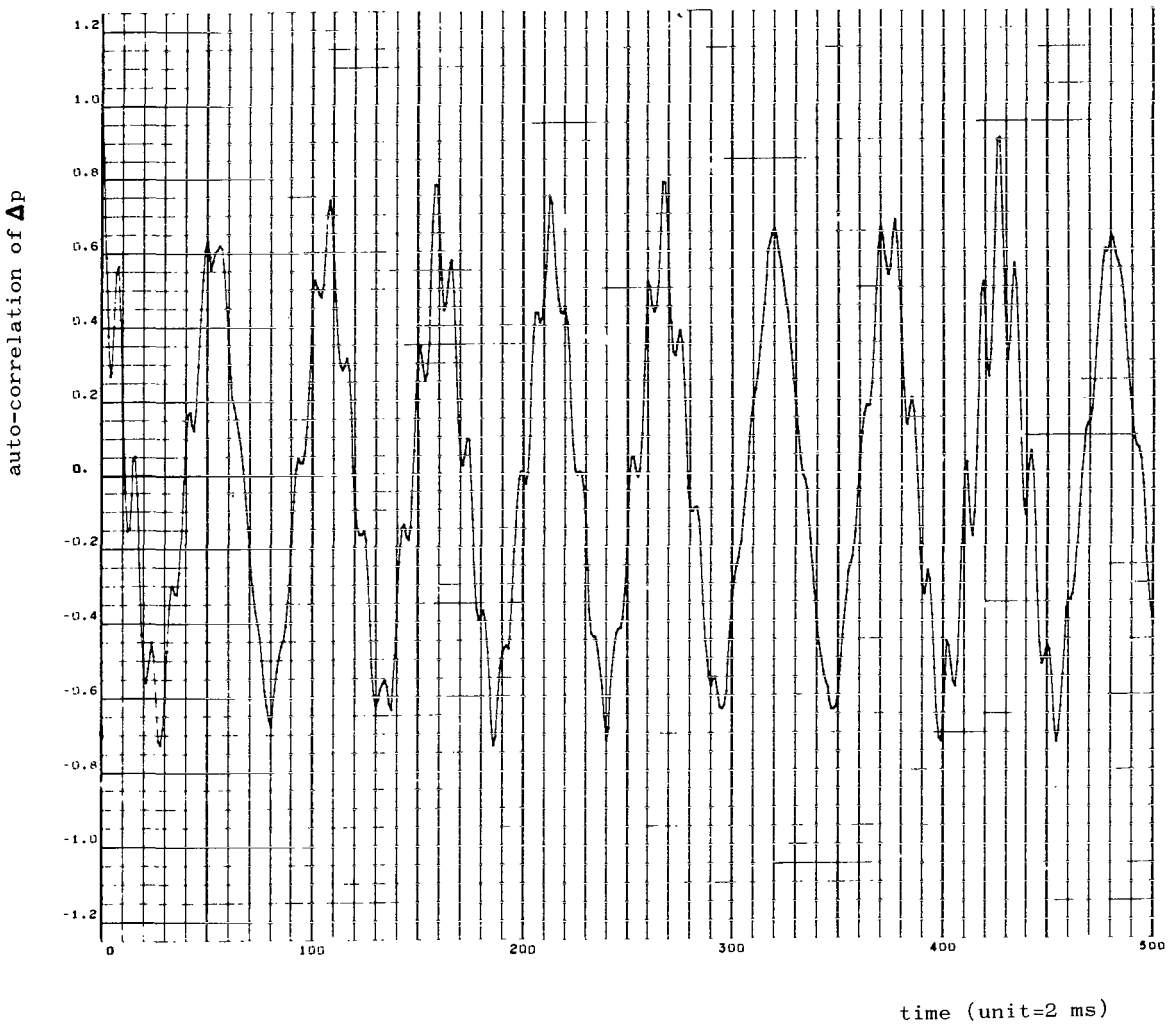

FIGURE 34-9. AUTO-CORRELATION OF Δp VERSUS LAG TIME

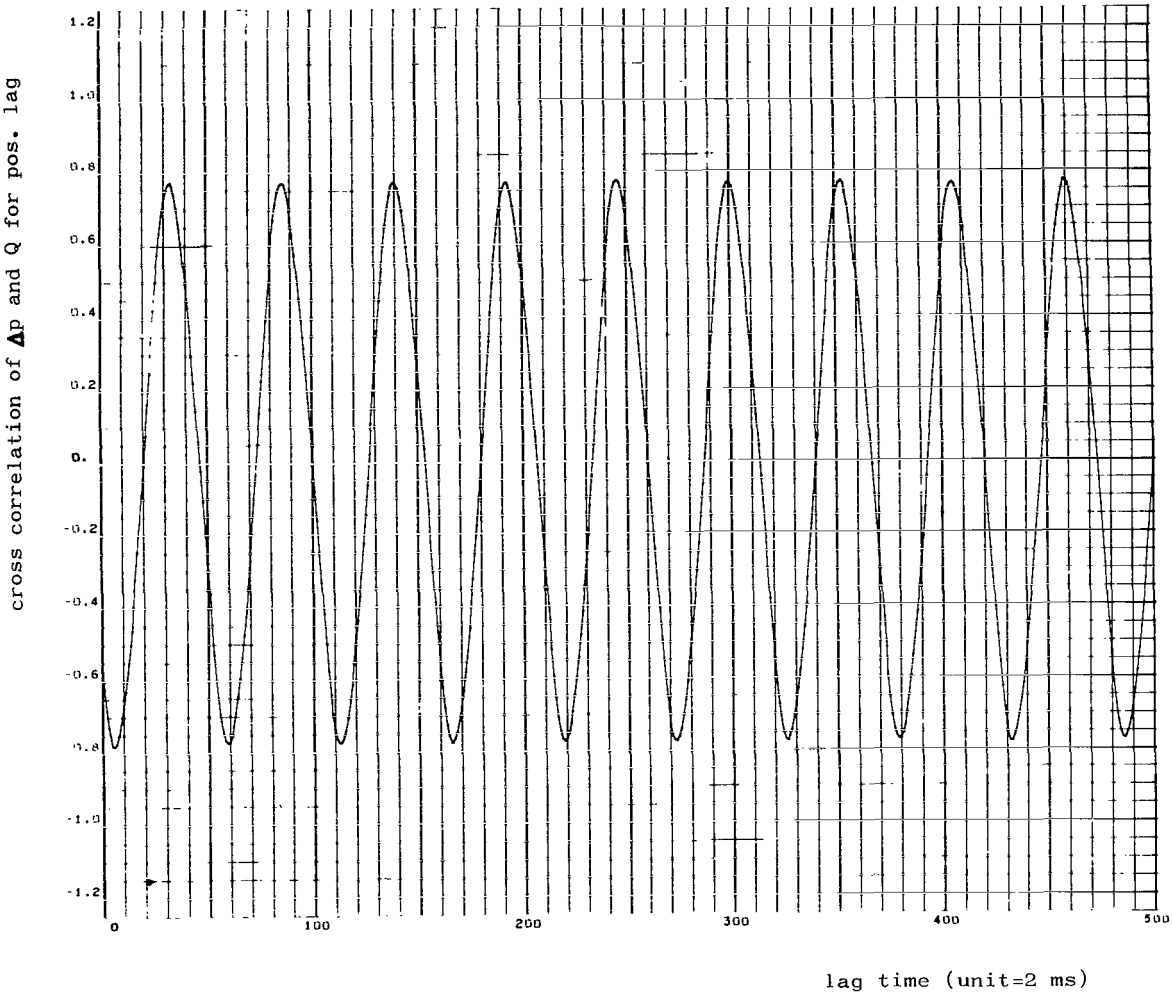

FIGURE 34-10. CROSS-CORRELATION OF Δp AND Q VERSUS POSITIVE LAG TIME

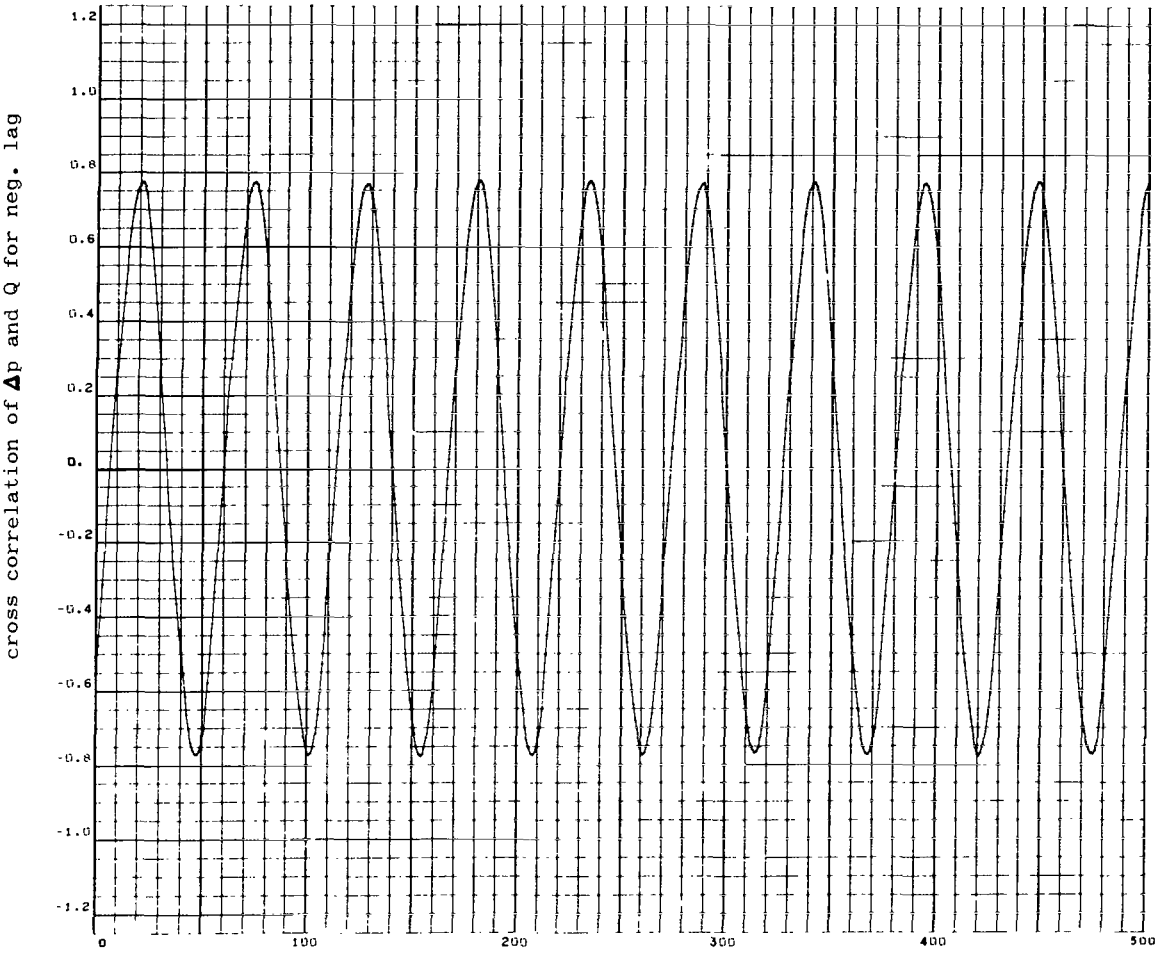

FIGURE 34-11. CROSS-CORRELATION OF Δp AND Q VERSUS NEGATIVE LAG TIME

PREDOMINANT FREQUENCIES

FREQ.	RMS AMP.	FREQ.	RMS AMP.	FREQ.	RMS AMP.	FREQ.	RMS AMP.
+9.5024	+3.5402	+63.5162	+1.2465	+60.0153	+1.2358	+28.0071	+1.0386
+65.5168	+0.8168	+69.0177	+0.5369	+56.0143	+0.4870	+73.0187	+0.4662
+50.5129	+0.4308	+54.0138	+0.4237	+75.0192	+0.2977	+37.5096	+0.2784
+85.0218	+0.2663	+103.0264	+0.2455	+18.5047	+0.2103	+22.5057	+0.1886
+12.0030	+0.1762	+67.5173	+0.1536	+0.5001	+0.1390	+47.0120	+0.1303

CHI-SQUARE- +116.2198 2.5 PERCENT- +23.3367 5 PER CENT-- +21.0261 12 DEGREES OF FREEDOM
N= 1999 RANGE= -13.263550 TO +11.281904
MEAN= +0.000279 S.D.= +4.709350 SKEW= -0.094365 KURTOSIS= +2.255822
N(.025)= +1.962469 N(.975)= +1.748218 N(MEAN)= +1.855343

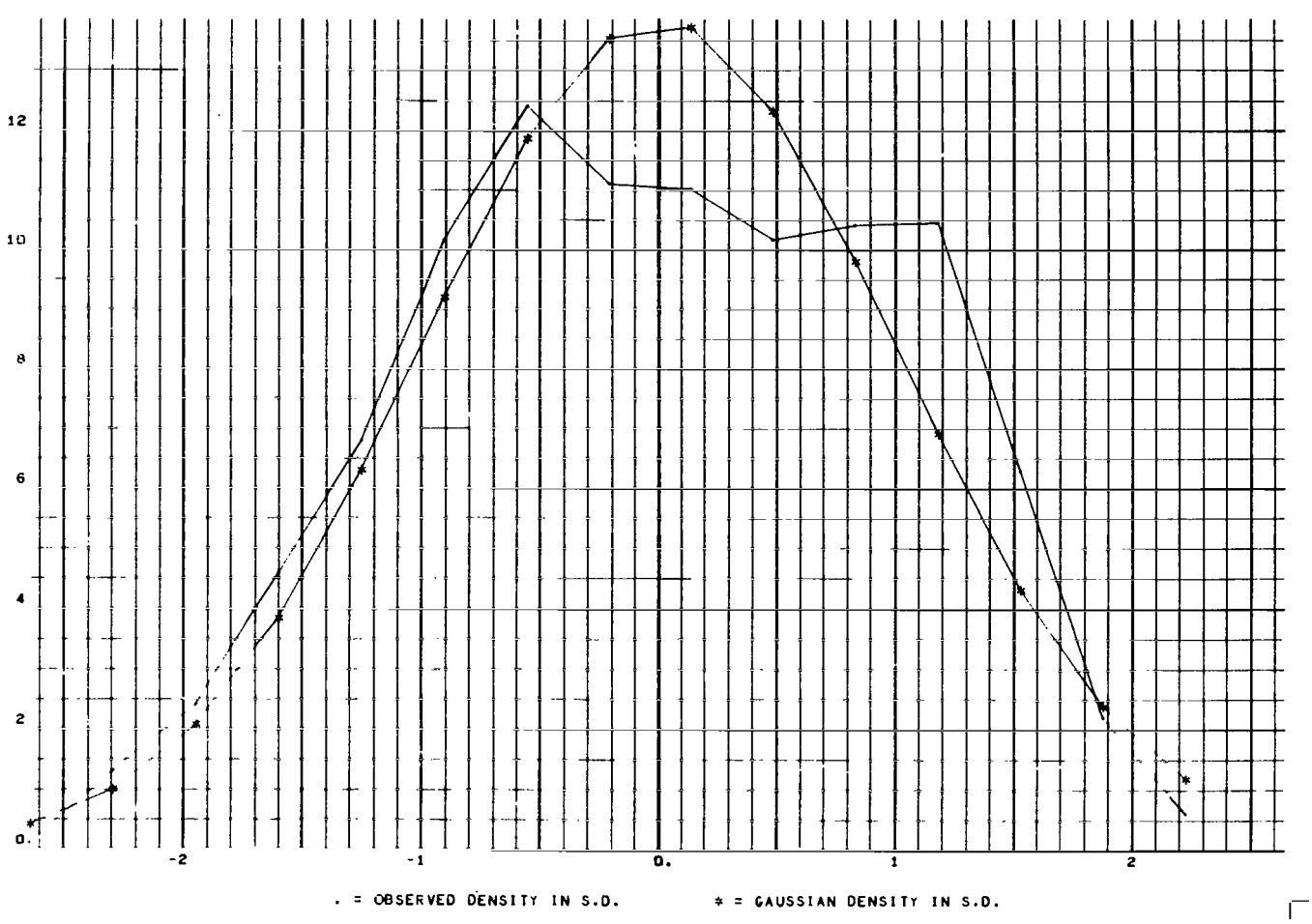

FIGURE 34-12. PROBABILITY DENSITY PLOT OF Δp VERSUS AMPLITUDE DEVIATION

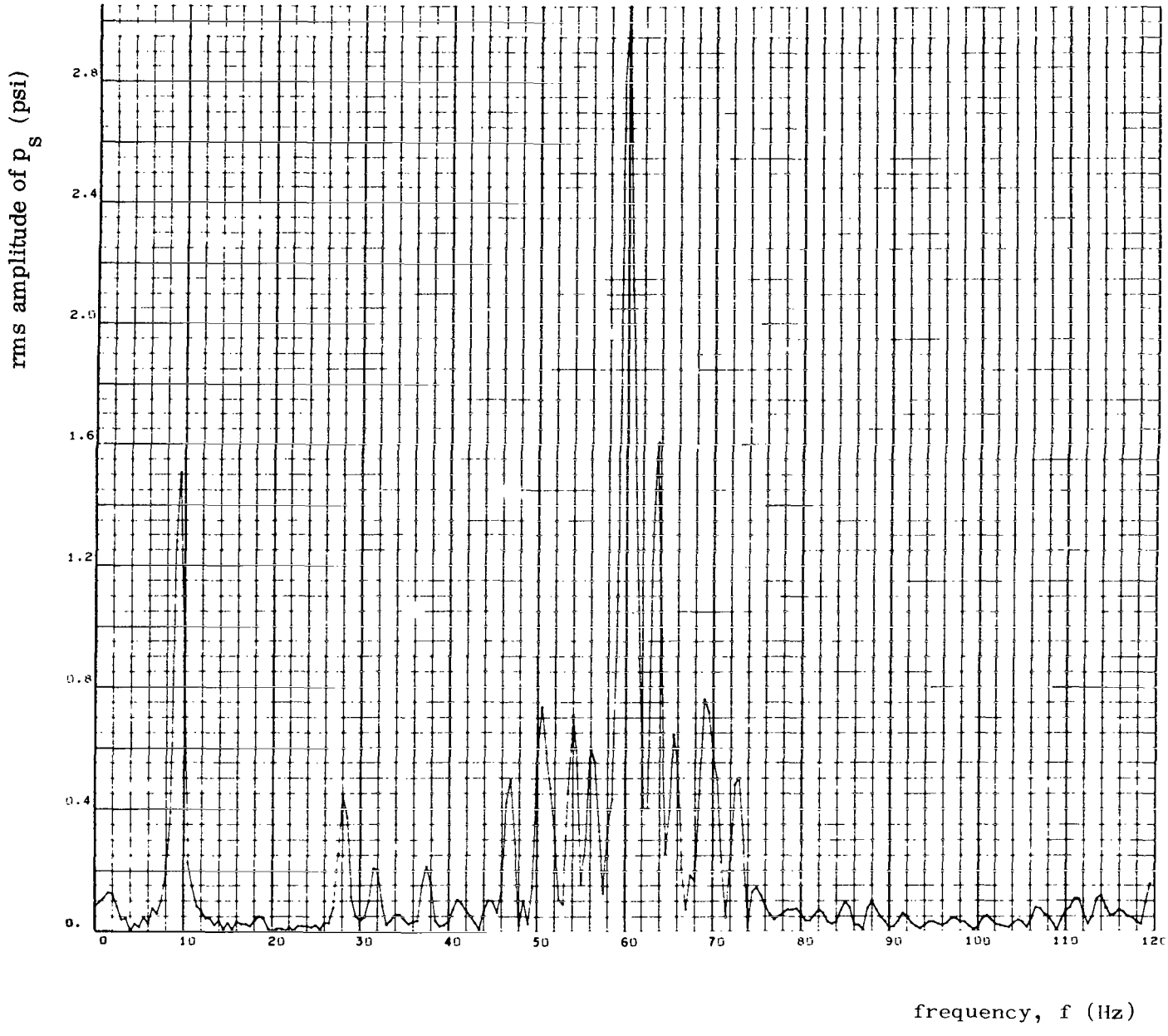

FIGURE 34-13. rms AMPLITUDE DISTRIBUTION OF SUCTION PRESSURE, p_s, VERSUS FREQUENCY

FIGURE 34-14 rms AMPLITUDE DISTRIBUTION OF DELIVERY PRESSURE, p_d, VERSUS FREQUENCY

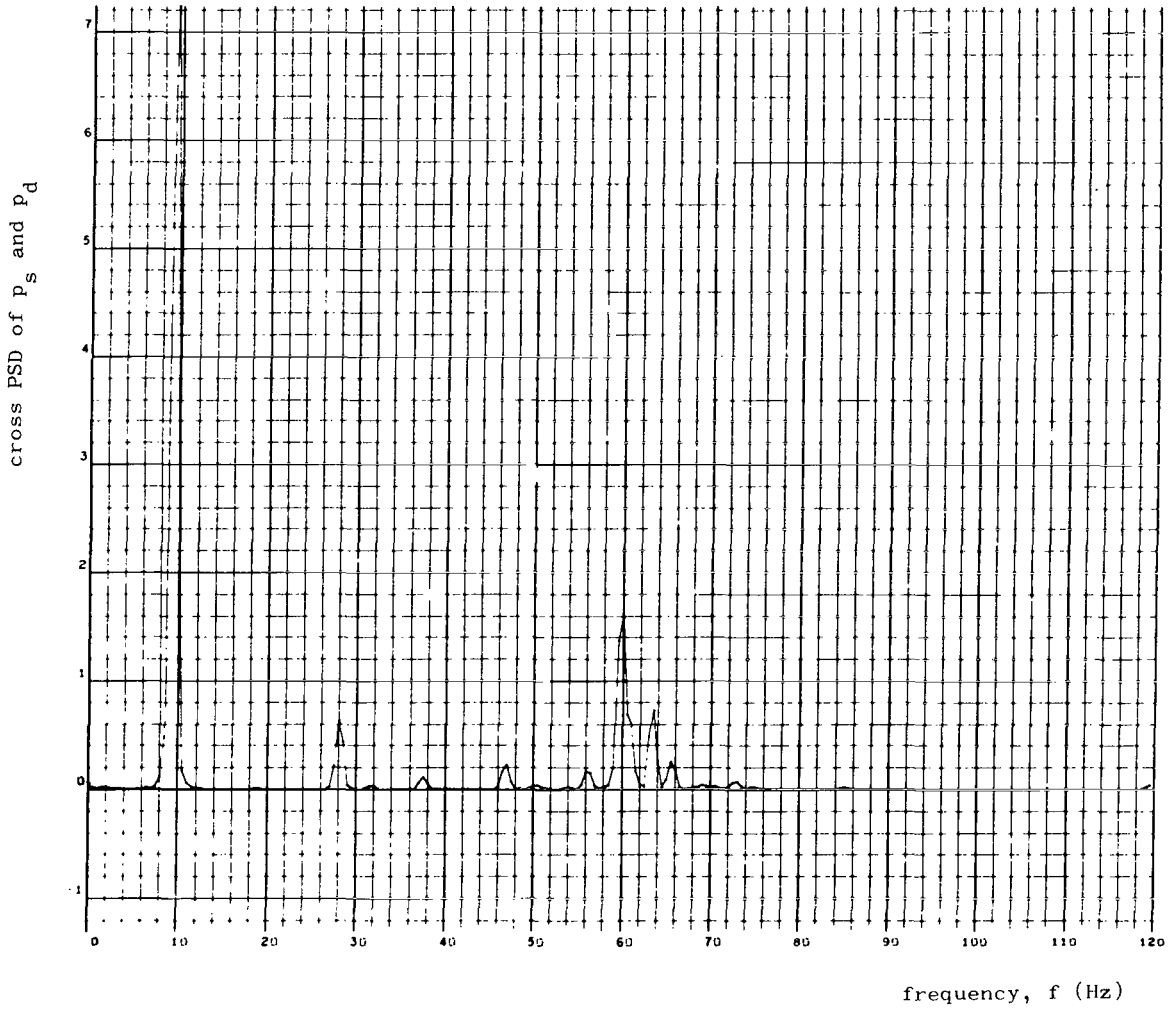

FIGURE 34-15. CROSS POWER SPECTRAL DENSITY OF p_s and p_d VERSUS FREQUENCY

FIGURE 34-16. CROSS PHASE CORRELATION OF p_s AND p_d VERSUS FREQUENCY

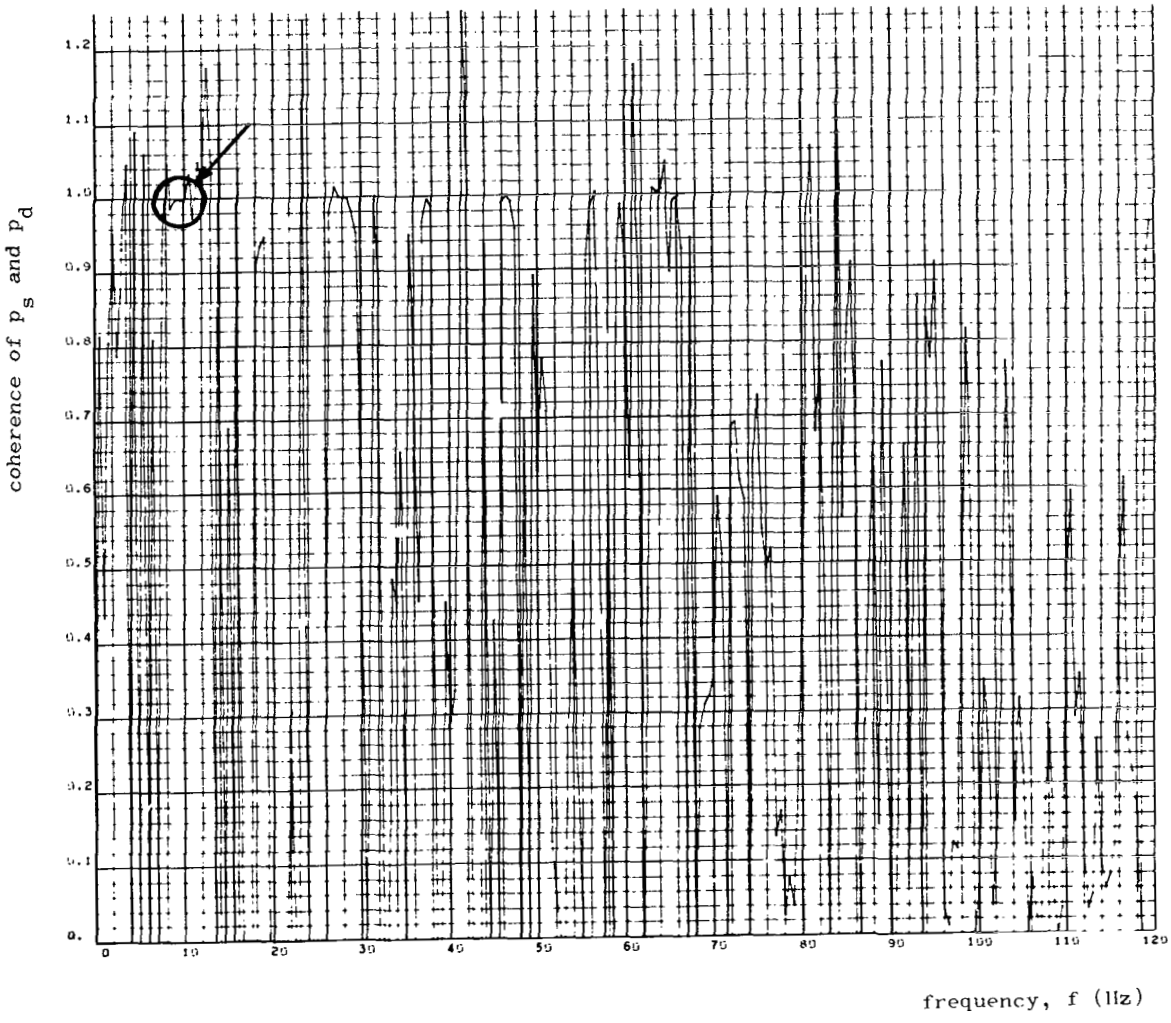

FIGURE 34-17. COHERENCE OF p_s AND p_d VERSUS FREQUENCY

PREDOMINANT FREQUENCIES

FREQ.	RMS AMP.	FREQ.	RMS AMP.	FREQ.	RMS AMP.	FREQ.	RMS AMP.
+9.5024	+4.8087	+28.0071	+1.4075	+60.0153	+0.5425	+37.5096	+0.5174
+63.5162	+0.4522	+47.0120	+0.4467	+65.5168	+0.4000	+56.0143	+0.2704
+6.5016	+0.2564	+18.5047	+0.2502	+85.0218	+0.2067	+5.5014	+0.2018
+75.0192	+0.1942	+2.5006	+0.1929	+73.0187	+0.1914	+103.0264	+0.1856
+3.5008	+0.1721	+31.5080	+0.1643	+4.5011	+0.1101	+14.5037	+0.0968

CHI-SQUARE- +698.8458 2.5 PERCENT- +26.1190 5 PER CENT-- +23.6848 14 DEGREES OF FREEDOM
N= 1999 RANGE= -11.721657 TO +10.314671
MEAN= +0.000365 S.D.= +5.334625 SKEW= -0.045189 KURTOSIS= +1.673803
N(.025)= +1.635299 N(.975)= +1.640710 N(MEAN)= +1.638004

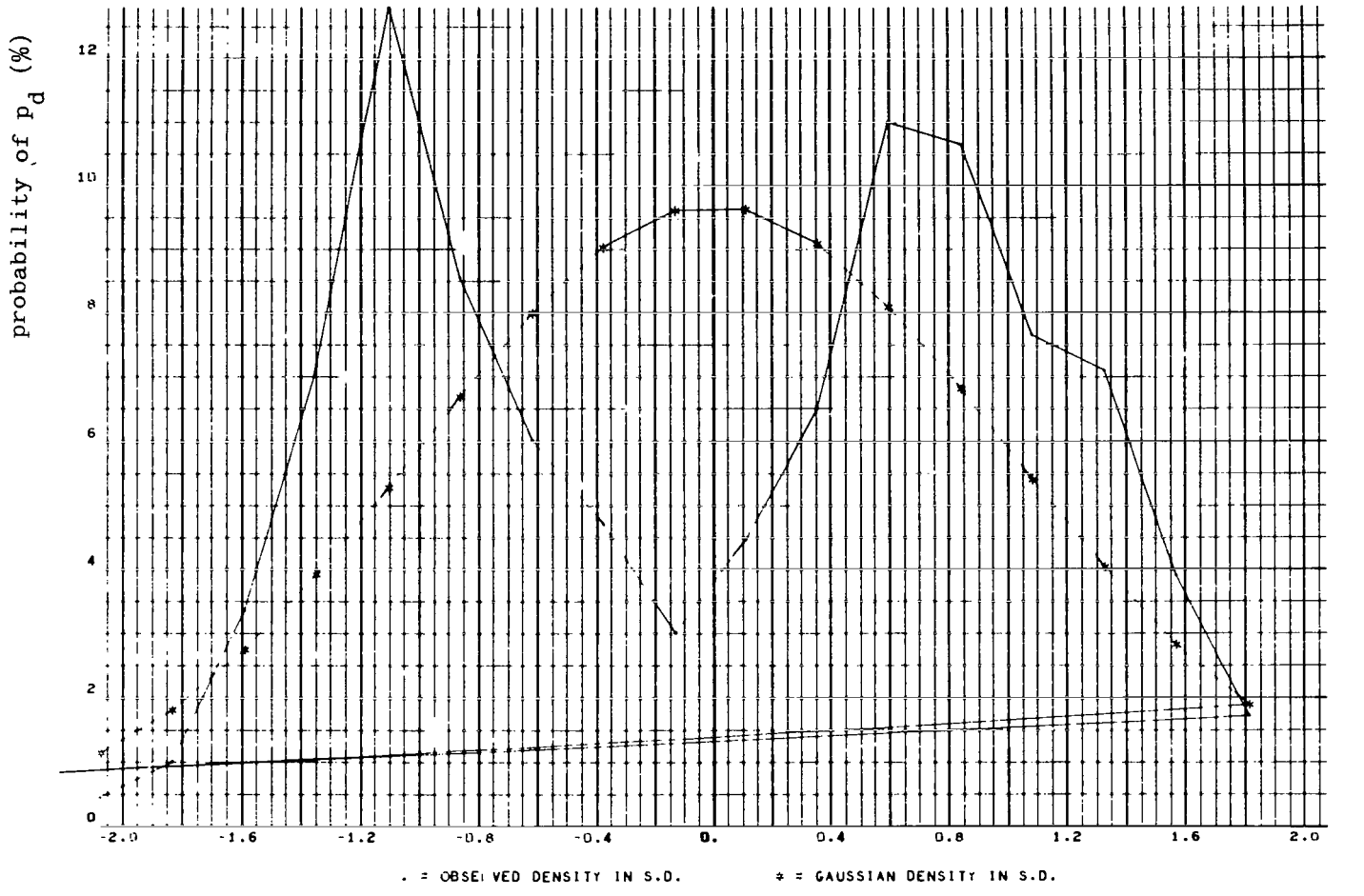

FIGURE 34-18. PROBABILITY DENSITY PLOT OF p_d VERSUS AMPLITUDE DEVIATION

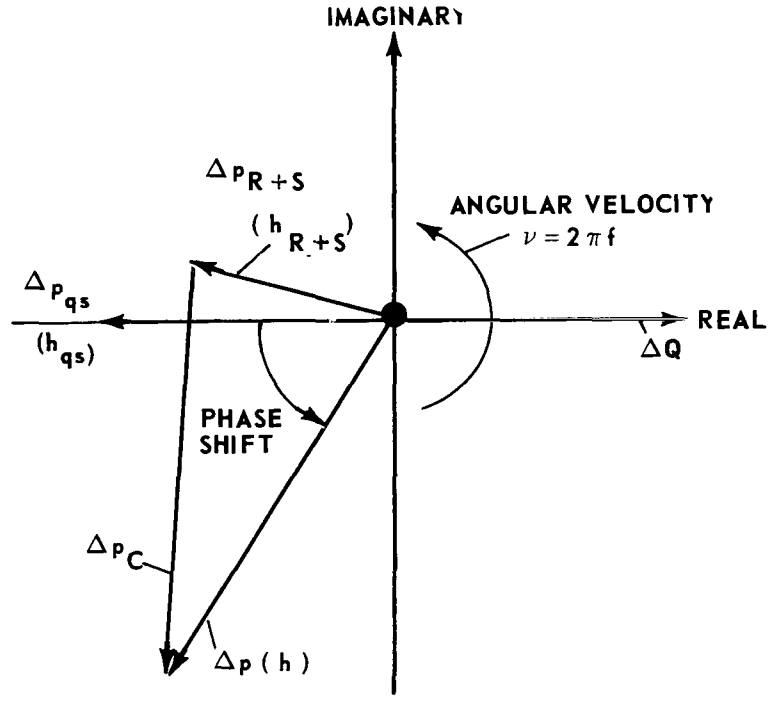

FIGURE 35. AMPLITUDE AND PHASE CORRELATION BETWEEN FLOW AND PRESSURE FLUCTUATION

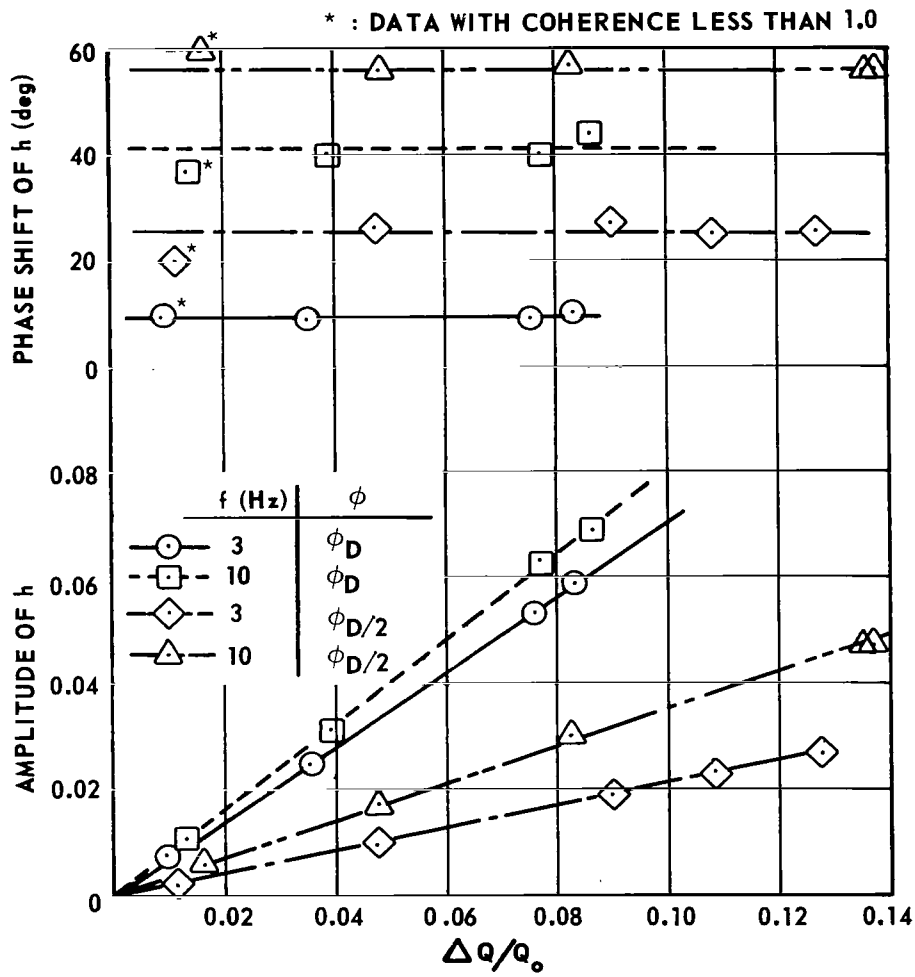

FIGURE 36-1. LINEARITY TEST, n = 60 rps
(SERIES 6)

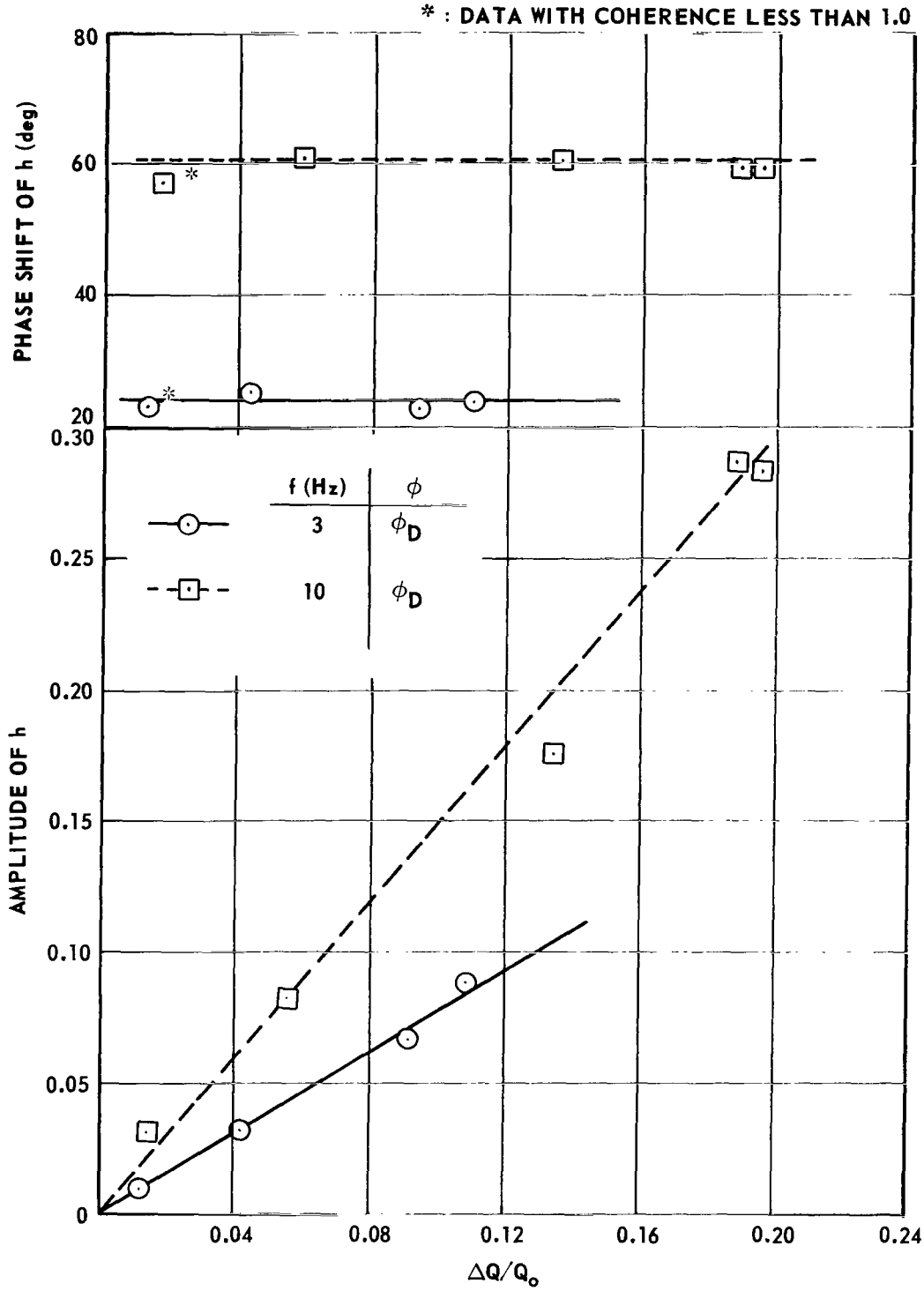

FIGURE 36-2. LINEARITY TEST, n = 30 rps
(SERIES 10)

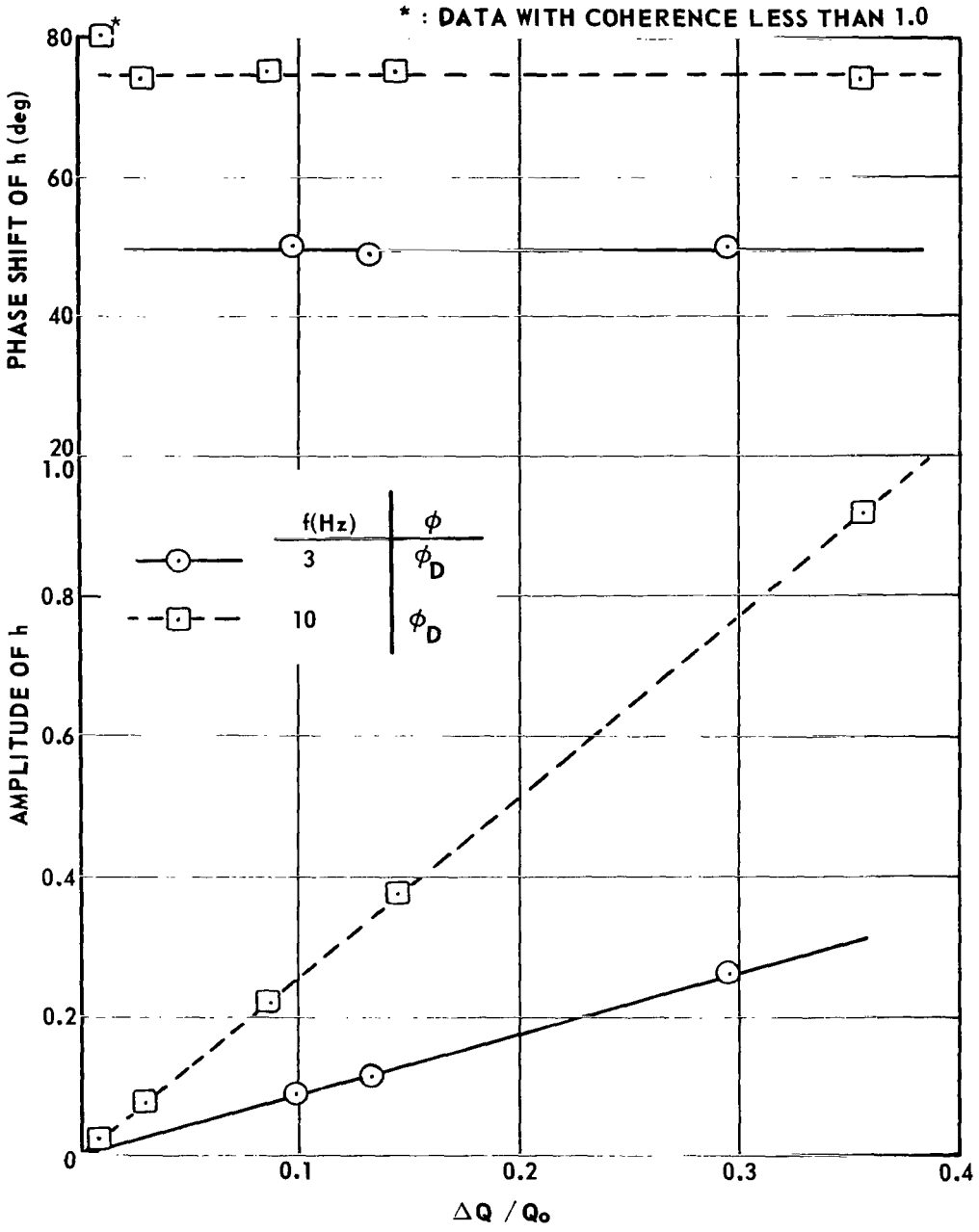

FIGURE 36-3. LINEARITY TEST, n = 15 rps
(SERIES 14)

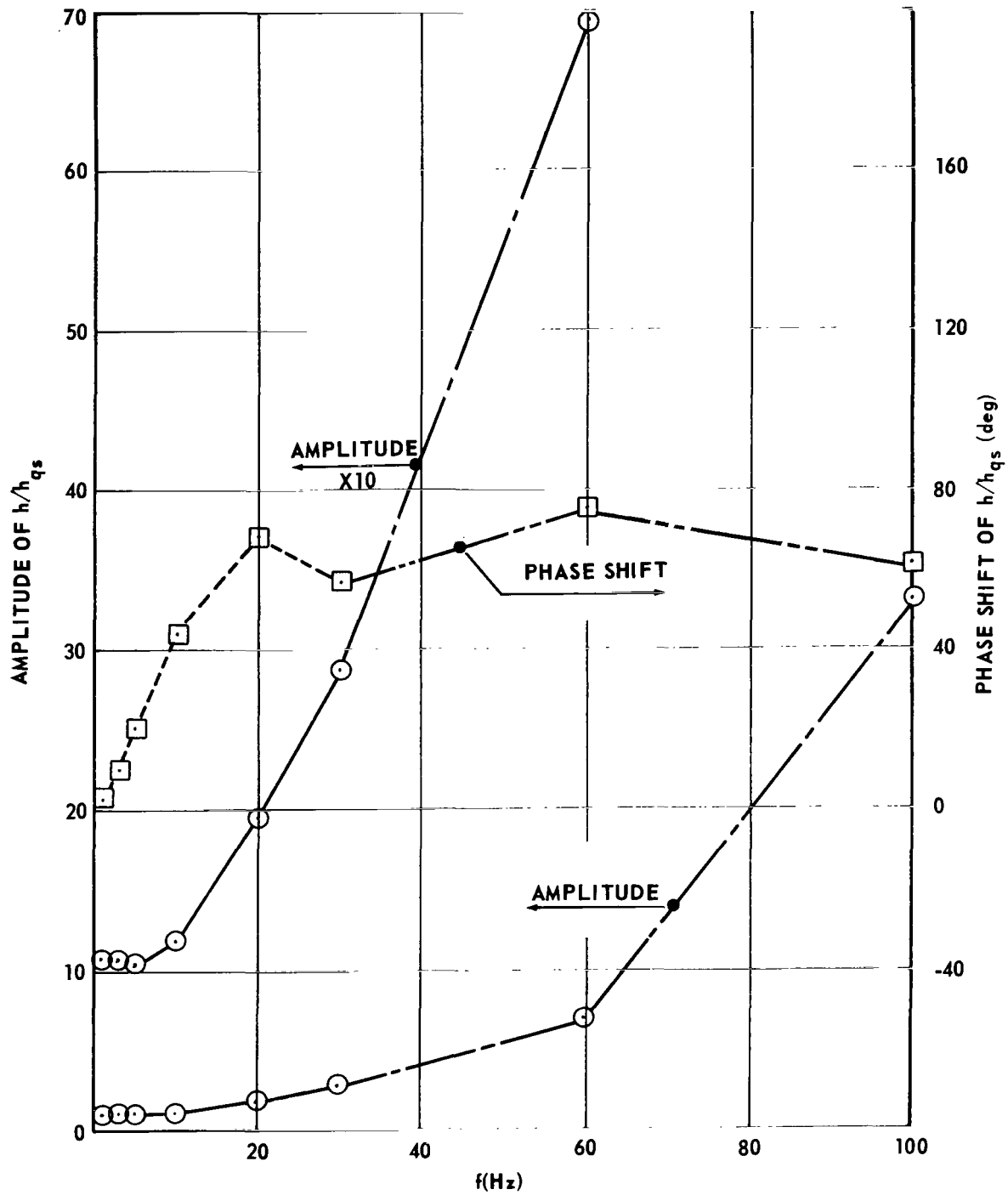

FIGURE 37. RESPONSE OF PRESSURE DIFFERENCE OBTAINED FROM PULSATING TEST: n = 60 rps, $\phi = \phi_D$ (SERIES 4)

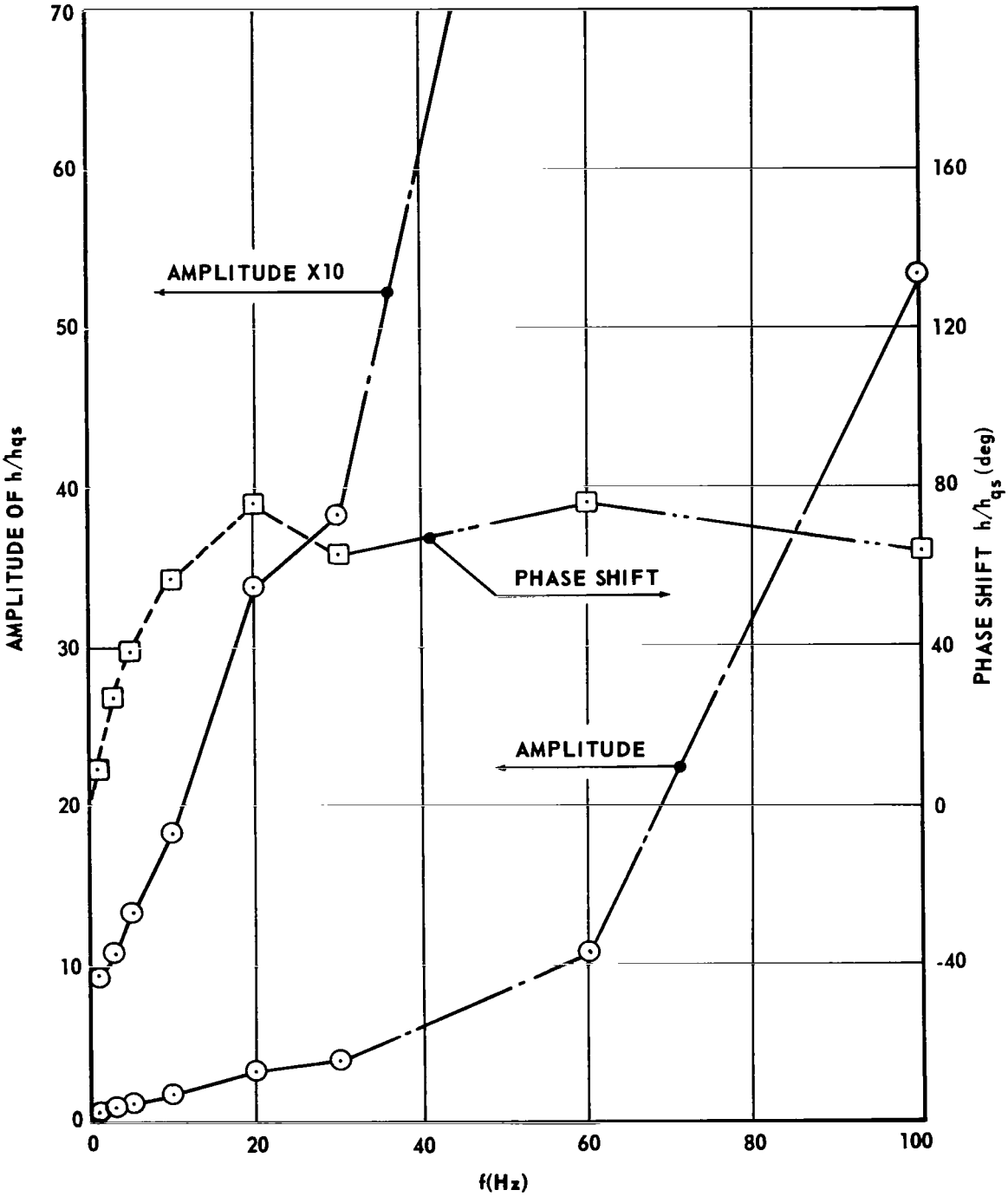

FIGURE 38. RESPONSE OF PRESSURE DIFFERENCE OBTAINED FROM PULSATING TEST: n = 60 rps, $\phi = \phi_D/2$ (SERIES 5)

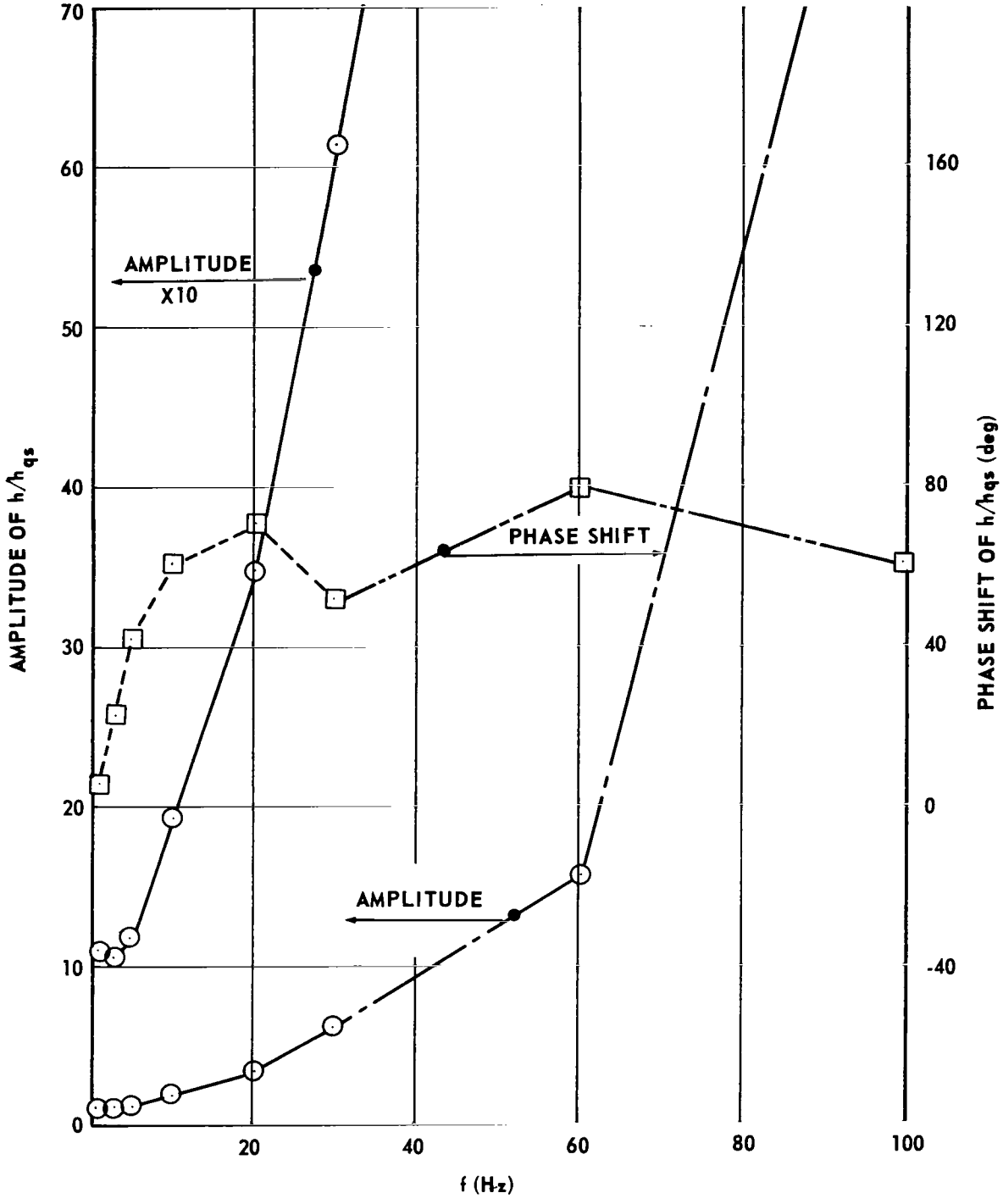

FIGURE 39. RESPONSE OF PRESSURE DIFFERENCE OBTAINED FROM PULSATING TEST: n = 30 rps, $\phi = \phi_D$ (SERIES 8)

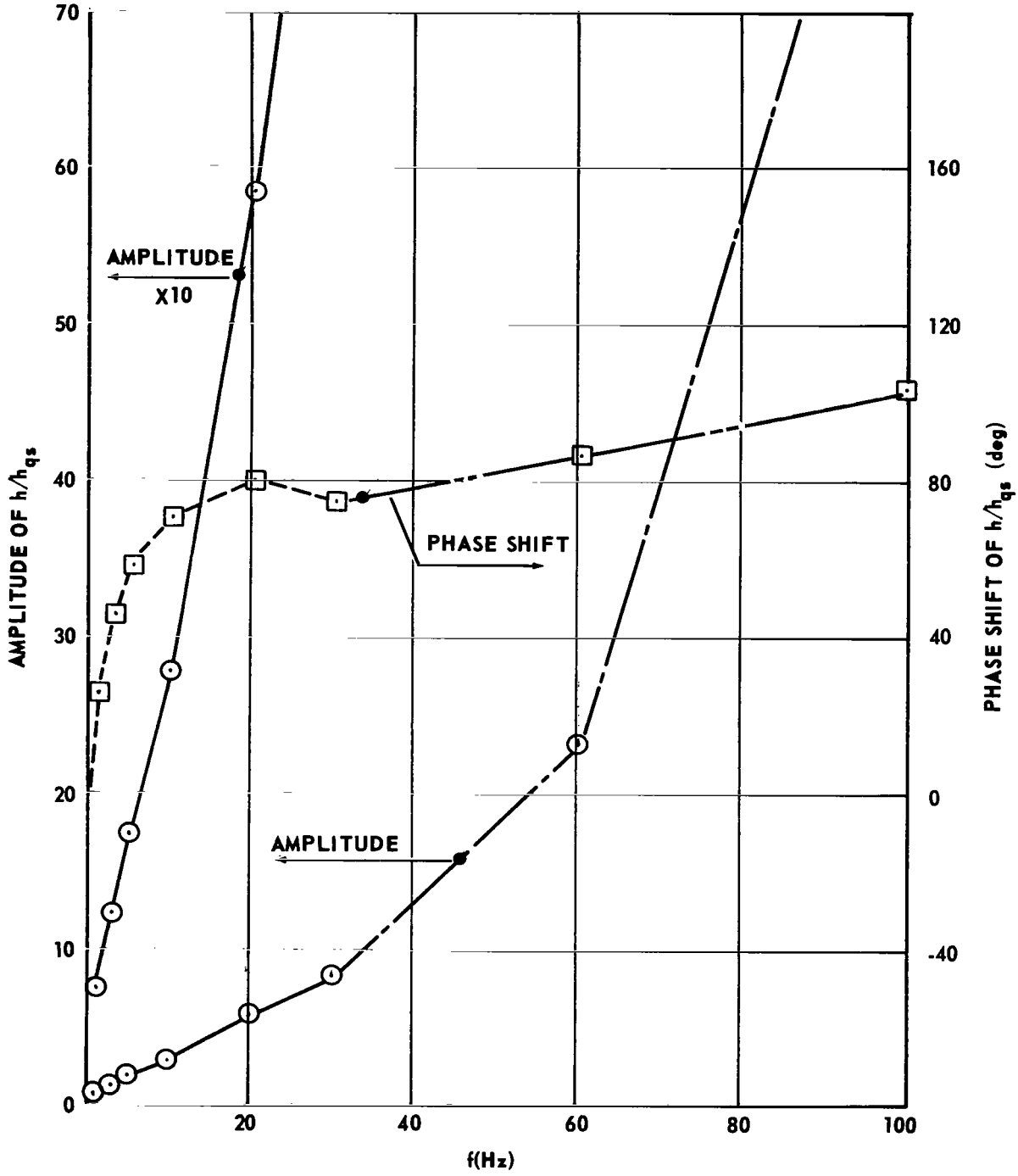

FIGURE 40. RESPONSE OF PRESSURE DIFFERENCE OBTAINED FROM PULSATING TEST: n = 30 rps, $\phi = \phi_D/2$ (SERIES 9)

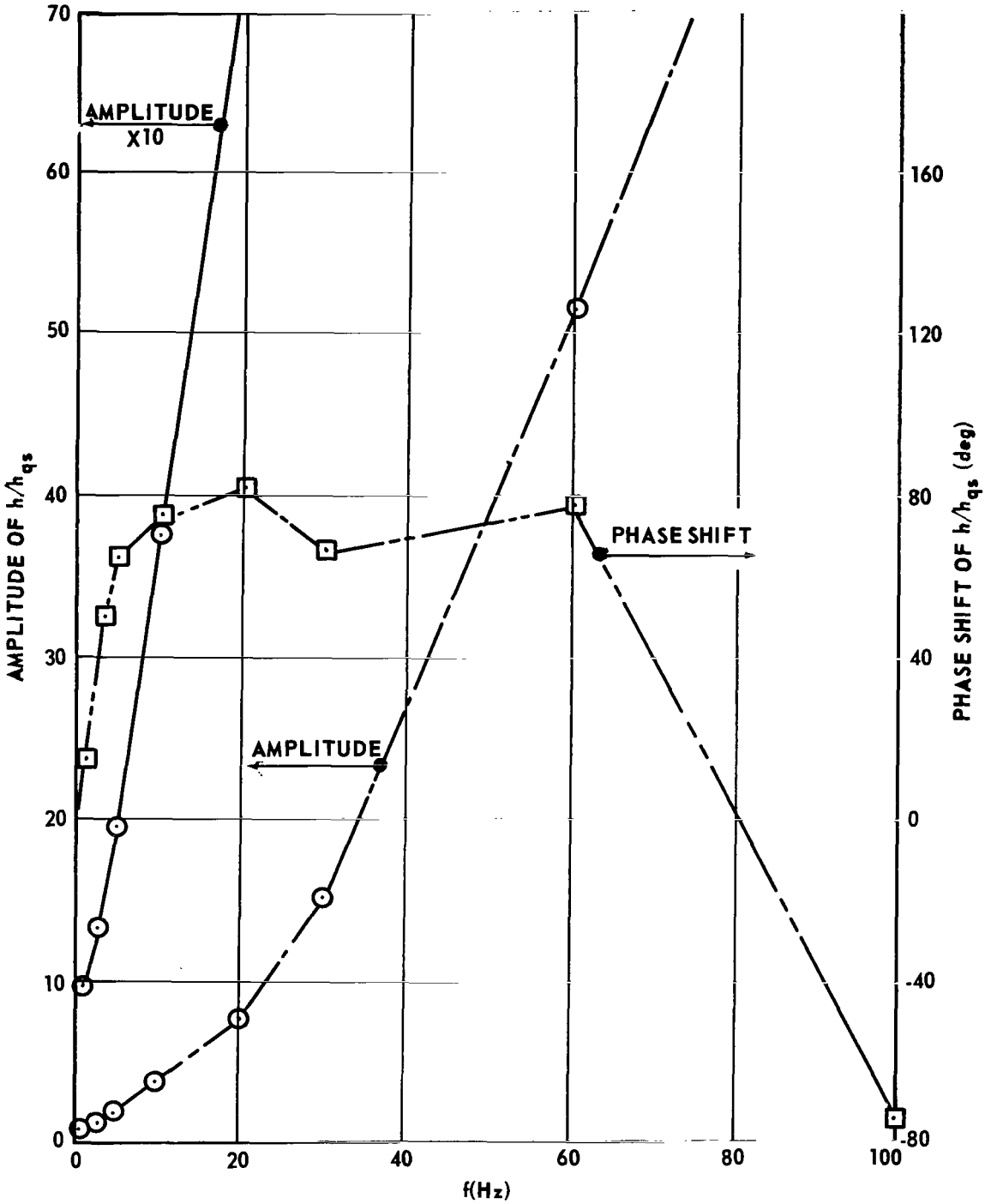

FIGURE 41. RESPONSE OF PRESSURE DIFFERENCE OBTAINED FROM PULSATING TEST: n = 15 rps, $\phi = \phi_D$ (SERIES 12)

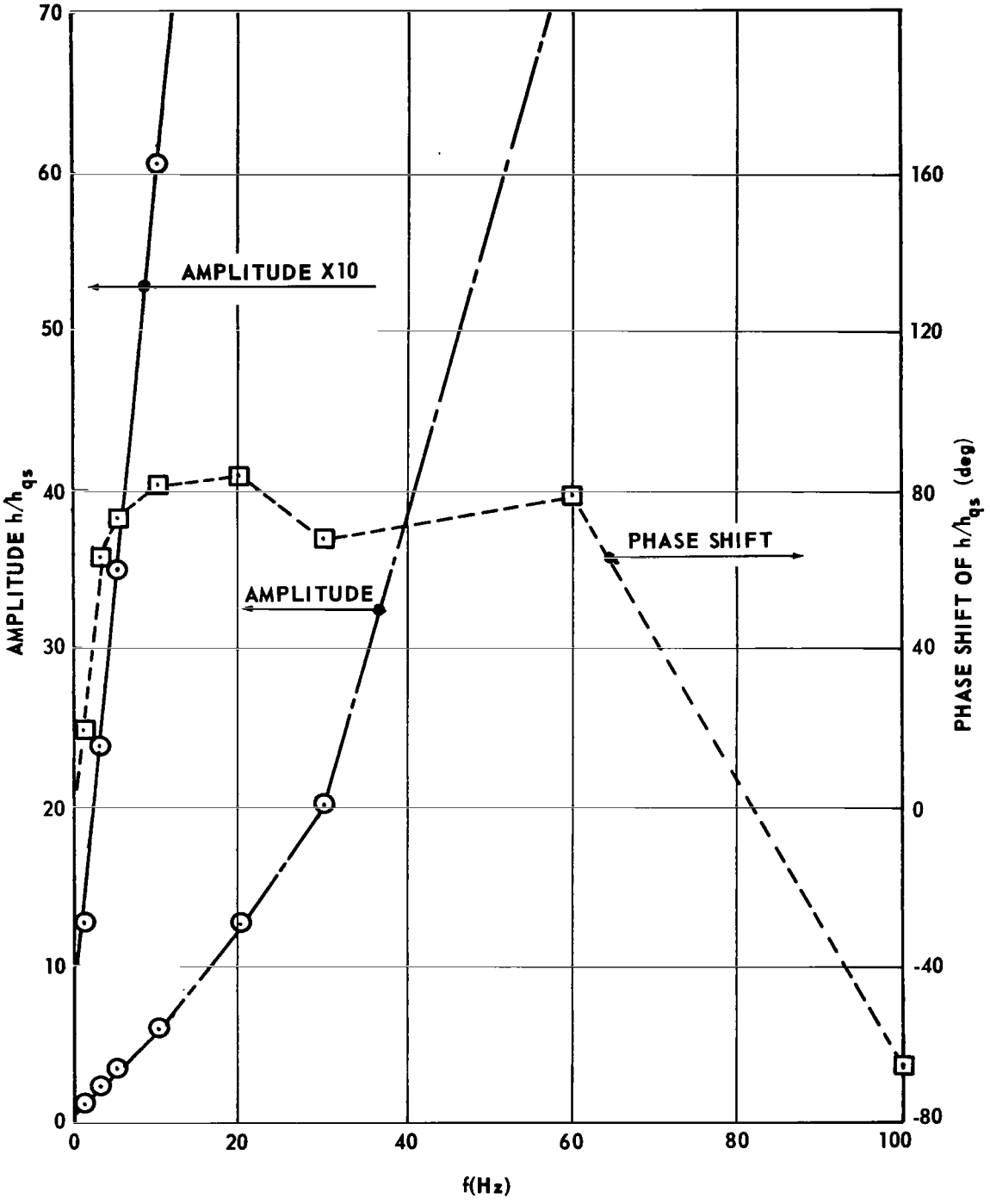

FIGURE 42. RESPONSE OF PRESSURE DIFFERENCE OBTAINED FROM PULSATING TEST: n = 15 rps, $\phi = \phi_D/2$ (SERIES 13)

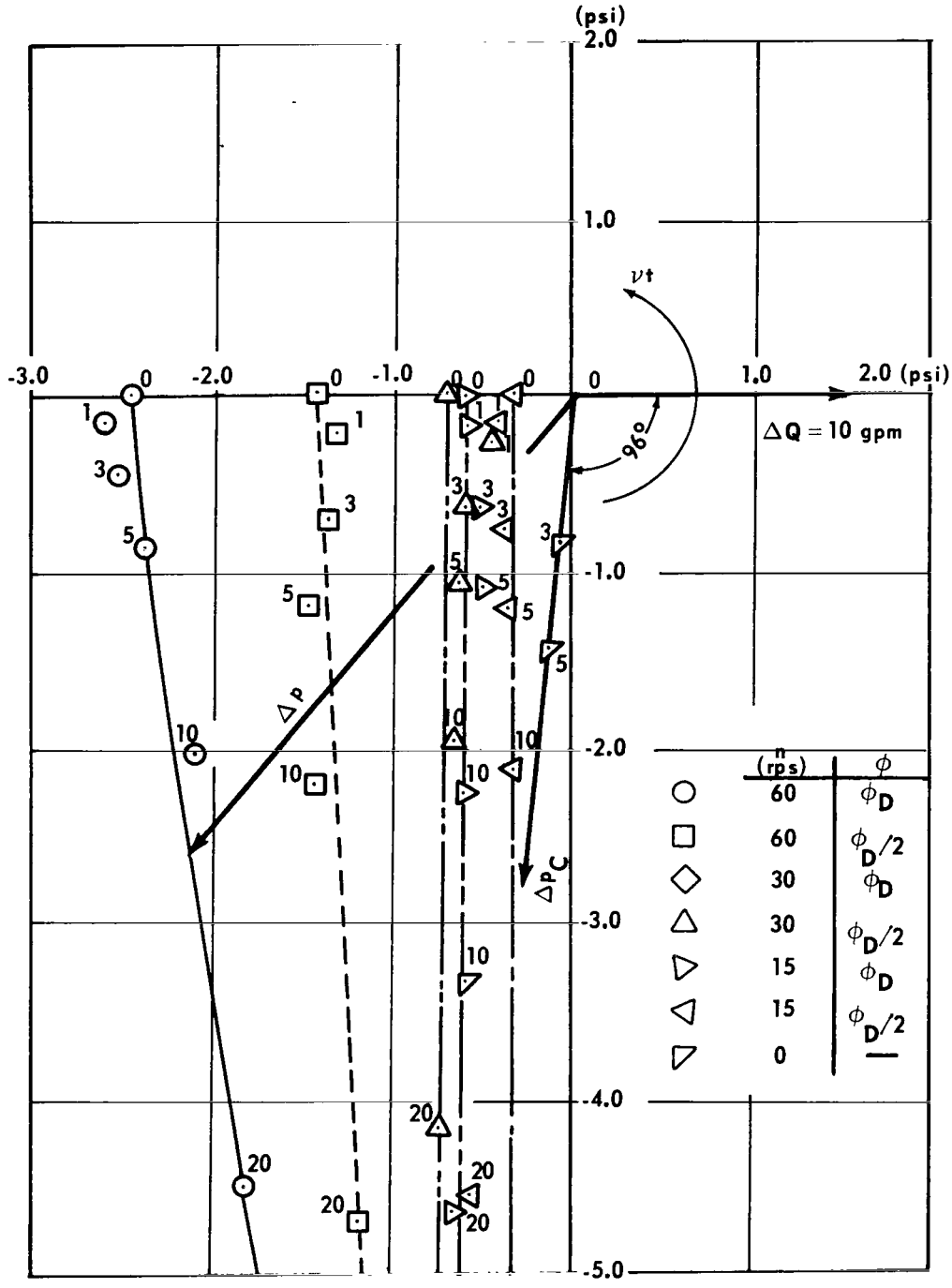

(Number attached to symbols indicates the applied frequency, f.)

FIGURE 43. POLAR DIAGRAM DESCRIBING RESPONSE OF PRESSURE DIFFERENCE FOR THE FLOW FLUCTUATION OF ΔQ = 10 gpm (SERIES 4, 5, 8, 9, 12, 13, and 15)

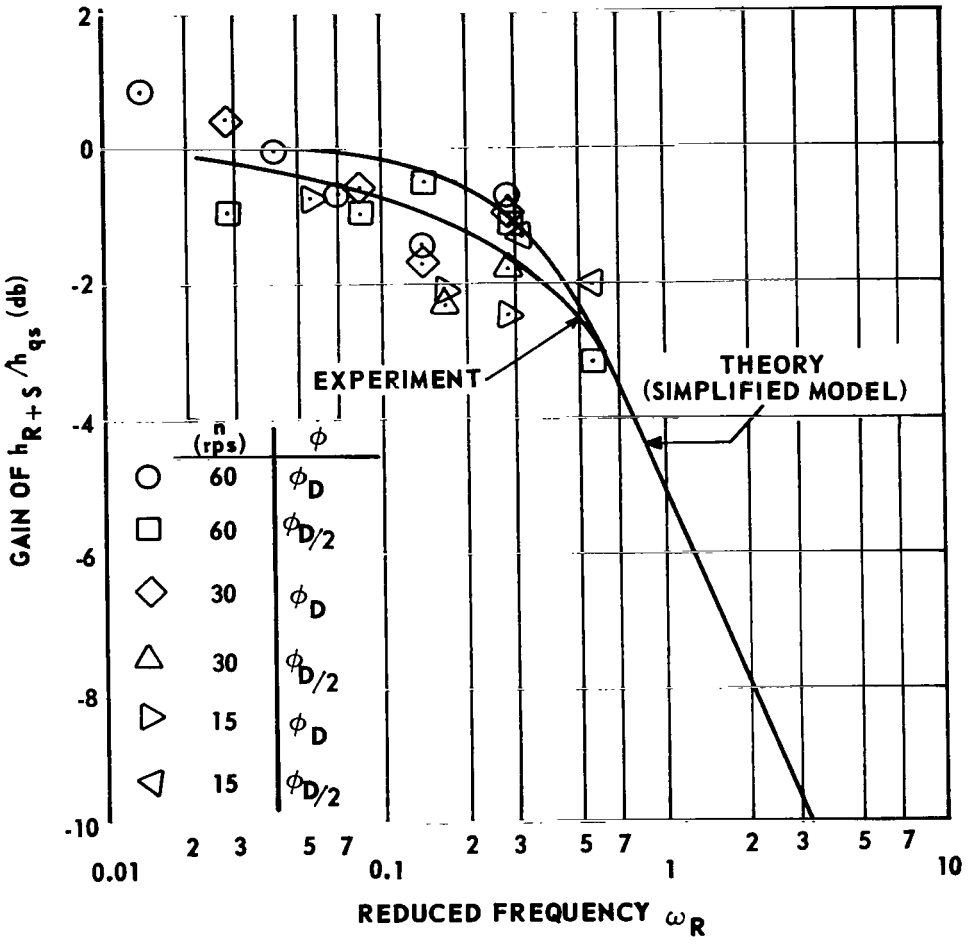

FIGURE 44-1. FREQUENCY RESPONSE OF h_{R+S}/h_{qs}, GAIN VERSUS REDUCED FREQUENCY

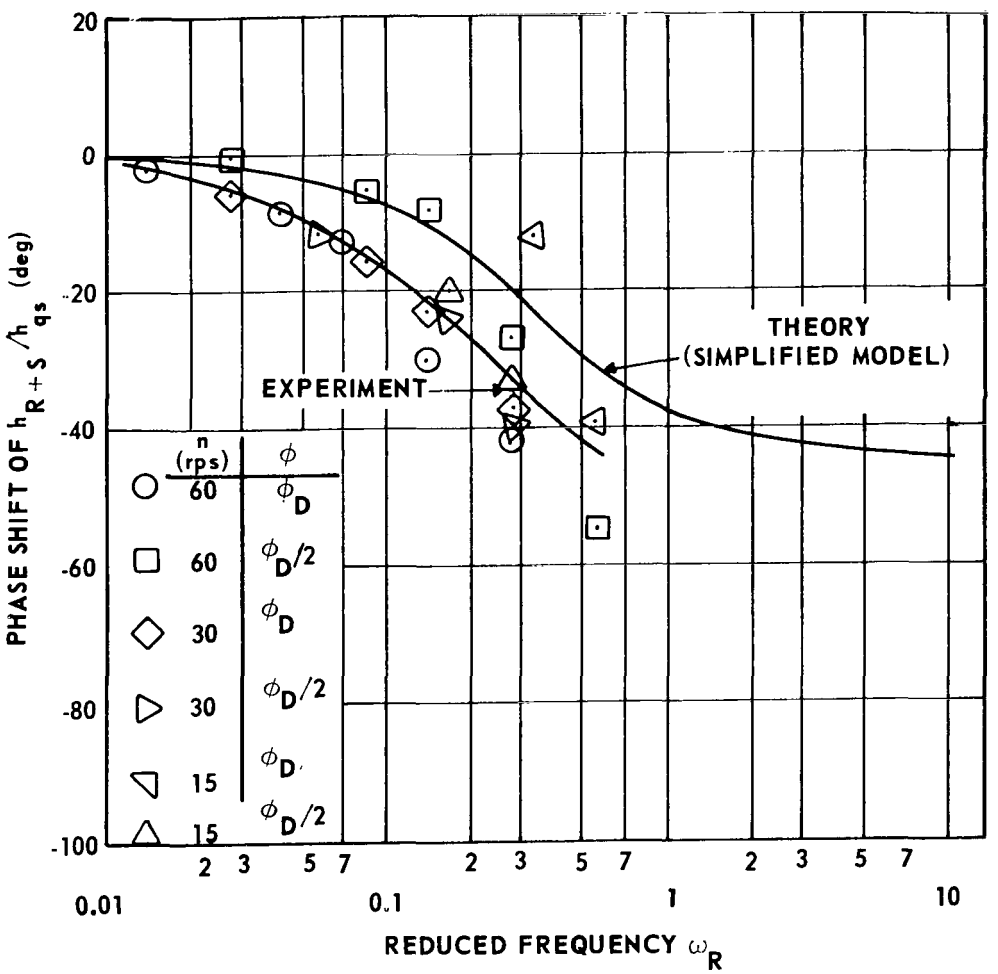

FIGURE 44-2. FREQUENCY RESPONSE OF h_{R+S}/h_{qs}, PHASE SHIFT VERSUS REDUCED FREQUENCY

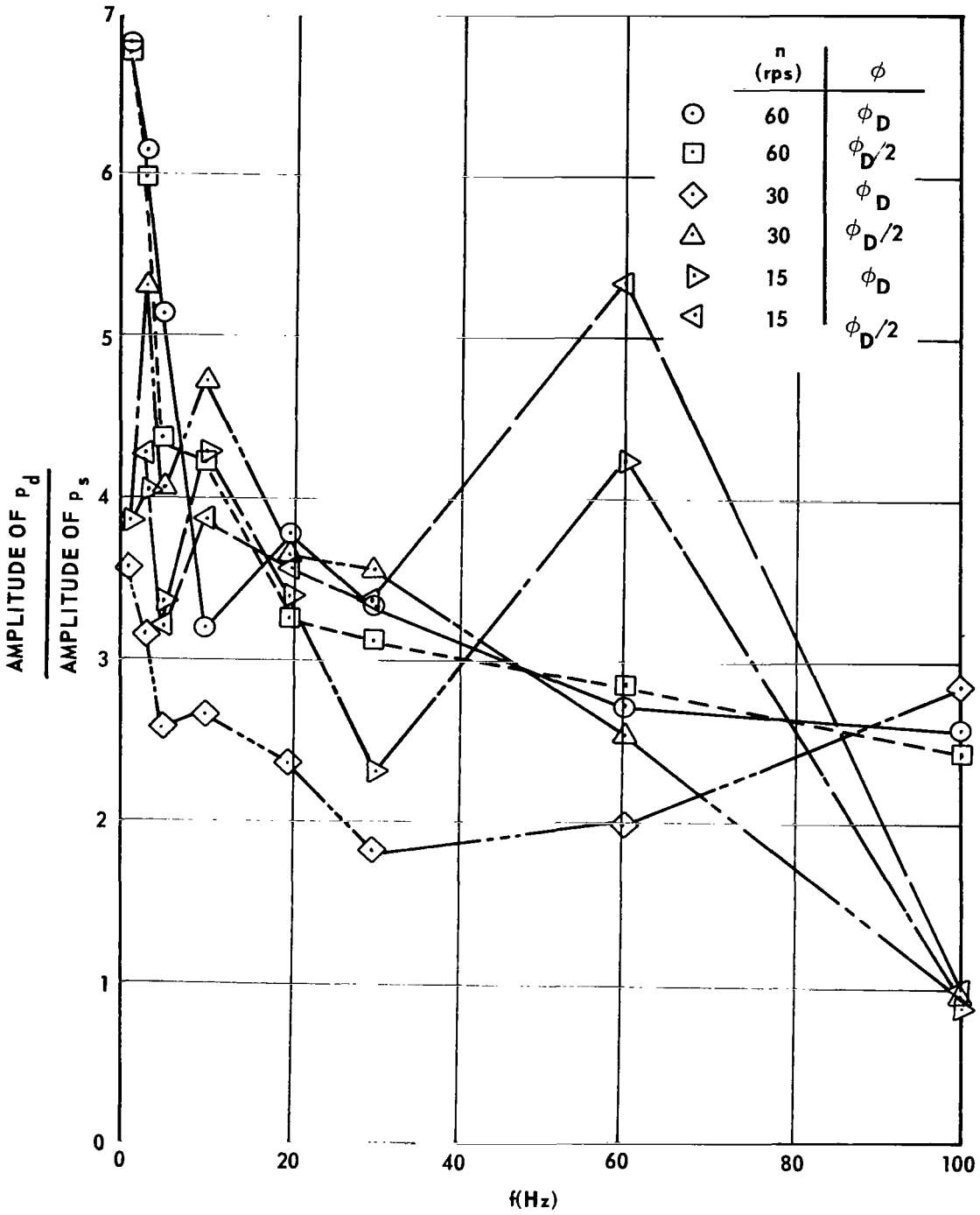

FIGURE 45. AMPLITUDE RATIO OF DELIVERY AND SUCTION PRESSURE

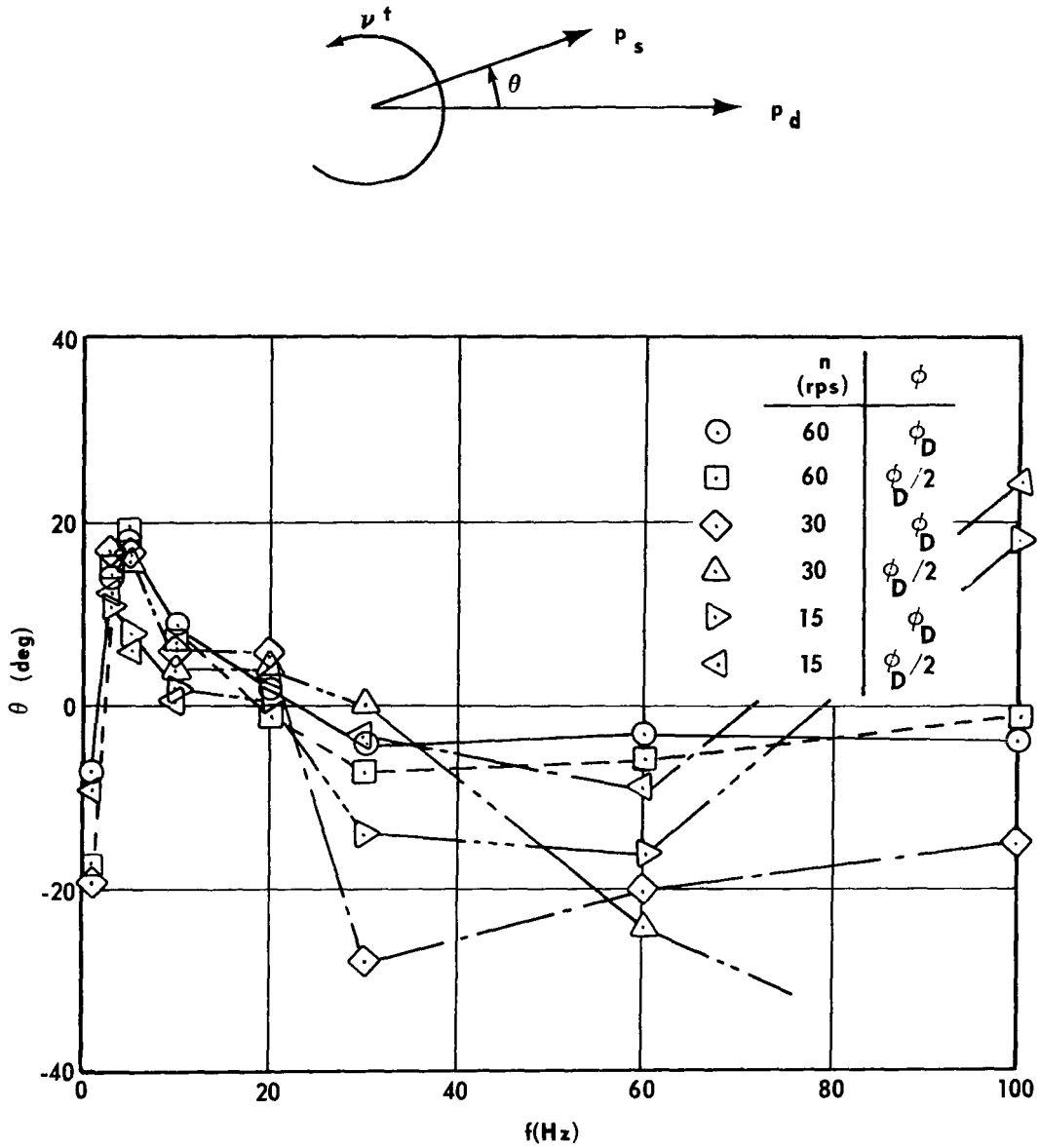

FIGURE 46. PHASE CORRELATION BETWEEN DELIVERY AND SUCTION PRESSURE

NASA-Langley, 1968 — 3 M349

05U 001 28 51 3DS 68106 00903
AIR FORCE WEAPONS LABORATORY/AFWL/
KIRTLAND AIR FORCE BASE, NEW MEXICO 8711[illegible]

ATT MISS MADELINE F. CANOVA, CHIEF TECHNI
LIBRARY /WLIL/

POSTMASTER: If Undeliverable (Section 158 Postal Manual) Do Not Return

"The aeronautical and space activities of the United States shall be conducted so as to contribute . . . to the expansion of human knowledge of phenomena in the atmosphere and space. The Administration shall provide for the widest practicable and appropriate dissemination of information concerning its activities and the results thereof."

—NATIONAL AERONAUTICS AND SPACE ACT OF 1958

NASA SCIENTIFIC AND TECHNICAL PUBLICATIONS

TECHNICAL REPORTS: Scientific and technical information considered important, complete, and a lasting contribution to existing knowledge.

TECHNICAL NOTES: Information less broad in scope but nevertheless of importance as a contribution to existing knowledge.

TECHNICAL MEMORANDUMS: Information receiving limited distribution because of preliminary data, security classification, or other reasons.

CONTRACTOR REPORTS: Scientific and technical information generated under a NASA contract or grant and considered an important contribution to existing knowledge.

TECHNICAL TRANSLATIONS: Information published in a foreign language considered to merit NASA distribution in English.

SPECIAL PUBLICATIONS: Information derived from or of value to NASA activities. Publications include conference proceedings, monographs, data compilations, handbooks, sourcebooks, and special bibliographies.

TECHNOLOGY UTILIZATION PUBLICATIONS: Information on technology used by NASA that may be of particular interest in commercial and other non-aerospace applications. Publications include Tech Briefs, Technology Utilization Reports and Notes, and Technology Surveys.

Details on the availability of these publications may be obtained from:

SCIENTIFIC AND TECHNICAL INFORMATION DIVISION

NATIONAL AERONAUTICS AND SPACE ADMINISTRATION

Washington, D.C. 20546